JPL PUBLICATION 77-5

# JPL Basic Research Review



National Aeronautics and
Space Administration

Jet Propulsion Laboratory
California Institute of Technology
Pasadena, California 91103

TECHNICAL REPORT STANDARD TITLE PAGE

| 1. Report No. 77-5 | 2. Government Accession No. | 3. Recipient's Catalog No. |
|---|---|---|
| 4. Title and Subtitle<br>JPL BASIC RESEARCH REVIEW | | 5. Report Date<br>March 16-17, 1977<br>6. Performing Organization Code |
| 7. Author(s)<br>JPL Staff | | 8. Performing Organization Report No. |
| 9. Performing Organization Name and Address<br>JET PROPULSION LABORATORY<br>California Institute of Technology<br>4800 Oak Grove Drive<br>Pasadena, California 91103 | | 10. Work Unit No.<br>11. Contract or Grant No.<br>NAS 7-100<br>13. Type of Report and Period Covered<br>JPL Publication |
| 12. Sponsoring Agency Name and Address<br>NATIONAL AERONAUTICS AND SPACE ADMINISTRATION<br>Washington, D.C. 20546 | | 14. Sponsoring Agency Code |

15. Supplementary Notes

16. Abstract

Results, current status and projected goals for some fifty Research and Advanced Development programs at the Jet Propulsion Laboratory are reported in abstract form.

Some of the papers will be presented orally to the NASA OAST Council while others are provided to delineate additional work in progress at the Laboratory.

| 17. Key Words (Selected by Author(s)) | 18. Distribution Statement |
|---|---|
| Chemistry and Materials (General)<br>Engineering (General)<br>Mathematical and Computer Sciences (General)<br>Physics (General) | Unclassified -- Unlimited |

| 19. Security Classif. (of this report) | 20. Security Classif. (of this page) | 21. No. of Pages | 22. Price |
|---|---|---|---|
| Unclassified | Unclassified | 107 | |

## HOW TO FILL OUT THE TECHNICAL REPORT STANDARD TITLE PAGE

Make items 1, 4, 5, 9, 12, and 13 agree with the corresponding information on the report cover. Use all capital letters for title (item 4). Leave items 2, 6, and 14 blank. Complete the remaining items as follows:

3. Recipient's Catalog No. Reserved for use by report recipients.

7. Author(s). Include corresponding information from the report cover. In addition, list the affiliation of an author if it differs from that of the performing organization.

8. Performing Organization Report No. Insert if performing organization wishes to assign this number.

10. Work Unit No. Use the agency-wide code (for example, 923-50-10-06-72), which uniquely identifies the work unit under which the work was authorized. Non-NASA performing organizations will leave this blank.

11. Insert the number of the contract or grant under which the report was prepared.

15. Supplementary Notes. Enter information not included elsewhere but useful, such as: Prepared in cooperation with... Translation of (or by)... Presented at conference of... To be published in...

16. Abstract. Include a brief (not to exceed 200 words) factual summary of the most significant information contained in the report. If possible, the abstract of a classified report should be unclassified. If the report contains a significant bibliography or literature survey, mention it here.

17. Key Words. Insert terms or short phrases selected by the author that identify the principal subjects covered in the report, and that are sufficiently specific and precise to be used for cataloging.

18. Distribution Statement. Enter one of the authorized statements used to denote releasability to the public or a limitation on dissemination for reasons other than security of defense information. Authorized statements are "Unclassified—Unlimited," "U. S. Government and Contractors only," "U. S. Government Agencies only," and "NASA and NASA Contractors only."

19. Security Classification (of report). NOTE: Reports carrying a security classification will require additional markings giving security and downgrading information as specified by the Security Requirements Checklist and the DoD Industrial Security Manual (DoD 5220.22-M).

20. Security Classification (of this page). NOTE: Because this page may be used in preparing announcements, bibliographies, and data banks, it should be unclassified if possible. If a classification is required, indicate separately the classification of the title and the abstract by following these items with either "(U)" for unclassified, or "(C)" or "(S)" as applicable for classified items.

21. No. of Pages. Insert the number of pages.

22. Price. Insert the price set by the Clearinghouse for Federal Scientific and Technical Information or the Government Printing Office, if known.

## PREFACE

This document is a compilation of text and figures which reflect the Basic Research Program on-going at the Jet Propulsion Laboratory, particularly those projects actively carried out in CY'76.

## ABSTRACT

Results, current status and projected goals for some fifty Research and Advanced Development programs at the Jet Propulsion Laboratory are reported in abstract form.

Some of the papers will be presented orally to the NASA OAST Council while others are provided to delineate additional work in progress at the Laboratory.

# CONTENTS

## CONTENTS (contd)

## CONTENTS (contd)

# Aerodynamics and Fluid Mechanics

RTOP 188-78-51
Suballotment from Marshall Space Flight Center
Advanced Technology – Liquid Helium
P. V. Mason*

# SUPERFLUID HELIUM EXPERIMENTS IN ZERO GRAVITY

Liquid helium will be used in space in the next few years, both as a cryogen to cool devices such as masers, superconducting electronics, and far infrared detectors, and in the superfluid form, as a subject of investigation in its own right. Normal helium He I will provide cooling to 2.2°K, superfluid helium HeII to 1.0°K, and the rare isotope $^3$He can provide temperatures down to 0.3°K. Below this point, temperatures as low as 0.01°K can be obtained by using the $^3$He-$^4$He dilution refrigerator.

Superfluid helium will be used as a cryogen both in the NASA-sponsored investigation of general relativity using the Stanford-developed superconducting gyroscope, and in the Infrared Astronomy Satellite (IRAS) to be launched in 1981. In support of these missions, an investigation was made of the properties of superfluid helium in zero gravity. The goal of the work was to demonstrate that the remarkable quantum properties of superfluid helium, such as thermal superfluidity and fountain effect pressure can be used to obtain a nearly ideal cryogen in the zero-gravity of space, and that no undesirable effects would interfere with its use.

At the time of the initial design of the IRAS satellite, there was considerable concern that unexpected effects in the superfluid might lead to rapid loss of helium and of the mission. The results of the tests described have given the program managers sufficient confidence in superfluid helium to permit it to be specified in preference to a supercritical helium system.

Five experiments were designed to test the crucial properties, and were flown for short periods in a NASA zero-g airplane, and in a 10-min rocket flight. The general configuration is shown in Fig. 1.

These experiments were done in collaboration with Los Alamos Scientific Laboratories, who supplied the cryostat and conducted the copper/helium interface experiments, and Sandia Laboratories, who provided major elements of the payload and range facilities. The booster rocket was supplied by Goddard Space Flight Center.

The experiments were:

(1) Demonstration and measurement of the properties and operation of a liquid-vapor separation device using the fountain effect for venting of the boil-off gas without loss of the cryogen. Figure 2 shows a laboratory experiment demonstrating fountain effect retention of superfluid helium.

(2) Determination of the distribution and oscillation frequencies and damping of bulk liquid helium in zero gravity [Fig. 3(a)].

(3) Determination of the effects of gravity on the thickness of nearly saturated films of superfluid helium [Fig. 3(b)].

(4) Measurements of the critical heat flow for the breakdown of superfluidity in thin films in zero gravity as a function of acceleration, film thickness and temperature [Fig. 3(b)].

(5) Determination of the heat flux for transition from pool to film boiling at the interface between copper and superfluid helium.

The results of the experimental flight demonstrated that superfluid helium can be successfully used as a cryogen in zero gravity. Specifically,

(1) The fluid is retained efficiently by a porous plug utilizing the fountain pressure. Temperature fluctuations caused by varying heat loads are small and do not lead to runaway thermal behavior.

(2) Film thickness is a strong function of temperature and acceleration in the saturated regime.

(3) Thermal superconductivity is retained even in thin films, as long as the accelerations are small. Proper design of cryogenic systems will be necessary if it is desired to maintain temperature uniformity to the millikelvin level, and account will have to be taken of the residual accelerations of the spacecraft.

(4) Bulk fluid tends to distribute itself on the walls of the containing vessel. The bulk sloshing oscillations are small in amplitude and settle out within seconds after the removal of disturbing accelerations. Both of these properties are desirable for use as a cryogen; see Fig. 4.

(5) The critical heat-flow data for copper/helium interfaces are still being analyzed.

Work is continuing in the following areas:

(1) Determination of the amplitude and spectral distribution of temperature fluctuations in bulk liquid due to the sloshing.

(2) Methods of controlling the sloshing by capillary, electrostatic, and electromagnetic forces.

(3) Methods of cooling devices to temperatures below 1°K, taking into account that $^3$He is not a superfluid.

(4) Methods of measuring waves on thin films of superfluid, with the intention of conducting experiments in zero gravity in frequency and wavelength regimes not available on earth.

*Earth and Space Sciences Division, Physics Section

RTOP 505-06-01
Airframe Noise Reduction
J. M. Kendall*

## AIRFRAME NOISE DUE TO TURBULENT FLOW

Wind tunnel studies of the noise production by turbulent flow past models which represent aircraft configuration elements have continued. As reported previously, the principal experimental technique involves the use of a highly directional microphone system which is located outside the tunnel, and which receives acoustic signals through an opening in the side of the tunnel. The spatial resolution of the system is such that the location of a point source of sound can be determined to within a centimeter. By scanning the system with respect to a flow region to be analyzed, the noise source distribtion is obtained, and is represented pictorially for each of several frequency bands.

A number of improvements to equipment and technique have been developed. These will increase the data acquisition speed, and improve the microphone spatial resolution through incorporation of the point-source response in the data reduction. Also, a three-axis traverse mechanism which supports a hot-wire anemometer or other probe has been interfaced to the computer for flow field and turbulence measurements.

Studies have been made on two- and three-dimensional bluff bodies, on cavity flows, and on aircraft model components. Through these measurements, the following results and observations are obtained:

(1) For these flows, the principal noise production zones are generally quite localized within the flow, rather than being of extended dimension.

(2) These zones can be identified with specific fluid-dynamic features, such as wake closure, flow attachment to or separation from a surface, transition to turbulence, etc.

(3) In certain cases, small geometrical changes affect the noise production by alterning the occurrence or extent of these fluid-dynamic features.

(4) The interaction between configurational components can significantly affect noise production because the presence of one element alters the flow about another.

(5) In most cases, a flow zone which is noisy radiates across a fairly wide spectrum.

Some of these points are illustrated by the results presented here. In each figure, the intensity of a signal measured at a point is represented by the arc length of the symbol; the flow speed of the measurement was 18 m/sec. Figure 1, top, shows in horizontal section the turbulence intensity distribution for the flow past a 5-cm-diameter cylinder extending from the tunnel floor to ceiling. This result is intended for qualitative identification of the shear layer and wake closure locations only. The lower portion shows the noise distribution as recorded in side view. The noise emanates from the closure region.

Figure 2 displays the noise distribution due to flow over an axisymmetric cutout. A 7.5-cm-diameter cylinder aligned with the flow, and upon which the boundary layer is turbulent, is reduced in radius by 0.63 cm over a 10-cm length to form the cutout. Of interest here is the observation that the noise apparently radiates radially outward; lower intensity is measured at the upper and lower edges of the model, where the "acoustic depth" is greater, than at the centerline height.

Figures 3 and 4 show two views of the noise distribution for flow past a model aircraft flap and landing gear, the latter emerging from a cavity within the mounting panel. The noise originates principally at the ends of the flap, and at the location where the turbulent boundary layer on the panel interacts with the wheel strut. Removal of the flap was accompanied by an increase in the strut noise, presumably because of an increase in the local flow speed there.

*Earth and Space Sciences Division, Physics Section

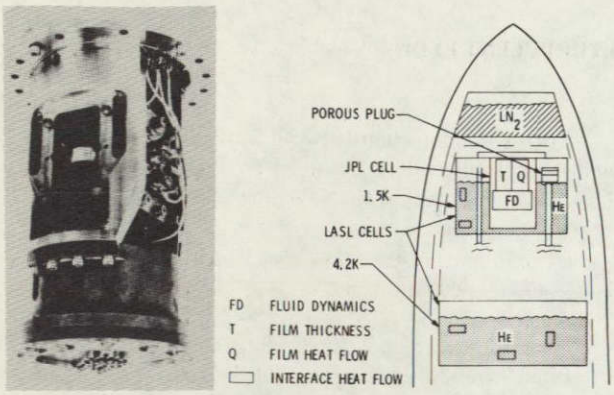


Figure 1. JPL Helium in Zero-Gravity Rocket Experiment

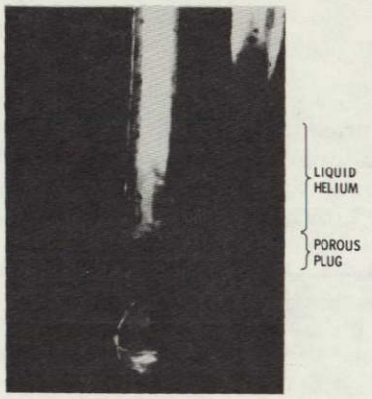


Figure 2. Porous Plug – Laboratory Tests

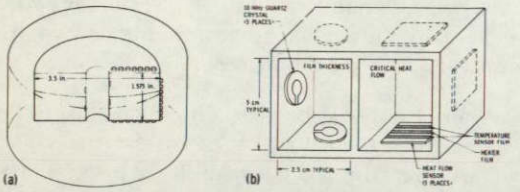


Figure 3. (a) Fluid Dynamics Experiment Configuration
(b) Nearly Saturated Helium Film Experiment Configuration

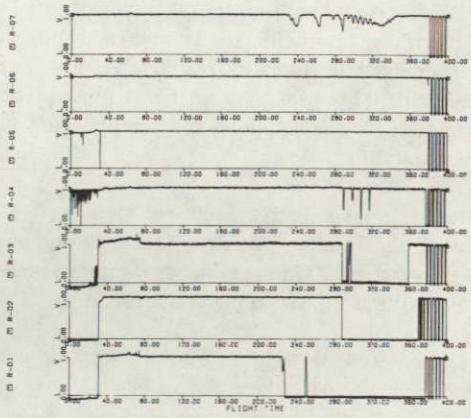

Figure 4. Fluid Dynamics Experimental Results

RTOP 505-06-41
Quiet Wind Tunnel Support
RTOP 514-55-01
Transition Prediction/Swept Wings
L. M. Mack*

# BOUNDARY LAYER STABILITY AND TRANSITION

The use of linear stability theory as a means of understanding the initial phase of boundary-layer transition, and as a technique for predicting the location of transition, is continuing under the sponsorship of Langley Research Center (LaRC). Two different problems were taken up in the reporting period. The first is one that has arisen in connection with the development at LaRC of a "quiet" supersonic wind tunnel, i.e., a tunnel in which the test model is not exposed to sound radiation from a turbulent boundary layer. The question was to determine how much of an incident Mach radiation field is reflected from a laminar boundary layer. The second problem is connected with the NASA Laminar Flow Control project. Here the objective is to produce a computer program based on the conventional parallel-flow stability theory that can compute the stability characteristics of three-dimensional boundary layers. This program will be used to determine the amount of suction required to maintain laminar flow on a transonic swept wing. Some remarks on these two problems follow.

The JPL stability program has the capability of calculating the reflection of a periodic Mach radiation field from a laminar boundary layer. The strength of the reflected radiation helps answer the question of how effective a given laminar boundary layer is as a sound absorber. In this approach, the sound field is decomposed into plane-wave components which all move with the average velocity of the acoustic sources in the radiating turbulent boundary layer. As the source velocity is supersonic relative to the freestream velocity, the theoretical sound field may be regarded as the far-field produced by the Phillips mechanism of supersonic sound generation. Typical results for $A_r/A_i$, the ratio of the amplitude of the reflected wave to that of the incoming wave, are shown in Fig. 1 as a function of Reynolds number ($Re = U_1^* \times^* / \nu_1^*$) for an insulated flat-plate at freestream Mach number $M_1 = 4.5$ for several dimensionless frequencies $F = \omega^* \nu_1^* / U_1^*$, where the asterisks refer to dimensional quantities and the subscript 1 to the freestream quantities. The average source velocity is $0.65\ U_1^*$, and the waves are two dimensional. An attenuation region exists near the leading edge for each frequency. The amount of attenuation increases with increasing frequency, while the extent of the attenuation region decreases. Work currently in progress is directed toward examining the effect of boundary-layer parameters such as wall cooling, suction and pressure gradient in order to find combinations which maximize the attenuation.

A three-dimensional boundary layer differs from its two-dimensional counterpart in having cross-flow instability in addition to the usual instability of the velocity profile in the potential-flow direction. The early work of Stuart and Brown brought out the nature of cross-flow instability and provided some useful numerical results, but no computations were made of either the spatial amplification rate or the all important amplitude history of constant-frequency disturbances. The goal of the current work is to develop both a method for obtaining the amplitude histories and a computer program to implement the method. A major modification of the JPL two-dimensional stability program was needed to meet the special requirements of three-dimensional boundary layers and is now in progress.

The amplitude ratio $A/A_0$, where $A_0$ is the amplitude at the neutral stability point, is obtained by integrating the spatial amplification rate in the direction of maximum amplification. This rate may be obtained directly from the spatial amplification theory, or from the temporal theory by the approximate relation $-\omega_i/|c_g|$, where $\omega_i$ is the temporal amplification rate and $|c_g|$ is the magnitude of the group velocity. It is not correct to assume that the spatial theory makes it unnecessary to compute the group velocity. Before eigenvalues of three-dimensional spatial disturbances can be computed, even in a two-dimensional boundary-layer, it is necessary to know the direction of maximum amplification. This direction is most plausibly taken to be the direction of the group velocity. The necessity of computing the group velocity gives the temporal theory an advantage as the eigenvalues can be obtained independently of the group velocity.

The boundary layer on a rotating disk offers an example of a boundary layer where cross-flow instability is dominant, and has been used to develop ideas and gain experience with three-dimensional boundary layers before moving on to the swept-wing problem. The temporal amplification rate of the rotating disk boundary layer is shown in Fig. 2 as a function of $\alpha$, the dimensionless wave number (with respect to $L^* = (\nu^*/\Omega^*)^{1/2}$, where $\Omega^*$ is the angular velocity of the disk) in the direction of the wave normal, for several wave orientations. The orientation angle, $\psi$, is the angle between the wave normal and the radial direction measured opposite to the direction of rotation. The Reynolds number $R = \Omega^* r^* L^* / \nu^*$, is equal to 1000. The unstable waves have orientations between 20° and −60° with the maximum amplification rate at about −16°. Not all of these waves are plotted in Fig. 2, because, for $\psi < -11°$, the peak amplification rate for a given orientation occurs at a wave number for which the phase velocity, $c_{ph}$, is negative, as shown in Fig. 3. These inward moving waves cannot influence transition. Consequently, the maximum amplification rate, subject to the constraint $c_{ph} \geq 0$, occurs for $\psi = -11°$, $\alpha = 0.35$ and $c_{ph} = 0$. The group velocity at $R = 1000$ was found by numerical differentiation of the vector dispersion relation to have a magnitude of about 0.5 for wave angles near −10°, and a direction of about 80°, i.e., nearly in the direction of the tangential velocity. With the unknown direction of maximum amplification also assumed to be 80°, spatial computations were carried out to determine the amplitude

*Earth and Space Sciences Division, Physics Section

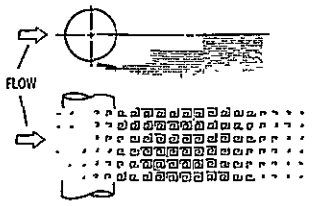


Figure 1. Turbulence Intensity (Top) and Noise Source Distribution (Bottom) for Flow Past Circular Cylinder

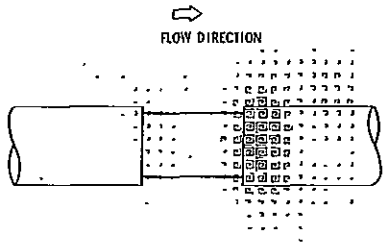


Figure 2. Noise Distribution for Flow Past an Axisymmetric Cutout

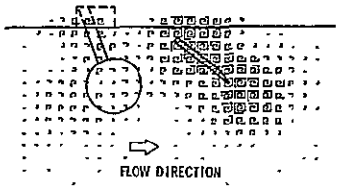


Figure 3. Noise Distribution for Flow Past Landing Gear and Flap, Side View

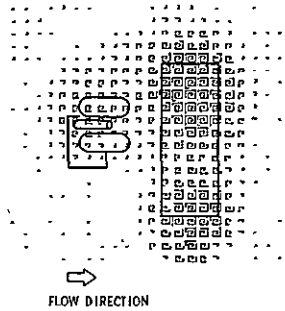


Figure 4. Noise Distribution for Flow Past Landing Gear and Flap, Plan View

RTOP 506-26-23
Planetary/Probe Design/Outer Planets
P. T. Y. Poon*

# RADIATIVE GASDYNAMICS OF SHOCK-HEATED HYDROGEN-HELIUM PLASMAS

As an entry probe enters into the atmosphere of an outer planet such as Jupiter, Saturn, or Uranus, the radiative heat flux plays a significant role in the total heating to the surface of the heat shield. The bow shock layer can be divided into four regions according to their physical properties: (1) weakly radiating nonequilibrium region, (2) highly radiating equilibrium region, (3) radiative cooling region and (4) ablation layer composed of evaporated carbon diffused with hydrogen-helium. The JPL annular arc accelerator shock tube (ANAA), with its ability to prepare shock-heated test samples which simulate Jovian entry conditions, has been successfully employed to carry out experimental investigations of the chemical kinetics and the emission as well as absorption characteristics. Figure 1 shows the annular arc accelerator shock tube which consists of a cold gas driver and expansion section, high-voltage electrode sections and the shock tube test section. The shock speed is monitored by fast-rise photo multiplier tubes at nine stations along the test section. Good quality hypervelocity flows have been achieved with shock velocities up to 50 km/s at an initial pressure of 1 torr into 84.17% $H_2$ - 15.83% He. Theoretical and experimental investigations in relative gasdynamics utilizing the high-performance shock tube have been carried out and documented in recent publications (Refs. 1-3). The following are highlights of the recent radiative gasdynamics effort:

(1) Radiative cooling measurements - The intense radiative flux emanating from the equilibrium region of the shock-heated plasma causes a drain of energy and cools the plasma. Since the radiative emission is sensitive to the temperature of the plasma, the radiative heat transfer is significantly reduced. Rapid computational algorithms have been developed to solve the coupled fluid dynamic-radiative transfer equations and applied to predict radiative cooling in the hypervelocity shock-tube test slug. In addition to on-axis cooling effects, there are off-axis temperature gradient effects due to greater cooling near the boundaries. Both effects have been accounted for in the calculations. Figure 2 shows a sample result of the comparison of the radiative cooling experiment with the prediction.

(2) Nonequilibrium relaxation distance measurements - The ionization relaxation distance is measured as a function of velocity by holographic interferometry techniques with a pulsed ruby laser system. Figure 3 shows the relaxation distances measured over a wide range of shock conditions (26-46 km/s at an initial pressure of 1 torr) for a realistic composition (84.17% $H_2$ - 15.83% He) simulating outer planet entry. The extent of the nonequilibrium zone determines the influence of nonequilibrium effects on total heating to the heat shield of the entry probe (Refs. 1 and 2).

(3) Equilibrium electron density measurements - The equilibrium electron density in the shock-heated plasma is measured by two independent diagnostic techniques: first, from the total fringe shift in the region immediately ahead of the gas dynamic shock wave to the quasi-uniform ionized region behind the gas dynamic shock wave, and second, from the spectroscopic measurements of Stark-broadened line profiles. Figure 4 shows the equilibrium electron density measurements and the theoretical results predicted by the JPL thermochemistry code. The verification of the thermochemistry calculations together with previous equilibrium radiative intensity measurements provide a firm basis for the computation of the "driver" radiative flux in the flow field surrounding the heat shield.

In conclusion, experimental and theoretical investigations have provided useful studies in the three regions of interest in the bow shock layer surrounding the entry probe.

References

1. Livingston, F. R., and Poon, P. T. Y., "Relaxation Distance and Equilibrium Electron Density Measurements in Hydrogen-Helium Plasmas," AIAA J., Vol. 14, pp. 1335-1337, Sept., 1976, presented as paper 76-121 at the AIAA 14th Aerospace Sciences Meeting, Washington, D.C., Jan. 26-28, 1976.

2. Leibowitz, L. P., and Kuo, T. J., "Ionization Nonequilibrium Heating During Outer Planet Entries," AIAA J., Vol. 14, pp. 1324-1329, Sept., 1976.

3. Poon, P. T. Y., and Stickford, G., "Radiative Cooling in Shock-Heated Hydrogen-Helium Plasmas," to be published.

*Applied Mechanics Division, Thermophysics Section

ratio $A/A_0$ of stationary waves. The results are shown in Fig. 4 for four Reynolds numbers. The abscissa is $-R\beta_r$, where $\beta_r$ is the dimensionless wave number in the tangential direction. Transition, which is observed to occur at about R = 525 on a rotating disk, corresponds to a $\ln(A/A_0)$ of about 15, a much larger value than is commonly associated with transition in a two-dimensional boundary layer. The maximum amplitude ratio at R = 525 occurs at $-R\beta_r = 25$ with $\psi = 12.1°$. It may be noted that the number of cycles around any circumference is given by $-R\beta_r$ and that the integration of the spatial amplification rate to yield $\ln(A/A_0)$ was performed with $-R\beta_r$ held constant.

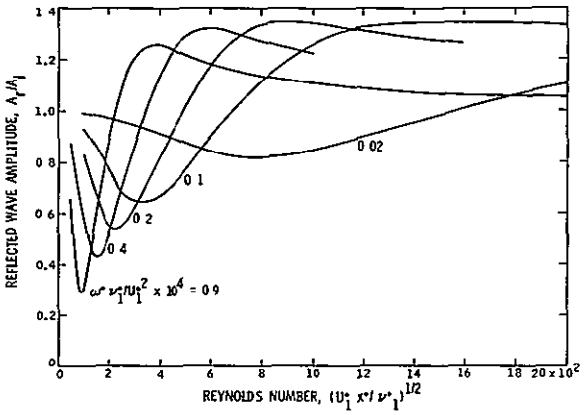


Figure 1. Ratio of Amplitude of Reflected Wave from Insulated-Wall, Flat Plate Boundary Layer at $M_1 = 4.5$ to Amplitude of Incoming Wave

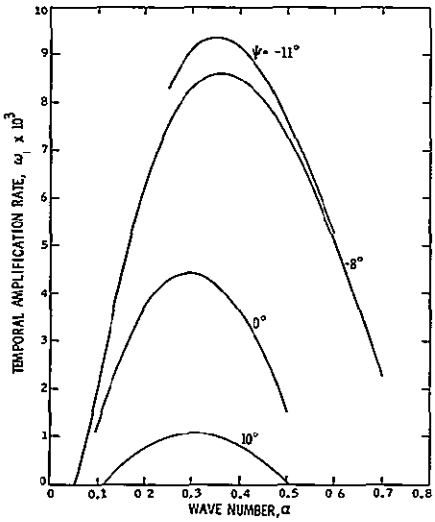


Figure 2. Temporal Amplification Rate of Rotating Disk Boundary Layer at R = 1000

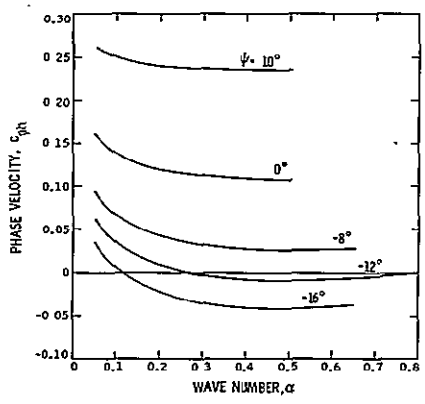


Figure 3. Temporal Phase Velocity of Rotating Disk Boundary Layer at R = 1000

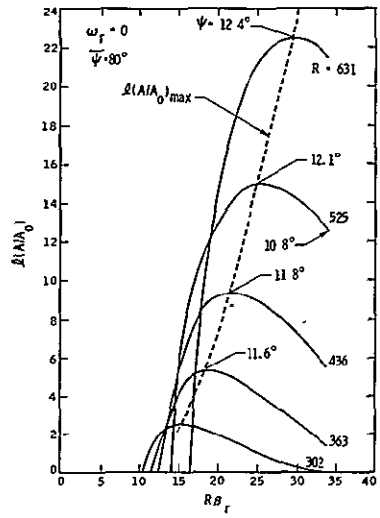


Figure 4. Amplitude Ratio of Stationary Waves in Rotating Disk Boundary Layer for Four Reynolds Numbers as a Function of Tangential Wave Number

Applied Mathematics and Computer Science

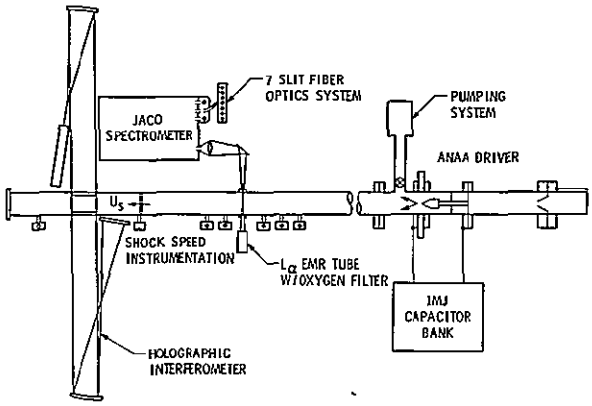


Figure 1. Annular Arc Accelerator Shock Tube and Optical Instrumentation

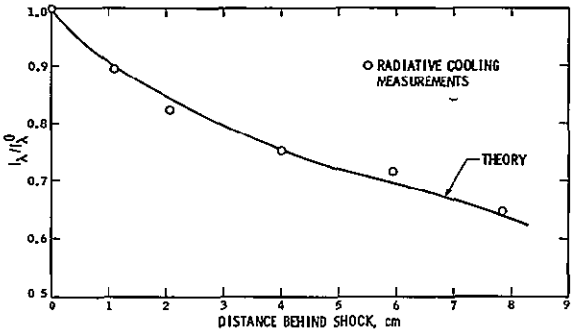


Figure 2. Radiative Cooling in 0.8417 torr $H_2$/0.1583 torr $H_e$ for Shock Speed of 38.53 km/s

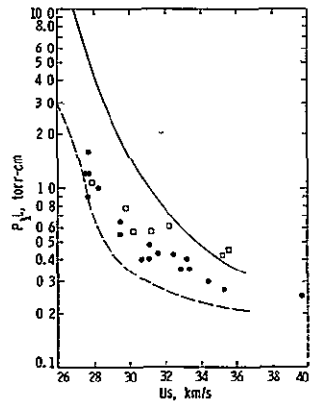


Figure 3. Nonequilibrium Relaxation Distance Obtained from Holographic Measurements (●) and Spectroscopic Measurements (□). Solid Curve and Dashed Curve are Calculations from Two References

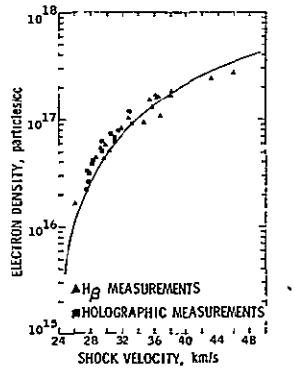


Figure 4. Equilibrium Electron Density from $H\beta$ and Holographic Measurements

RTOP 506-25-23
Solitons in Quasi One-Dimensional Systems
H. D. Wahlquist*



## SOLITONS IN QUASI ONE-DIMENSIONAL ORGANIC CONDUCTORS

New applied mathematics for nonlinear differential systems is being developed under the task Nonlinear Wave Interactions in Plasmas and Lasers (RTOP 505-15-35). This work has been reported to the OAST Research Council in past years, and so will be mentioned only briefly here before we discuss a new area of research to which it has led.

We do wish to report, however, the progress being made in application of our discovery of *prolongation structures* (PS) for nonlinear partial differential systems. These are so-called "free" Lie groups which we have shown can be systematically derived, and which generate a hierarchy of potentials and conservation laws for a partial differential system. The PS technique developed at JPL is being used by groups at Manchester, Iowa, Harvard, and Dublin. It is now clear from work by these groups that after deriving the PS, one can use it to implement well-known solution methods: the inverse-scattering equations, the "soliton" creation and destruction transformations, etc., – all methods which have been vital for progress the last few years in many nonlinear fields, from plasmas and lasers to fundamental particle theory. Efforts are under way also to extend the PS technique to develop needed methods for nonlinear systems in two- and three-space dimensions.

Another very important contribution to the theory of prolongation structures was published recently by Robert Hermann (Harvard): "The Pseudopotentials of Estabrook and Wahlquist, The Geometry of Solitons, and The Theory of Connections," Phys. Rev. Lett. 36, 835, 1976. He has shown that the hierarchy of conserved differential forms generated by the PS can be interpreted geometrically in a very natural way in terms of "connection" forms over higher dimensional manifolds. And it then follows that the original differential ideal (which represents the given partial differential system) corresponds to the "curvature" forms associated with that connection.

As a result of this insight, one now sees that almost all of the well-studied one-dimensional soliton equations can be given a unified geometrical description based on the group manifold of the Lie group, SL(2,R), which exists as a subalgebra of the PS's of all these equations. It further suggests fascinating possibilities for giving a fundamental topological interpretation of the soliton phenomenon in terms of the "winding" numbers associated with the global properties of solution manifolds. This work has also revealed close formal relationships between the PS's of known one-dimensional soliton equations and the nonlinear Yang-Mills fields which are becoming increasingly important in the theory of fundamental particles.

As an important outgrowth of the basic work on nonlinear systems, OAST has this year initiated a new task "Solitons in Quasi One-Dimensional Systems," (RTOP 506-25-23) which is a research collaboration of applied mathematics, quantum theoretical physics and experimental solid state physics.

The soliton represents a new type of low energy, mobile, elementary excitation and may be visualized in solid conductors as a solitary wave, or pulse, in the electronic charge density which propagates through a lattice. The soliton owes its existence to the presence of strong nonlinear interactions such as those associated with anharmonic potentials. Soliton conduction should be characterized by unusual electrical, magnetic, and optical properties since solitons do not appear to be scattered by impurities or defects as effectively as other charge carriers, e.g., electrons. At the present time, practically nothing is known about the soliton contribution to the transport properties. The complexities associated with nonlinear processes of soliton conduction are greatly reduced by considering systems of quasi 1-D geometry for which new mathematical methods now exist.

A theoretical and experimental approach is under way which is focused on the nonlinear process of soliton conduction in quasi 1-D materials such as (TTF) (TCNQ). We are developing a theoretical model incorporating soliton charge carriers from the beginning as fundamental constituents. Basic elements of such a soliton conduction model already existed as a result of one of the papers written under the task on Nonlinear Wave Interactions at JPL (RTOP 505-15-35): Wahlquist, H. D., "Backlund Transformations of Potentials of the Korteweg-de Vries Equation and the Interaction of Solitons with Cnoidal Waves," in Robert M. Miura, Ed., "Backlund Transformations, the Inverse Scattering Method. Solitons and Their Application," Lecture Notes in Mathematics, No. 515 (Springer-Verlag, Berlin, New York, 1976).

This theory gives the exact energy level spectrum and corresponding eigenfunctions of electrons in a 1-D lattice containing traveling domain walls. These results show that the moving "domain wall" soliton opens up a new discrete energy level for electrons, below the lowest energy level of the band structure of the original periodic lattice potential. Thus, an electron can drop into a bound state, localized around the traveling soliton and be carried along with it – an exact quantum model of a stable, nonlinear, soliton charge carrier. In view of these properties this appears to be a very attractive model to investigate. Its obvious advantage is that of including the nonlinear many-soliton conduction effect exactly in lowest order.

*Earth and Space Sciences Division, Physics Section

Not Presently Funded
A. L. Fymat*

# MATHEMATICS OF INVERSION THEORY OF PHYSICAL PROCESSES

## Relevance of Proposed Work

Many of NASA's activities in space (planetary exploration including satellite imagery, remote sensing of our environment and of the Earth's natural resources, . . .) are confronted with one basic common problem: the interpretation of data gathered from a distance in terms of physical characteristics and parameters of the sensed medium. The solution to this problem can, at least in principle, be arrived at by modeling the physical situation and subsequently "inverting" the model using analytical and numerical tools. When successful, the approach can also be used for optimizing the very experiments providing these data. Unfortunately, the corresponding formulations are often mathematically ill-posed, i.e., they result in either a nonunique or an unstable solution, or both. Under such circumstances, the experiments may lose their significance no matter how crucial or useful they might have been. Two courses of actions are left open however: (1) ascertain that the failures of the conditions of uniqueness and stability are not the result of inappropriate formulations, and if so provide better formulations, and (2) identify those conditions under which the problems become well-posed, i.e., amenable to experimentation and inversion, and develop the corresponding solutions. The aim of the proposed work is to investigate these two avenues starting from current NASA problems in remote sensing of atmospheric structure and composition, and of environmental pollution.

## Current Work

We are currently investigating new methods and concepts for remotely sensing the vertical profiles of temperature, gaseous composition, and size distribution and refractive index spectrum of particulates in the Earth's atmosphere. Many of these methods and concepts are directly applicable to the study of the other planetary atmospheres, and to many other problems as well. First-kind Fredholm integral equations are encountered here. Unfortunately, such equations are known to be unstable and, while considerable efforts have been devoted to their solution, actual applications to atmospheric problems have achieved only a limited success. Also, owing to the very nature of these equations, convergence and error have been difficult to analyze. However, the physics of the problem is usually incompletely taken into account in several of the attempts at finding an inverse solution. For these reasons, the International Radiation Commission of the International Association of Meteorology and Atmospheric Physics has recently created an ad-hoc Working Group, chaired by the proposer, with charge of critically reviewing the current methodology in inversion theory, and setting forth areas where further research is needed. Work in this area has been on-going since November 1975 and will continue. While some of the basic difficulties have already been identified, actual research on their solution needs to be undertaken. Proposed work in some fundamental aspects of these problems is described below.

## Proposed Work

Since the actual solution of first-kind Fredholm integral equations cannot be obtained from the measurements, two approaches have been followed generally. (1) derivation of properties that all solutions share; these must then be properties of the true solution; (2) restriction of the class of admissible solutions by introducing *a priori* hypotheses on the solution. The former point is by now well-developed (this is the Backus-Gilbert method), and is being applied for optimizing the design of experiments. It does not however represent a method of inversion of experimental data but only a technique for assessing the significance of a solution, e.g., whether a particular feature is really resolved by the data or how much detail is available from a given distribution of observations. The validity of the solution obtained from the latter alternative depends of course critically on the *a priori* information employed. Nevertheless, even with the use of such information, first-kind equations are still being inverted. Unfortunately, the difficulties in the studies of convergence and error of such equations renders assessing the validity of the solutions obtained an equally difficult task. Two different procedures could however convert the original first-kind equations into second-kind equations whose convergence can be studied straightforwardly by any of a number of known, error-accountable methods. The latter equations are further free of the numerical difficulties associated with first-kind equations. These two procedures are (1) use the Tikhonov regularization concept; and (2) regard the first-kind equation as a limiting case of dual integral equations. It is proposed to investigate these two procedures and to provide new formulations and solutions of the atmospheric remote sensing equations.

## University Work

This work will be conducted in consultation with Prof. R. E. Kalaba, University of Southern California, who has initially suggested the concept of conversion to dual integral equations.

*Earth and Space Sciences Division, Planetary Atmospheres Section

In experiments on quasi 1-D systems, the temperature dependence of various physical properties is all important. Thermal averages will have to be computed from the theory, and this requires the knowledge of the quantum statistical partition function Z. In the proposed work, Z will be computed from the phenomenological Hamiltonian based on the model discussed above. For certain transport properties knowledge of Z is not sufficient, and one must calculate the so-called temperature Green's functions. The techniques for doing this are well-known and will be used to predict electric, thermoelectric and optical properties.

The initial experimental program will involve the measurement of the current voltage (I-V) characteristics as a function of electric field and temperature in (TTF) (TCNQ) and its derivatives. Special attention will be given to the range of electric fields and temperatures for which nonlinear I-V characteristics are observed. The temperature dependence of the electrical conductivity will be measured in both the low and high electric field regimes (if nonlinear behavior is discovered) to determine the excitation energies for solitonic and single particle conduction. A low frequency AC technique will be used to obtain the I-V curves directly. In addition, the noise spectrum will be measured at each temperature to obtain the resistance at zero electric field. This will improve the accuracy for the determination of the magnitude of the solitonic conductivity. (TTF) (TCNQ) will be studied since there is evidence for the presence of a pinned CDW at low temperatures ($T < 38°K$). (TTF) $(SCN)_{.58}$ will be studied since it semiconducts at higher, more accessible temperatures ($T < 200°K$), and may have the same structural instabilities as (TTF) (TCNQ). Since only one chain conducts in (TTF) $(SCN)_{.58}$ as opposed to both chains conducting in (TTF) (TCNQ), the data interpretation is simplified.

# Environmental Science

RTOP 505-03-32
Gas Turbine Engine Pollution Reduction Technology
R. M. Clayton*

# HYDROGEN ENRICHMENT FOR LOW EMISSION JET COMBUSTION

The Environmental Protection Agency has established standards for aircraft jet engines that, by 1981, will require as much as 65% reduction in emissions of oxides of nitrogen ($NO_X$) for newly certified engines under take-off power. Even greater levels of reduction of carbon monoxide (CO) and unburned hydrocarbons (HC) emissions will be required for ground-idle conditions. Moreover, concern over ozone depletion in the stratosphere from $NO_X$ may ultimately lead to very stringent standards for high altitude cruise operation. And even though it is understood that the $NO_X$ emissions are the result of high combustion temperatures under high-power operation and that CO and HC emissions are the result of reduced combustion efficiency under low-power operation, "conventional" approaches to combustor design changes generally fail to show promise of achieving the emission standards across the engine operating range. This lack of success is inherent in the opposing combustion requirements involved in reducing the two classes of emissions. Thus, the development of new combustor design concepts is required before combustion temperature can be reduced substantially without sacrificing flame stability and combustion efficiency.

The control over peak flame temperature that is available with premixed, fuel-lean combustion is well known. This mode of combustion is presumed to be necessary to greater or lesser degree in all advanced combustor concepts for minimizing $NO_X$ production. But the leanness required is seriously close to the lean burning limit of hydrocarbon and air; therefore, the attractiveness of the premixed, lean-burning concept is tempered by the narrow margin between the mixture strength and combustor dwell times required for $NO_X$ control and those required for flame stability, ignition and high combustion efficiency.

By virtue of its unique lean-burning qualities, molecular hydrogen substituted for a portion of the jet fuel significantly improves the combustion margin available for pollution control. This is illustrated in Fig. 1 for a subsonic-cruise power operating condition typical of a 30:1 compression ratio turbofan engine (inlet air, 11.6 atm at 850°F). The theoretical depression of the lean flammability limit as a function of the mixed-fuel composition is shown by the solid curve labeled $ER_{LM}$. The dashed lines show theoretical rich and lean engine-operating boundaries which, together with the ideal lean limit line, illustrate the potential benefits of using hydrogen enrichment for achieving acceptable lean-burning combustor operation. In principle, the addition of hydrogen permits efficient burning well to the lean side of the $NO_X$ control boundary which, without hydrogen, falls near the hydrocarbon/air lean limit ($ER_{LJP}$).

*Control and Energy Conversion Division, Energy and Materials Research Section

The objective of the research reported herein is to evaluate the practical feasibility of applying the hydrogen enrichment concept for the simultaneous reduction of $NO_X$, CO and HC emissions to *ultra low* levels. The target emission indexes (g pollutant/kg total fuel) are 1.0 for $NO_X$ and CO, and 0.5 for HC. The practical aspects of the evaluation are fulfilled by conducting experiments utilizing a cylindrical research combustor with inlet-air state conditions typical for 30:1 compression ratio, high-bypass, turbofan commercial aviation engines.

During the past year, experiments were conducted using the combustor, designated MOD 2, shown in Fig. 2. The combustor is housed in a pressure vessel into which unvitiated air is pumped by the JPL hypersonic wind tunnel compressors. This air is supplied at up to 30 atm pressure and 1000°F at 10 lbm/S. The air flows from the vessel through the mixing section of the combustor where metered amounts of hydrogen (from a bottle storage) and finely atomized jet fuel are mixed with the air. The total mixture then passes through a flameholder, and is ignited and burned in the water-cooled combustion chamber. The burned gases are sampled and analyzed for CO, HC, and $NO_X$ before being exhausted to atmosphere through a sonic nozzle.

Emissions data for $H_2$/jet fuel (JP-5) mixes and for jet fuel only were obtained over a wide range of equivalence ratio (ER) for the low and cruise power conditions. Data with jet fuel alone were obtained at the take-off power condition. In no case has the problem of flashback and flameholding in the premixing zone previously encountered in the original (MOD 1) burner been observed. However, flameholder durability was a persistent problem that ultimately precluded operating the MOD 2 burner with $H_2$ at the take-off power condition. Further burner development is required to demonstrate the concept at this severe operating condition (inlet air, 30 atm at 1000°F).

The ultra low emission goals were simultaneously achieved for the cruise power condition at an average burning equivalence ratio of 0.38 using 10-12% mass $H_2$ in the total fuel. This operating point is shown on Fig. 1. The emission goals were not achievable with jet fuel alone due to the onset of lean blowout at an equivalence ratio too high to sufficiently reduce the $NO_X$ emission. The emission goals were not achieved simultaneously for the low power condition, but any two of the three goals were achievable in the equivalence ratio range of 0.3 to 0.4 with a relatively small residual in the third. About 15% $H_2$ was required.

Typical emission results for the MOD 2 burner for the cruise condition are shown as a function of input ER in Fig. 3. The fact that the $NO_X$ emission level is considerably greater than theoretical estimates is believed to be the result of premixing deficiencies. The overall results for the three simulated power levels are summarized in Fig. 4.

On the basis of the present results, it is concluded that hydrogen enrichment: (1) can minimize *all* pollutants, (2) significantly improves flame stability, (3) requires good premixing to minimize required hydrogen, and (4) is not simple to implement but is feasible, given further dedicated development.

During FY'77 it is planned to improve premixing homogeneity and flameholder design and carry out additional higher power experiments using the bottled hydrogen supply. Assuming that the results continue to be positive, efforts to incorporate an integrated hydrogen generator using a partial oxidation reactor will be initiated.

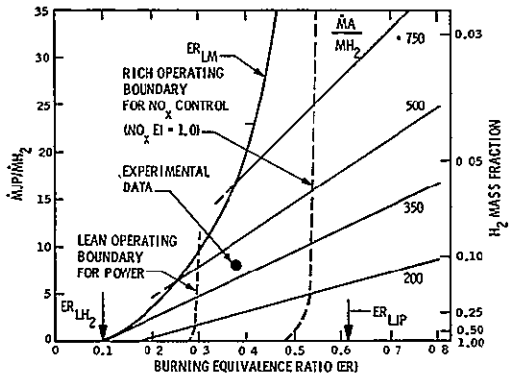


Figure 1. Operating Map for Hydrogen-Enrichment Concept, Cruise Condition

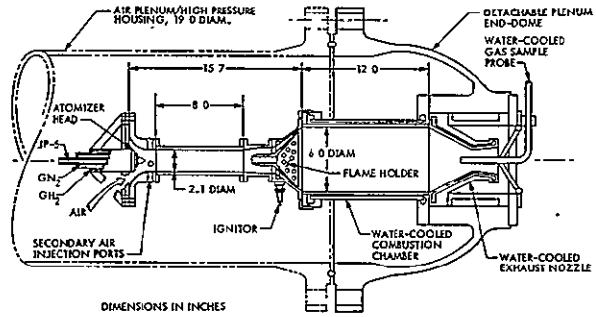


Figure 2. MOD 2 Burner Assembly

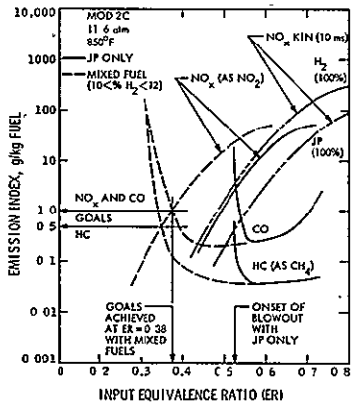


Figure 3. Emissions vs Equivalence Ratio, Cruise Condition

| | | SIMULATED POWER CONDITION | | | | | |
|---|---|---|---|---|---|---|---|
| | | LOW | | CRUISE | | T.O.* | |
| P, atm | | 4.4 | | 11.6 | | 30.0 | |
| T, °F | | 360.0 | | 850 0 | | 1000.0 | |
| AIR FLOW, lbm/s | | 1 3-2 2 | | 3 4-4 1 | | 8.0-9 3 | |
| EQUIV. RATIO | | 0.34 | 0.39 | 0.38 | 0.55 | 0.41 | 0.51 |
| $H_2$ MASS % | | 15 | 15 | 10 -12 | 0. | 0. | 0 |
| | JPL GOALS | | | | | | |
| PRESS. LOSS, % | ≤10.0 | 6 0 | 6.0 | 7 0 | 6 0 | 5.0 | 5.0 |
| COMB. EFF., % | 99. + | 99. + | 99 + | 99 + | 99. + | 99. + | 99. + |
| E.I. $NO_x$, g/kg | 1 0 | 1.0 | 2.5 | 1.0 | 5 0 | 3.0 | 50.0 |
| E.I. CO, g/kg | 1.0 | 4.0 | 1.0 | 1.0 | 0.4 | 30.0 | 1.0 |
| E.I. HC, g/kg | 0.5 | 0 35 | 0.25 | 0.1 | 0 04 | 0.06 | 0.07 |

*NOT YET RUN WITH $H_2$

Figure 4. MOD 2 Results Summary

RTOP 505-03-11
Basic Noise Research
S. P. Parthasarathy*

## MACH WAVE EMISSION FROM SUPERSONIC JETS

At high jet speeds, when turbulent eddies in a flow move at velocities greater than the ambient speed of sound, intense sound waves are generated. These would resemble the bow waves associated with solid bodies moving supersonically through a gaseous medium and are given the name eddy Mach waves. The objective of the Mach wave study was to determine the mechanism by which flow fluctuations are converted to that part of the radiated noise which constitutes Mach waves. In particular it was desired to relate these Mach waves to the flow parameters of a supersonic jet.

An experimental investigation has been conducted on supersonic jets at a Mach number of 1.43 over a temperature range from about 420 to 1370°K (300 to 2000°F) in which it was found that the noise in the far field was dominated by eddy Mach waves. It is shown both from experimental and theoretical considerations that the strength of the Mach waves is determined by the product of the mean shear and the density fluctuations of the jet.

Thus, the source of sound arises from the mixing of hot and cold streams as well as from those compressions and expansions that are intuitively associated with sound generation. For the temperature range investigated, the Mach waves were emitted at angles between 37 and 59 deg with respect to the jet axis with the smaller angle occurring at the lower temperature, which is also at the lower jet velocity. These values represent those in the region of the jet where the Mach angle was constant, that is, beginning at the nozzle exit and extending downstream to a distance ranging from 6 to 12 jet diameters, depending on temperature.

The density fluctuation expressed as the sum of mean squares of the contributions brought about by compressibility and by mixing of the hot and cold streams is consistent with the theory. At temperatures below 800°K, the density fluctuation is dominated by compressibility; whereas, at a temperature of 1300°K, the contributions of compressibility and of mixing are about equal. At much higher temperatures, mixing would dominate.

The time scale of the autocorrelation of Mach wave sound pressure increases linearly with axial distance downstream. This is consistent with a linear growth of the jet shear layer and a linear growth of the turbulent density fluctuation time scale. The Mach wave time scale varies inversely as the jet speed, indicating that the eddy length scales are independent of jet speed. The length scales of the eddies that contribute to Mach wave radiation grow linearly from a virtual origin for a jet of fixed Mach number.

Mach waves contribute from 50 to almost 100% of the noise radiation depending on the location of their origin. The lower contribution that occurs at locations near the nozzle exit is due to radiation that appears to be centered in the transonic portion of the jet.

After having shown that the eddy Mach waves are closely related to density fluctuations which arise from mixing of compressible streams, a logical next step is to determine the manner in which beneficial modifications to mixing can be accomplished. The benefits would be associated with noise reduction. An investigation of the mixing phenomenon, in particular the role in this regard of the large eddies or large scale structures that exist in turbulent jets, will be studied.

*Control and Energy Conversion Division, Energy and Materials Research Section

P. F. Massier*

## BASIC NOISE RESEARCH

The motivation for conducting Basic Noise Research resulted from the current need for reducing noise radiated from turbojet engines which are used for aircraft propulsion. A major contribution to the noise originates in the shear layer of the high-speed gas flow after it is discharged from the engine. Thus, it is believed that an understanding of the noise generation in this region will lead to methods of controlling the noise sources.

Also, disturbances that occur in the gas stream upstream of the nozzle can be transmitted to the core flow region of the jet and radiate as excess noise from the jet. This part of the disturbance-generated noise may originate either from acoustic or nonacoustic input fluctuations. The influence of these disturbances on the jet structure and, in turn, on the noise is as yet unknown.

At the present time there is controversy on the effect of forward flight of aircraft on jet noise, because this effect is not fully understood. Significant discrepancies exist between predictions and experiment. This is an important effect that requires clarification in order to predict whether aircraft will meet Federal regulations. The theoretical and experimental studies being conducted will lead to an understanding of this effect and possibly to a reduction of the noise radiated from aircraft in flight.

Thus, these investigations are oriented toward gaining an understanding of noise generation in jets. The ultimate goal, however, is that of noise reduction. This approach differs from the one used extensively in the past: namely, the utilization of structural materials and coatings to absorb sound. In the present studies the attack on the noise reduction problem is based on a more fundamental approach.

The investigations consist of combined experimental and theoretical work. Most of the experiments are conducted in an anechoic chamber on a steady flow basis. The temperature of the air flowing through the nozzle can be elevated to a maximum of 1370°K (2000°F) by burning methanol in a combustor as is done in a jet engine. However, the flow is mixed and controlled much more closely than in an actual engine. Compressed air is supplied by an air compressor facility. The experimental facilities are such that nozzle sizes up to about 11 cm in diameter at Mach numbers as high as 1.4 have been studied. Higher Mach numbers are easily attainable since the air supply pressure is 500 psia. Controlled disturbances upstream of the nozzle can be introduced by diverting the main gas flow through each of two electropneumatic transducers from which the flows pass through two divergent ducts. Then these flows discharge into a common rectangular plenum which is connected to the nozzle. Fluctuations in the upstream temperature can also be accomplished by introducing a high temperature gas flow through one of these transducers and low temperature gas flow through the other in opposite phase. The frequency range of the transducers is from about 100 to 5,000 Hz. Another facility available on an intermittent basis for use on this program is the reverberant chamber, used normally for testing spacecraft. This facility is beneficial whenever there is a need to obtain overall sound pressure levels. To acquire such information in an anechoic chamber would require the use of microphones in many locations and numerous geometrical integrations.

Current work is still oriented mostly toward understanding noise generation; however, some ideas on noise reduction have already evolved and are being pursued also.

The specific investigations that will be discussed are the next four topics on the agenda: (a) Mach Wave Emission from Supersonic Jets, (b) Core Noise, (c) Large Scale Coherent Structures in Jets, and (d) Effect of Forward Flight on Jet Noise. All of this work is being done in-house.



*Control and Energy Conversion Division, Energy and Materials Research Section

RTOP 505-03-11
Basic Noise Research
S. P. Parthasarathy*

## CORE NOISE

Core noise in a jet engine is attributed to noise caused by fluctuations upstream of the exhaust nozzle and is generally regarded as becoming important when the jet mixing noise is low. In jet engines, core noise consists of flow fluctuations, acoustic waves produced by turbomachinery and fluctuations of entropy caused by turbulent combustion.

The problem of core noise discussed here explains the mechanisms by which the various internal fluctuations interact with a jet in generating far field noise. This interaction can be the result of a number of factors. For example, a simple transmission of acoustic waves through a fluid jet can occur. However, a more complicated situation can also arise in which an input fluctuation triggers instabilities in the jet where these instabilities undergo nonlinear amplifications producing further turbulence and associated excess jet noise.

Experimental investigations were conducted on the transmission of pressure fluctuations and independently on the transmission of temperature fluctuations from a plenum through the exit of a nozzle to the surrounding atmosphere. The exit diameter of the nozzle was 4.2 cm. Experiments were conducted for discrete frequency inputs of both pressure and temperature fluctuations from 100 Hz to 5000 Hz and for an exit Mach number of 0.56. From the experiments, it was found that there was a direct proportionality between the generated pressure fluctuations and those sensed in the far field. Thus, there was no nonlinear amplification mechanism in the jet involved in the transmission. The far-field directivity pattern showed lobes for frequencies as low as 300 Hz, heretofore unobserved.

The transmission functions for both pressure and temperature fluctuations showed a number of peaks and valleys with differences of as much as 40 dB. However, the nondimensionalized sound pressure level for the two methods of generating fluctuations at a given Mach number of 0.56 showed that below 1000 Hz the sound pressure level in the far field was higher for the temperature fluctuations than for the pressure fluctuations.

Clarification is still needed, however, as to the manner in which the soundwaves and eddies behave individually when they are produced upstream and interact with the jet at the nozzle exit. Isolation of the sound waves and eddies can be accomplished by using screens to disintegrate eddies and cause them to mix; thus, in this case, allowing only sound waves to be present. Then to investigate only the behavior of the eddies, the sound can be absorbed with the use of sound absorbers in the shape of ducts thereby allowing only the eddies to pass through to the jet. More accurate measurements of the angular distribution of radiated noise will also be made by traversing a single microphone in the far field along a circular arc around the jet.

*Control and Energy Conversion Division, Energy and Materials Research Section

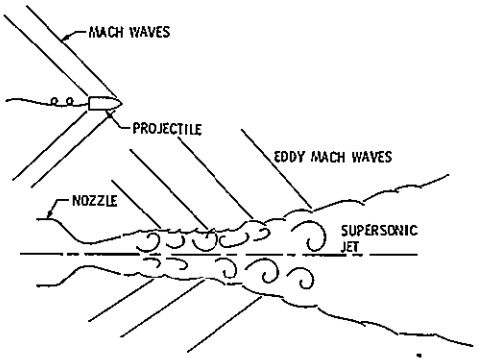


Figure 1. Mach Wave Emission

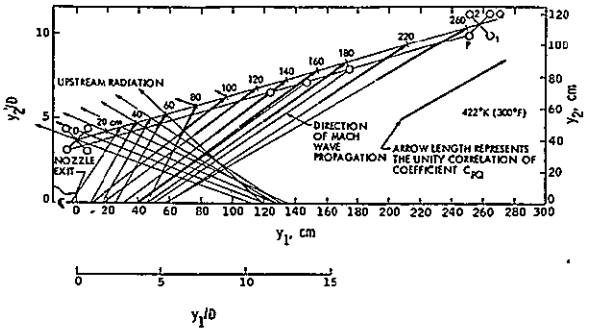


Figure 2. Mach Wave Field for a Jet Temperature of 422°K

- M = 1.43
- T = 420 TO 1370 °K (300 TO 2000 °F)
- DATA OBTAINED FROM NOZZLE EXIT TO 12 DIAMETERS DOWNSTREAM
- $D_e$ = 10.8 cm

Figure 3. Experimental Conditions

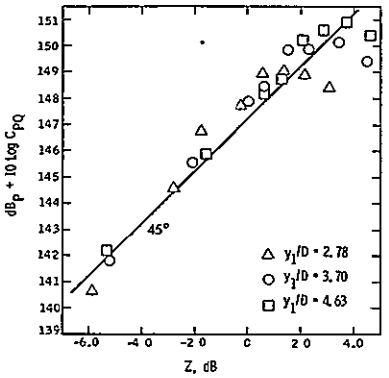


Figure 4. Intensity of Mach Wave Radiation at P vs Z

RTOP 505-03-11
Basic Noise Research
V. Sarohia*

# LARGE-SCALE COHERENT STRUCTURES IN JETS

In recent years, there has been a growing interest in the investigation of large-scale coherent structures in turbulent boundary shear flows, in jet flows and in wake flows. It has been recognized that the randomly merging and amalgamation processes accompanying the evolution of these orderly structures are responsible for entrainment and heat transfer processes across the turbulent shear flows. This merging process of large-scale coherent structures in shearing flows has also been shown to contribute largely to the Reynold stresses in the jet mixing layer. The present study has been undertaken to investigate the role that these large-scale coherent structures have in the production of jet noise.

Investigation of large-scale coherent structures in jet flows has been undertaken for both excited and nonexcited jet flows. For this purpose, high subsonic jet flow through a 4.2-cm-diameter nozzle was studied over a range of Reynolds numbers between $Re \simeq 10^5$ and $0.8 \times 10^6$ based on nozzle exit diameter. The flow exhausted from the nozzle into an anechoic chamber where jet noise measurements were made also. The jet flow was visualized by injecting $CO_2$ gas into the main nozzle air supply. The density gradient caused by the presence of $CO_2$ gas in the air resulted in a shadow effect which was employed to obtain spark shadowgraphs of the jet which were recorded on both photographic film and videotape.

The jet flow was excited by introducing disturbances of various frequencies between 100 and 2000 Hz into a plenum chamber located upstream of the nozzle. These upstream disturbances were generated by passing the flow through an electropneumatic transducer. The modulation of mass flow through the transducer could be varied by controlling the amplitude of the electrical input at a given frequency. Part of the fluctuating low energy resulted in large amplitude sound waves and the remainder resulted in flow fluctuations in the plenum chamber. The velocity fluctuations measured at the nozzle exit result from a combination of sound, mean flow fluctuations and possible instability waves or vortices generated in the jet shear layer. The velocity fluctuation at the center of the nozzle exit was as large as 15% of the mean jet velocity. This is much larger than the 2 to 3% values found in a typical jet engine. As a consequence of these large amplitude controlled velocity fluctuations at the nozzle exit, coherent vortex structures of a given frequency were artifically induced in the jet shear layer. The subsequent history of these artifically induced coherent jet structures will be studied to understand how they influence the small scale jet structure, the radiated jet noise, their interaction and amalgamation with each other, etc.

This investigation of the controlled, artifically created large structures in jet flows is being conducted along with the randomly occurring natural coherent structures of a nonexcited jet flow. It is believed that such a controlled jet flow study will lead to a fundamental understanding of the role that these coherent jet structures have in jet noise generation.

A spark shadowgraph of a nonexcited jet flow at $M \simeq 0.69$ and $Re_D \simeq 0.4 \times 10^6$ is shown in Fig. 1. The presence of coherent jet structures is quite evident. Amalgamation of these large-scale structures with each other as they convect farther downstream can be inferred.

Figure 2 shows a shadowgraph of an excited jet flow with large amplitude velocity fluctuations at the nozzle exit. The optical systems employed in taking Figs. 1 and 2 were different, as is clear from the shadowgraphs. The exit Mach number $M \simeq 0.4$ and excitation frequency $fD/U_e \simeq 0.15$ where f is excitation frequency in Hz, D is the nozzle diameter and $U_e$ is the mean nozzle exit velocity. Because of the large input mass fluctuations in the plenum chamber, periodic vortex structures resulted in the jet shear layer at the nozzle exit at the excitation frequency. For the excited jet shown in Fig. 2, as large-scale jet structures convected downstream the two initial vortex structures amalgamated into one. The jet mixing layer farther downstream showed large amplitude velocity fluctuations at half the frequency of the initial large scale disturbances. On comparing the behavior of these artifically controlled coherent structures with the structures observed in a nonexcited jet flow (Fig. 1), a striking similarity in jet behavior is evident; e.g., amalgamation and pairing of the large structures. Therefore, a more detailed investigation of this artificially excited jet is being undertaken. Such a study will shed light on the amalgamation mechanism of large coherent jet structures and also will lead to methods of controlling noise sources in jet flows.

Experiments as indicated in Fig. 3 are planned to study the role of these large scale structures in producing the shearing stresses in the jet mixing layer which in turn are responsible for jet noise. This will be achieved by simultaneously measuring the velocity fluctuations in the jet mixing layer along with the radiated noise. These measurements will be synchronized with high-speed schlieren motion pictures of the large-scale structures as they convect past the velocity and pressure signal sensors. A frame-by-frame investigation of large-scale structures and associated velocity and radiated near-field noise will shed light on the role of these large-scale structures in producing jet noise.

*Control and Energy Conversion Division, Energy and Materials Research Section

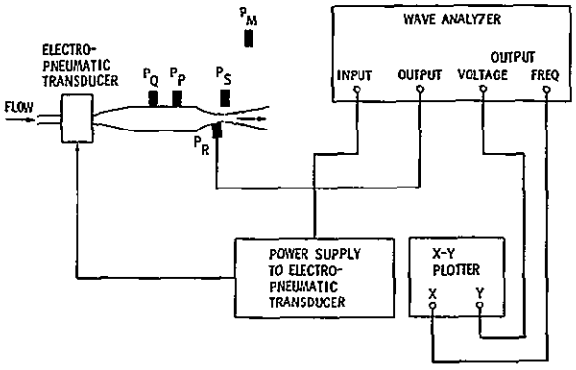


Figure 1. Instrumentation Diagram

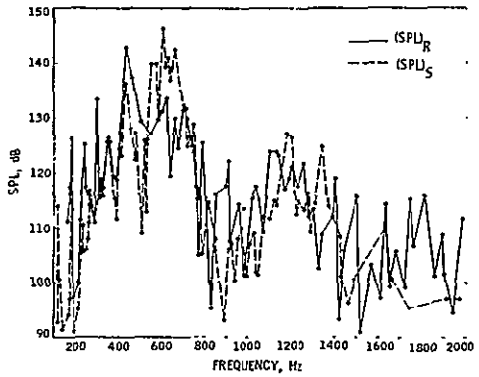


Figure 2. Sound Pressure Levels at R and S vs f

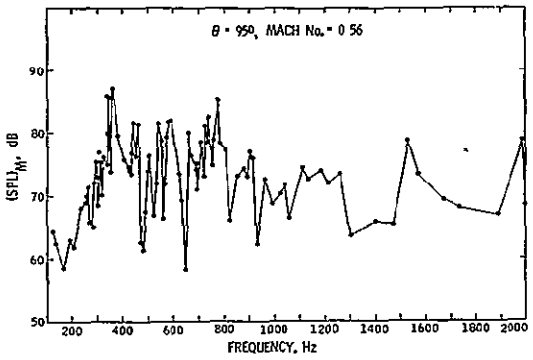


Figure 3. Far Field Sound Pressure Level for Internally Generated Pressure Fluctuations

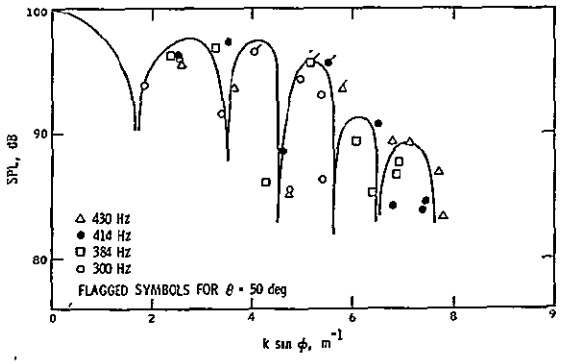


Figure 4. Far Field Diffraction Pattern

RTOP 505-03-11
Basic Noise Research
V. Sarohia*

## EFFECT OF FORWARD FLIGHT ON JET NOISE

To understand how the forward velocity of an aircraft influences the source of jet noise in flight is the main objective of this investigation. According to the present prediction models of aerodynamic noise from a turbulent jet, the effect of forward velocity of an aircraft on the far-field jet noise level is that the radiated noise should decrease with an increase in the forward flight velocity. This noise reduction results from reduced shear in the jet mixing layer which, in flight, is assumed to scale with the relative velocity $V_{rel} \equiv V_J - V_1$, where $V_J$ is the mean jet velocity and $V_1$ is the forward velocity of the aircraft. Flight data of jet noise results, on the contrary, show little or no decrease in jet noise perpendicular to the jet axis; that is, at close to $\theta_I = 90^\circ$ and in the forward quadrant where $\theta_I$ is the angle of the observer to the jet intake axis.

Results of wind tunnel simulation of a jet in flight show that a reduction in jet noise occurs with an increase in flight speed, but this decrease is not as large a power of relative velocity as expected. Furthermore, it is observed that noise reduction follows a power law relationship, $(V_{ref})^n$ where n is a strong function of $\theta_I$, the angle to the intake. The exponent has a value of approximately n = 7 close to the jet axis as expected theoretically and decreases gradually to a value of n = 5 or less close to $\theta_I = 90^\circ$. Flight tests also show such a reduction in far-field jet noise close to the jet axis but little reduction at $\theta_I = 90^\circ$, and even an increase in the forward quadrant.

The directional distribution of the forward velocity effect on radiated noise strongly suggests the importance of the boundary layer flow over the engine cowl on the development of jet flow in flight. The presence of the outer boundary layer flow at the nozzle exit will strongly affect the development of the self-preserving plane mixing layer region of the axisymmetric jet flow. The relative velocity effect on turbulence-generated noise may not be observed due to masking of the jet by the outer flow (engine cowl boundary layer flow). In this part of the flow, jet flow may generate noise like a static jet in flight. As one would expect, in this region, Reynolds stresses $\overline{u'v'}$ will not scale with $V_{rel} \equiv V_J - V_1$. The noise generated from this region (relatively high frequency noise) contributes significantly to radiated noise near $\theta_I = 90^\circ$ and in the forward quadrant. It is believed that improper accounting of the noise sources from the initial part of the jet flow in flight is one of the main causes for disagreement between the predicted results and results obtained from the flight measurements.

To clarify the role of the engine cowl boundary layer flow on jet noise in flight, flight simulation experiments have been performed in an anechoic chamber. The experimental setup consists of basically a 1.27-cm-diameter primary nozzle jet flow surrounded by a 12.7-cm-diameter free-jet flow. Measurements of the fluctuating and mean velocities in the jet shear layer as well as of the radiated jet noise were made at various flight simulation conditions. The influence of the initial outer boundary layer flow (simulating the engine cowl boundary layer) on jet noise was investigated. These measurements, along with spark shadowgraphs of the jet flow under flight simulated conditions, were taken to understand the basic mechanism of jet noise production from aircraft in flight. Such a basic investigation will lead to an accurate prediction of jet noise from aircraft in flight and methods of jet noise reduction in flight.

Results of flight simulation experiments indicating the effects of outer boundary layer flow on jet noise are shown in Fig. 1. These experiments showed that the radiated jet noise for a given flight velocity increased for a thick outer boundary layer as compared to a thin one. Spark shadowgraphs for a fixed flight velocity also showed that the influence of changing the initial boundary layer thickness on jet structure was noticed many diameters downstream (Fig. 2). Because of the increased jet spreading with the thicker boundary layer as compared to a thin one, it is expected that more noise would be radiated when the outer boundary layer was thicker because of increased Reynolds stresses.

The results of the flight simulation experiments strongly demonstrate the influence of the engine cowl boundary layer flow on the radiated noise from aircraft in flight. Since this outer jet flow differs from one flight simulation experiment to another and also among various flyover experiments, the influence of the outer flow on jet noise source will be variable. This is probably the main reason for the disparity among various flight noise data, e.g., some do and others do not observe the presence of forward arc lift. Also, the reduction of jet noise due to forward velocity may be minimized if there is a separation of the boundary layer flow on the engine cowl. This may happen for certain airplane engine cowl configurations when the thrust line is at an angle of attack at takeoff or landing of the airplane.

The present study also suggests that due to a shielding effect by the outer boundary layer flow, the turbulence generated, and consequently the radiated noise in the initial few jet diameters downstream of the nozzle exit, do not scale with the relative velocity. Instead, it appears more appropriate to assume that noise generated from this part of the jet flow from aircraft in flight scales with jet absolute velocity instead of the relative velocity. This leads to a modification of the present prediction model of jet noise in flight. A comparison of the flight data with this modified

*Control and Energy Conversion Division, Energy and Materials Research Section

An investigation to predict these large-scale structures for a given jet flow also will be undertaken. The governing inviscid, incompressible, two-dimensional equations of motion will be integrated numerically to compute the various frequencies to which a given jet flow is unstable. An investigation of the integrated amplification of the disturbances at these frequencies as they propagate through the jet will be computed. It is believed that such a study will shed light on the pairing and amalgamation of the large-scale structure in the jet shear layer. The results of this analytical investigation will also be of considerable assistance in investigating which upstream disturbances (core noise) will influence the large-scale coherent jet structures. This can lead to modification of the jet noise source. The alteration of the jet noise source is caused by a complicated interaction mechanism of upstream disturbances with the jet flow. Experiments will be conducted to verify the theoretical results.

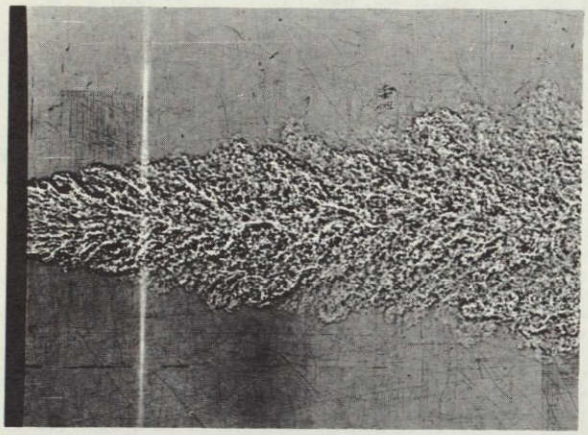

Figure 1. Large Scale Coherent Jet Structures in Non-Excited Jet Flow at $M_{exit} \simeq 0.69$ and $Re_D \simeq 0.86 \times 10^6$

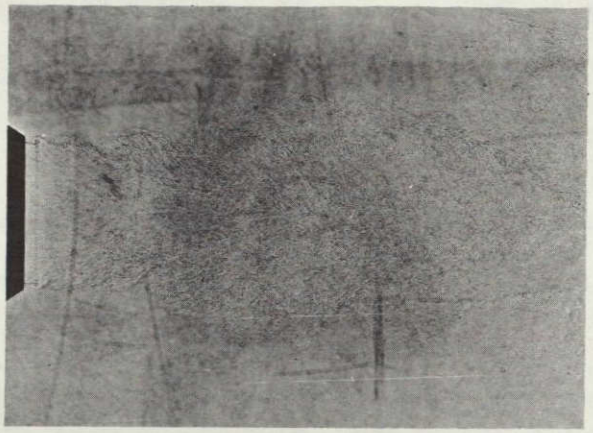

Figure 2. Large Scale Coherent Structures in Excited Jet Flow at $M_{exit} \simeq 0.4$; $Re_D \simeq 0.5 \times 10^6$ and $\frac{fD}{U_{exit}} = 0.15$

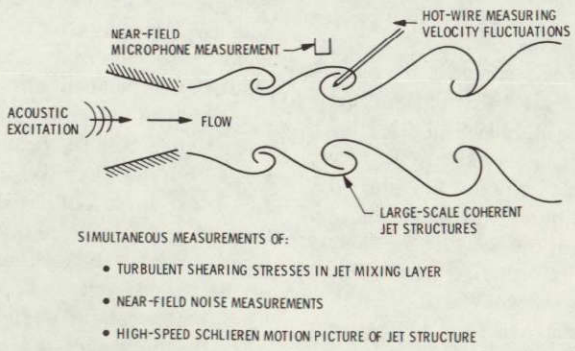


Figure 3. Experimental Setup for Investigation of the Role of the Large-Scale Structures in Radiated Jet Noise

prediction is shown in Fig. 3. These results reflect good agreement of predictions with flight data.

Design of a large-scale flight simulation experimental setup has been undertaken to study systematically and in detail the influence of outer boundary layer flow on the jet mixing layer in flight. The influence of the freestream turbulence on flight simulated jet noise will be investigated. Various methods will be used to enhance the jet mixing which will lead to a reduction of jet noise in flight.

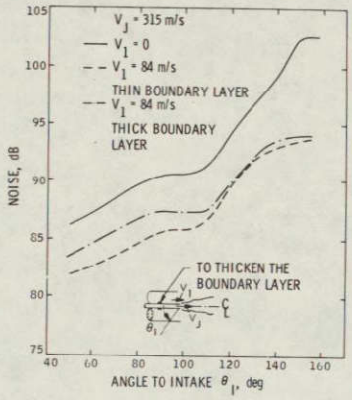


Figure 1. Effect of Outer Boundary Layer Flow on Jet Noise in Flight

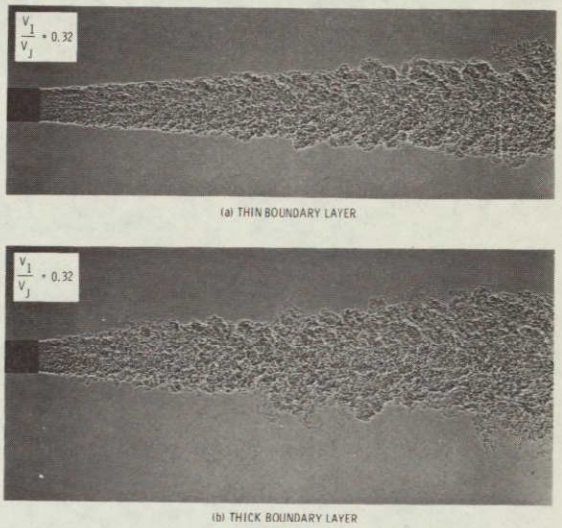


Figure 2. Shadowgraphs Showing the Effect of Outer Boundary Layer Flow on the Development of Jet Flow

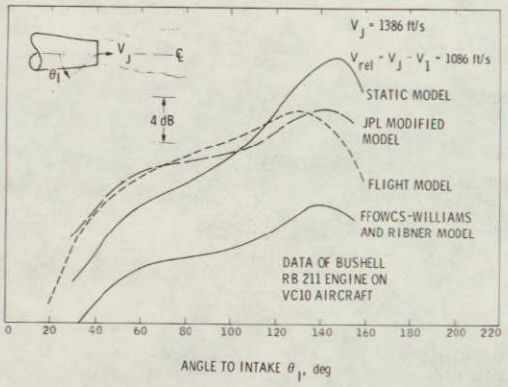


Figure 3. Comparison with Predictions of Jet Noise Under Static and Flight Conditions

# Materials

RTOP 506-15-28
Nonmetallic Superconductors
R. B. Somoano*

## SUPERCONDUCTIVITY AT HIGH TEMPERATURES

The primary objective of the Nonmetallic Superconductor Program at JPL is to investigate the possibility of synthesizing a high temperature superconductor. The overall approach stresses two types of mechanisms for achieving high temperature superconductivity with $T_c \sim 10^2$ °K: (1) the excitonic mechanism, and (2) the Peierls-Fröhlich giant charge density wave mechanism. The contributions of both mechanisms are optimized in quasi-one dimensional (1D) metallic structures.

A material which superconducts at high temperatures will be of vital importance in future uses of alternative energy sources. Examples of these uses are thermonuclear fusion (magnetic field containment of the plasma), spaceborne and airborne generators and motors, and electrical power transmission. These applications, coupled with the limited and dwindling supply of helium, emphasize the importance of achieving high temperature superconductivity.

The approach of the JPL program consists of experimental and theoretical studies of the physics and chemistry of quasi-1D organic and organometallic systems. The experimental effort involves chemical synthesis and physical measurements tasks. The chemistry effort is focused on the synthesis of compounds in which charge transport is due to a single carrier (holes) or to two different types of carriers (electrons and holes). The physics effort involves the study of the electrical, magnetic, optical, and structural properties of these materials. Specific goals are to determine the advantages or disadvantages of compounds containing one or two types of electrical carriers and to elucidate the nature of the deleterious metal-insulator (MI) transition. The theoretical effort focuses on the investigation of the strength of the excitonic mechanism in organic and organometallic structures.

The current (FY'76) program consists of the study of: (1) single carrier organic compounds based on TTF and its derivatives with halogens and pseudo-halogens, (2) new two carrier organic compounds, such as (TTF) (HTP), (3) organometallic compounds containing chains of rhodium, iridium, and platinum atoms, and (4) new polymorphs of the metallic, and superconducting, quasi-1D inorganic polymer, $(SN)_x$.

The results are: (a) finding that the excitonic mechanism cannot lead to superconductivity in organic structures, but only in organometallic systems, (b) discovery of the most highly conducting, and metal-like, single-carrier organic compound, (c) elucidation of an important correlation between the structure, electronic bandwidth, and the stability of the metallic state, (d) discovery of several new highly conducting rhodium chain compounds (these are the only conducting rhodium chain compounds known), and (e) a discovery of a new polymorph of $(SN)_x$ and measurements of its electrical and structural properties.

Some of the conclusions are: (1) single carrier cation radical structures are as conducting as most two-carrier compounds, but the metallic state is most stable in the latter and (2) the Peirls-Fröhlich mechanism for infinite conductivity is more promising than excitonic superconductivity, especially in organic compounds.

Future work (FY'77) will emphasize the synthesis of new two-carrier organic compounds and focus further attention on understanding and controlling the MI transition.

Several collaborative tasks, as part of the JPL program, have contributed to this effort. Prof. W. Little of Stanford University is involved in the theoretical study of the excitonic mechanism, Prof. A. M. Hermann of Tulane University carries out thermoelectric power studies of single crystal samples furnished by JPL, Prof. S. Samson of California Institute of Technology collaborates in the x-ray structural analysis of the organometallic compounds, and Prof. M. Labes of Temple University carried out the $(SN)_x$ study.



*Control and Energy Conversion Division, Energy and Materials Research Section.

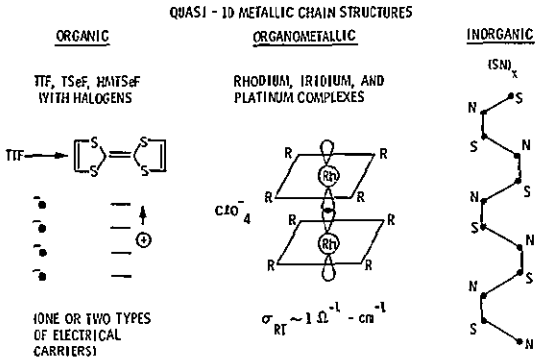


Figure 1. Current Experimental Program

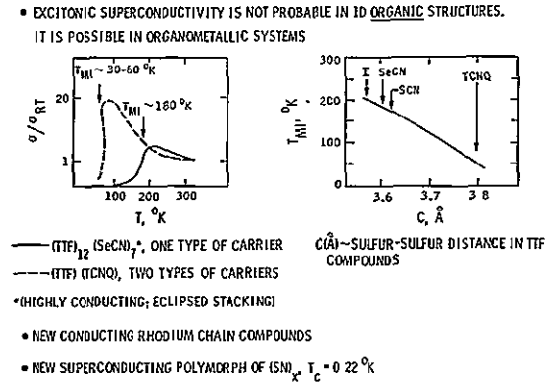


Figure 2. Results

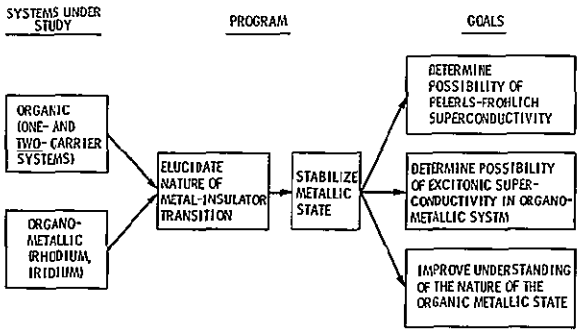


Figure 3. FY'77 Program

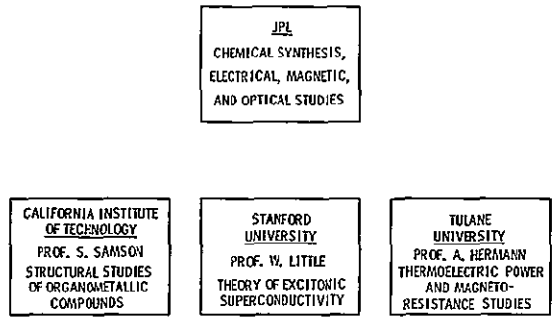


Figure 4. Nonmetallic Superconductors Effort

Not Presently Funded
R. F. Landel*

## CHEMILUMINESCENCE

There is frequently a need in material research to study trace reactions. Sometimes the sample is too small to permit anything but a micro-analytical technique, as with surface reactions. Often the material is so sensitive that marked change in properties occur long before there is any detectable chemical change by conventional techniques, as with the degradation of rubber-like polymers (where modulus changes are one or two orders of magnitude more sensitive than infrared or nuclear magnetic resonance analysis). In other cases, the reaction is too slow to give measurable changes in a reasonable time period, as in aging. Here, an attempt to increase the rate of reaction by raising the temperature can lead to different reactions, defeating the purpose.

We are currently faced with all of these problems – in trying to: (1) measure and enhance the stability of coatings for solar cells, (2) understand the aging of solid propellant binders, (3) assess the thermal stability of sealant materials for aircraft fuel tanks and (4) determine the UV, thermal and space stability of candidate solar soil materials. Indeed, there is a NASA-wide need for the solution to such problems. What is required therefore is support for the development and use of new analytical techniques specifically directed toward the resolution of such problems.

One of these is chemiluminescence, in which the reaction of a material is followed by measuring the light emitted by activated species produced during the course of the reaction. With sophisticated detection systems and the use of fluorescent additives, this light can be detected at extraordinarily low levels. Hence chemiluminescence offers a powerful new tool for determining kinetic and mechanistic details about a reaction pathway and the slow chemical changes which occur on aging.

Such light-detection measurements are closely related to those we have previously employed in studies of thermoluminescence, where light is emitted from a disordered solid as the disorder is annealed out on heating. (We had developed thermoluminescence for the forensic identification of glass and soil. Figures 1 and 2 depict the apparatus; Fig. 3 shows a comparison of two glass samples.) Support is being sought to adapt the existing equipment and expertise to the solution of this all-pervasive need of NASA for a hypersensitive analysis tool.

The work would concentrate on reactions which occur in solar cell encapsulants and solar soil materials, where early lifetime predictions could be markedly enhanced if the course of the reaction and reliable kinetic data were available. The present thermoluminescence apparatus, with its photomultiplier detector, can probably measure rates as low as $10^{-12}$ moles/sec. It is estimated that more sophisticated detection systems can raise this by 6 – 10 *orders of magnitude*. This means that reactions of a few tens of molecules per second can be followed, making chemiluminescence by far the most sensitive technique known for following degradation.

*Control and Energy Conversion Division, Energy and Materials Research Section

RTOP 506-16-17
Viscoelastic Properties of Polymers
R. F. Landel*

## POLYMER MATERIALS

Research on polymeric materials at JPL has as its chief goal the development of physical theories which describe their behavior under mechanical, thermal and electrical stresses, and the determination of those molecular parameters of the theory which control the physical properties, and hence the response. We have progressed very far in the first area, mechanical properties, where a unified theory now exists. Current work is devoted to the investigation of certain key areas thus identified and to the application of the theory to the practical problem of estimating, *a priori*, the lifetime of elastomers under load. This is work unique in NASA.

Dr. Steven Peng describes in this Report, work on large deformation behavior, where classical theory of elastomers no longer applies. We have developed a thermodynamically and geometrically correct extension of classical theory and are experimentally pursuing its ramification and validation. A rather straightforward constitutive equation for viscoelastic materials results, which is valid over wide ranges in time and temperature.

As for the lifetime of elastomers under load, Dr. Jovan Moacanin presents our unified theory, indicating the appropriate reduced variables or normalized coordinates of stress, strain and temperature which are required to describe the response of an elastomer, time dependence of failure included. In the past year we have completed a major portion of our effort by determining explicitly one of the key parameters required to handle filled rubbers. His report concludes with some remarks on the JPL approach in studying the behavior of the glassy.

The unified theory for mechanical properties, as described herein, is only applicable to stable materials. However, the theory can accommodate the effects of degradation (though many important aspects remain to be worked out in detail), if the degradation can be appropriately measured. It is one of the peculiarities of rubber-like polymers that trace amounts of chemical reaction can produce profound change in physical properties long before evidence of a chemical reaction can be detected by a conventional analytical technique. Hence the change in physical properties must be used as a measure of the chemical reaction, rather than vice versa. Unfortunately, this usually gives little or no insight as to what has actually occurred. Because of the great need for more sensitive analytical tools the following article describes a new technique for studying such trace reactions, chemiluminescence.

*Control and Energy Conversion Division, Energy and Materials Research Section

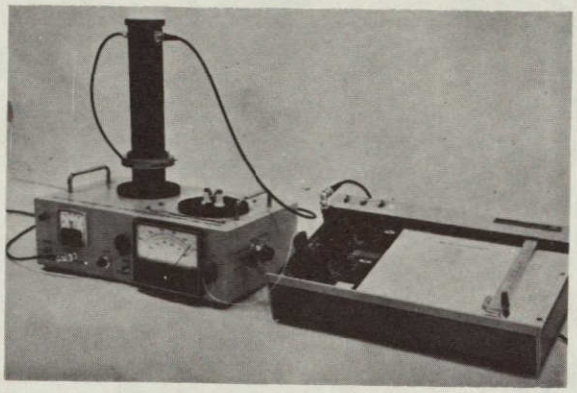

Figure 1. The JPL Thermoluminescence (TL) Apparatus

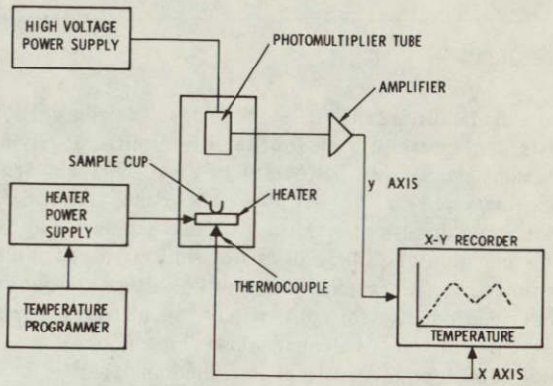


Figure 2. Schematic of the JPL Thermoluminescence Apparatus

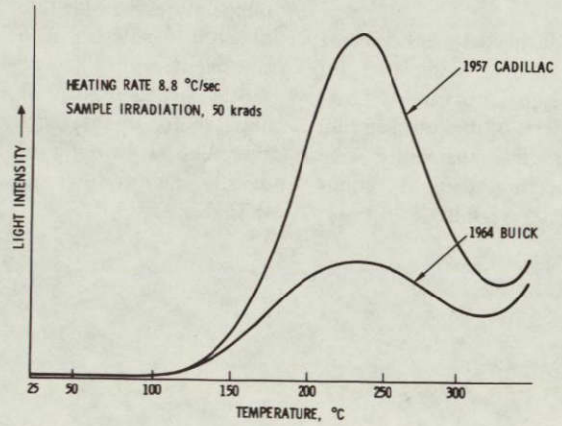


Figure 3. Relative Light Emitted by Two Samples of Glass from Turn-Signal Bulbs

RTOP 506-21-52
Solid Propellant Research
S. T. Peng*

## THERMOVISCOELASTICITY

Some further analysis of the general biaxial relaxation tests at room temperature for five SBR materials of varying crosslink density, $\nu_e$, has helped to generalize the conclusions reported in the last Research Council Review. In particular, the use of a reduced variable approach and the determination of a time-crosslinking shift factor, $a_X$, representing the effect of changing crosslink density allow the time dependency for this family of materials to be established over extremely long ranges of time. A normalized terminal relaxation function, $\phi_X$, has been established for 16 decades of log time (Fig. 1). The equilibrium moduli for all five crosslink densities determined from this curve are in good agreement with other results for SBR. Thus, the isothermal behavior of a whole family of elastomers can be predicted using a reduced relaxation shear modulus, $G_X(t/a_X)$, and reduced time, $t/a_X$.

A more recent test program of biaxial measurements on one of the SBR materials has been completed for temperatures ranging from room temperature to −45°C. As in the previous room temperature tests of the full spectrum of SBR compositions, strain and time separability were demonstrated. Moreover, the relaxation data at various temperatures produced time-temperature shift factors, $a_T$, that closely approximated the temperature dependence of the WLF equation (Fig. 2). This correlation together with the previous results means that the complete mechanical behavior of the gum SBR family can be represented by generalized reduced variables, the reduced modulus $G_X(T_O/T)$ where $T_O$ is a reference temperature, and the reduced time $t/a_X a_T$.

In addition, the 10-min isochronal Valanis-Landel $w'(\lambda)$ representation obtained from strip biaxial data at different temperatures could be normalized by dividing by the 10-min relaxation modulus, E(10) (Fig. 3). Similarly, the general applicability of a single functional form of $w(\lambda_i)$ for all SBR materials was strongly confirmed by a check plot of $\lambda_3 w'(\lambda_3)/2G$ vs $\lambda_3$ where the single curve obtained from strip biaxial data (in the thickness or $\lambda_3$-direction) at all temperatures was identical to that from the previous tests of all SBR materials at room temperature (Fig. 4). Similar agreement with this curve by the data, from both test series, for all degrees of biaxiality verifies the universal applicability of the functional form of W to the complete spectrum of behavior of SBR at all values of crosslink density, temperatures, degrees of biaxiality, and level of strain tested.

*Control and Energy Conversion Division, Energy and Materials Research Section

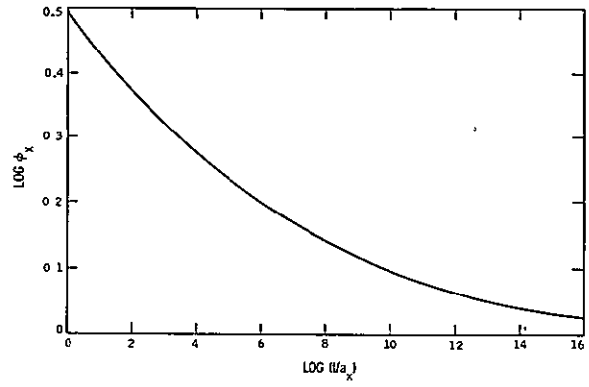


Figure 1. Normalized Terminal Relaxation Function vs Reduced Time

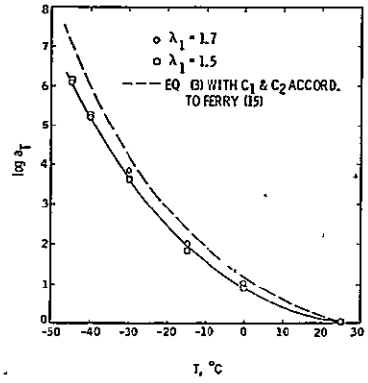


Figure 2. Temperature Dependence of the Shift

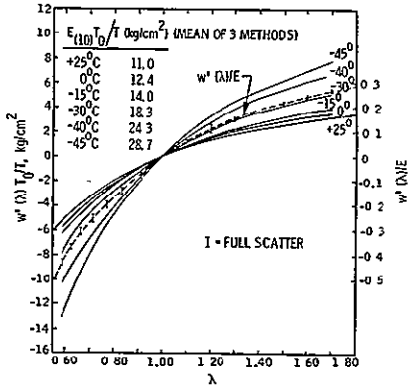


Figure 3. Normalization of w' (λ) $T_0/T$ vs Curves

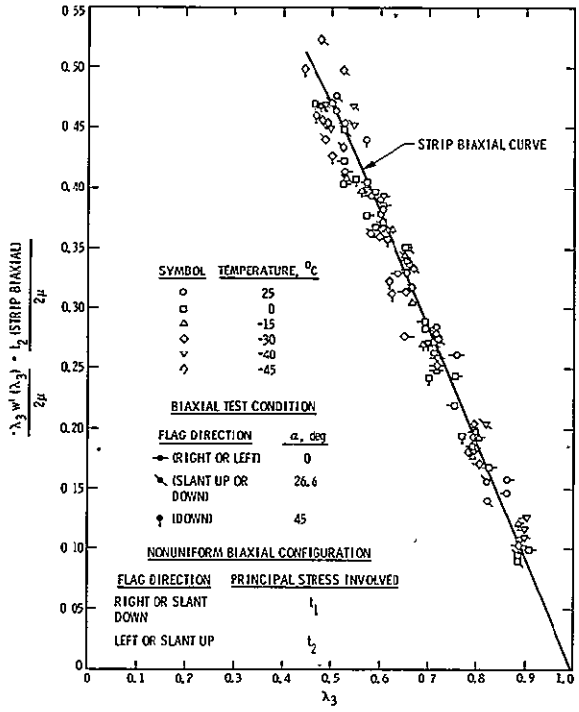


Figure 4. Confirmation of V-L w' (λ) Functional Form SBR Material

RTOP 506-16-17
Viscoelastic Properties of Polymers
J. Moacanin*

## LIFETIME OF ELASTOMERS UNDER LOAD

A general description of elastomer response in the stress-strain-time representation (i.e., "tensile property surface," Fig. 1) was completed. The time scaling parameter, $a_\phi$, for the effect of filler has been determined. Analysis of uniaxial tensile measurements performed on specially prepared styrene-butadiene rubber (SBR) elastomer formulations covering a range of carbon black loadings and crosslink density levels allowed separation of the filler contribution (Fig. 2). The effect on the scaling parameter depends exponentially on the reciprocal of the increase in modulus. The effect is reciprocal to that of crosslink density, where the effect depends directly on the increase in modulus viz., $a_X = (\nu_{ref}/\nu_e)^{-7.7}$. The effect of filler on modulus is given by two different equations (Fig. 2) which depend on the type of filler; in either case the quantity $\psi$ is determined by the filler volume fraction, $\phi$, a formulation parameter, and by the maximum possible volume fraction, $\phi_{max}$, a material parameter characteristic of the filler-rubber combination. Composite curves for the time-to-break, $t_b$, dependence on stress, $\sigma$, and strain, $\epsilon$, are shown in Fig. 3 (a) and (b). The data are experimental points for the above SBR formulations and the smooth curves represent the response for other elastomers studied previously, e.g., fluorosilicone, fluorocarbon, ethylene propylene, rubber, etc. These curves confirm that the shape of elastomer response is universal and that now the effect of filler can be predicted quantitatively.

*Control and Energy Conversion Division, Energy and Materials Research Section

COORDINATES:

$$\frac{\sigma}{\nu_e h(\phi) v_2^{1/3}} \frac{T_0}{T}, \epsilon, \text{ AND } \frac{t}{a_T a_x a_\phi a_c}$$

RELATIONSHIPS

| | $\sigma$ | $\epsilon$ | $t$ |
|---|---|---|---|
| TEMPERATURE | $T_o/T$ | 1 | $a_T$ |
| CROSSLINK DENSITY | $\nu_e$ | 1 | $a_x$ |
| FILLER | $h(\phi)$ | 1 | $a_\phi$ |
| PLASTICIZER (AND/OR SOL FRACTION) | $v_2^{1/3}$ | 1 | $a_c$ |

Figure 1. "Property Surface" is Universal in Normalized Coordinates

$$a_\phi = (E_\phi/E_0)^{-7.7}$$

$$E_\phi/E_0 = (1 + 1.25\psi)^2$$

WHERE

$$\psi = \begin{cases} \dfrac{\phi_{max}\phi}{\phi_{max} - \phi} & \text{REGULAR, NON-AGGREGATING PARTICLES} \\ \dfrac{\phi}{\phi_{max} - \phi} & \text{IRREGULAR PARTICLES} \end{cases}$$

Figure 2. Time-Scaling Parameter, $\alpha_\phi$ for Filler

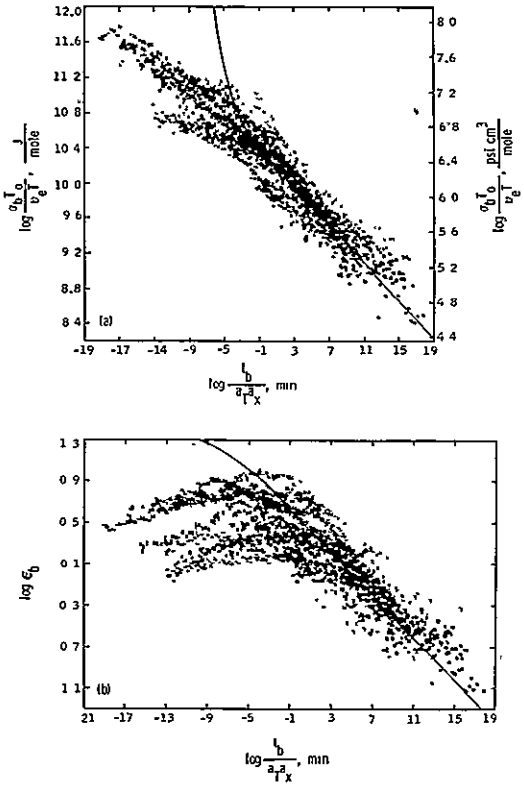


Figure 3. Ultimate Property Master Curves (a) Reduced Stress at Break vs Time to Break (b) Strain at Break vs Time to Break.

RTOP 506-15-25
Properties of Materials for Electronic Applications
F. J. Grunthaner*

## THIN MOS STRUCTURES

In the past few years there has been an unprecedented growth in the commercial microelectronics industry. One of the fastest growing technologies in this industry is that of large-scale integration (LSI) based on complementary metal-oxide-semiconductor (CMOS) devices. This technology is capable of amazing advances in the foreseeable future which could lead to radiation-hard microcircuits and ultra-high-density logic ($10^9$ bits per chip). Such advances would have a major impact on NASA missions.

The key components of these field-effect devices are the $Si/SiO_2$ interface, and the thin $SiO_2$ gate oxide. Chemical variations of device processing lead to large changes in the performance, reliability and lifetime of such devices, yet basic "bulk" methods of analysis are not adequate to monitor such variations. The recent development of surface analytical techniques now makes it possible to study and characterize this interface systematically. With such understanding it may be possible not only to predict but also improve reliability and lifetime.

Over the last five years, these surface techniques have seen rapid instrumental development in which JPL has actively participated. Our program is based upon the simultaneous application of surface analytical techniques and new electrical characterization procedures to the study of the $SiO_2/Si$ interface, and the defects present in thin $SiO_2$ oxide layers. This program enables us to directly correlate the electrical parameters of a device with the chemical and physical nature of this interface. The resulting observations will significantly accelerate the development of such thin oxide structures.

Modern surface analytical techniques offer chemical information in XPS or ESCA (x-ray photoelectron spectroscopy), spatial elemental distributions in SAM or AES (Auger electron spectroscopy), and elemental distributions as a function of depth in SIMS (secondary ion mass spectroscopy). These methods derive their information from the first 30 to 100 Å of material, and each has important data to offer the experimenter. The JPL Surface Analysis Laboratory (Fig. 1) has been designed to implement all of these techniques within the same UHV vacuum system and includes extensive facilities for the *in situ* preparation of $SiO_2/Si$ samples which consequently do not see laboratory contamination. This laboratory, by means of extensive JPL modifications, has the highest resolution x-ray photoelectron and Auger electron spectrometers known. The facility is completely computer-controlled and enables real time data reduction.

Our current program emphasizes the application of these methods to thin oxide structures (<60Å), while future efforts will increasingly employ depth profiling techniques to extend the region of characterization to include thick oxides (100 - 800 Å). The basic approach has been to study the chemistry of the interface by examination of this region through thin oxides up to 60 Å in thickness by XPS, which gives extensive chemical and elemental information.

To verify this approach, experiments were devised to determine the electron mean free path at these energies and in these structures. Typical values of this parameter are 10 - 20 Å, which give a maximum information depth of 30 - 60 Å. In our work, performed in collaboration with colleagues at the University of Hawaii, we determined the first extensive self-consistent data set characterizing this parameter by means of angular-dependent XPS. In Fig. 2, a set of three such spectra are given for a 15-Å $SiO_2$ film on silicon. When electrons are sampled normal to the surface, the underlying substrate is emphasized while, at glazing angles, the surface of the oxide dominates the spectrum. Here, we determined the mean free path (MFP) to be 37 ±4 Å in $SiO_2$ (one of the largest values yet recorded), and demonstrated the presence of several reduced oxide species in a transition zone at the interface. This MFP value gives a "study depth" of 110 to 150 Å.

In recent work, these experimental techniques have been used to characterize the effect of residual carbon contamination at the $SiO_2/Si$ interface on device performance. We had previously shown that organic material on the silicon substrate was not removed by industrial cleaning procedures. Figure 3 gives the silicon spectra of a highly cleaned (by new wet chemical techniques) substrate (lower insert) and the subsequent spectra of this sample after the growth of an approximately 60-Å oxide in the *in situ* facility. These samples were subsequently metallized in a low-temperature shadow-mask procedure, and surface state density $N_{SS}$ was determined in our automated electronic measurements system. Preliminary results are plotted in Fig. 4 for two different energies within the band gap. Three basic regions of behavior are observed in these unannealed 60-Å samples. The leakage currents in the MOS capacitor structure were below $10^{-13}$ A. These results are being prepared for publication.

This effort benefits from strong collaboration with colleagues at the University of Hawaii, Caltech, and M.I.T.

*Information Systems Division, Information Systems Research Section

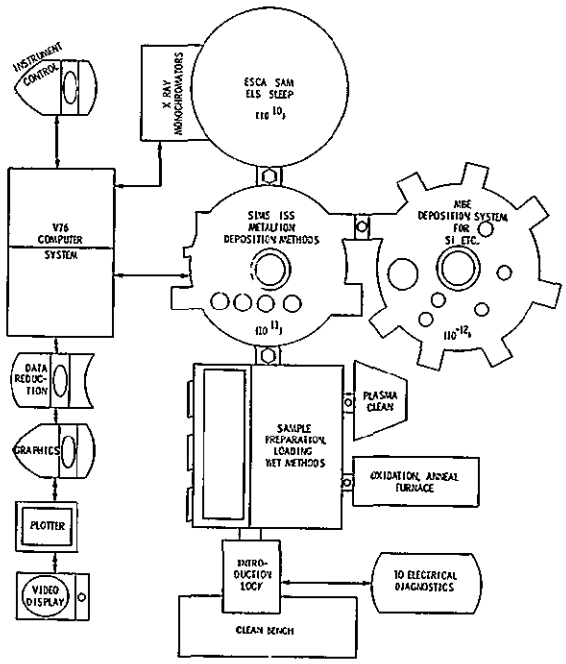


Figure 1. Capability Diagram of JPL Surface Analysis Facility

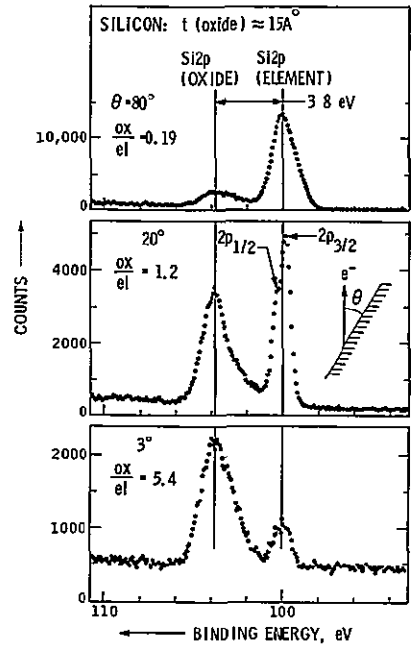


Figure 2. Angular Dependent X-ray Photoelectron Spectra of ~ 15-Å $SiO_2$ Film on Silicon

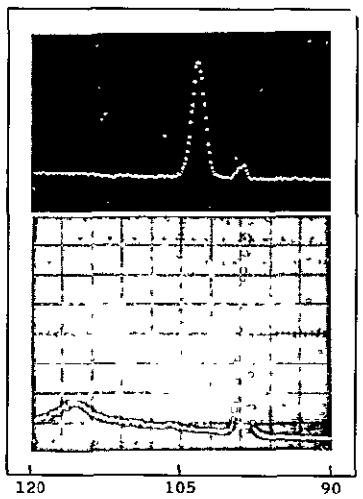


Figure 3. Silicon 2P XPS Spectra of Clean Substrate (Lower) and ~ 60-Å Thermal Oxide (Upper) Grown on the Same Substrate

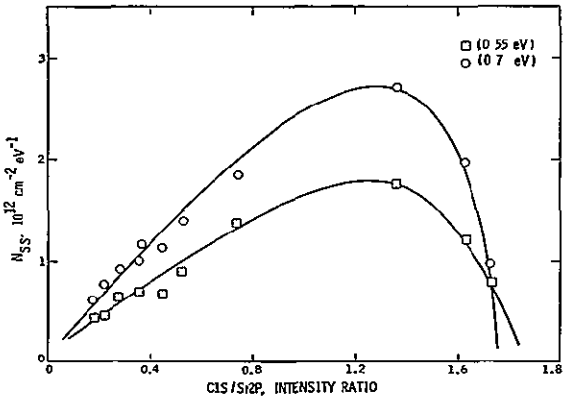


Figure 4. Plot of Measured Surface State Densities vs ClS/Si 2P Intensity Ratio

# Propulsion

RTOP 506-21-51
Liquid Propulsion Research
RTOP 506-21-52
Solid Propulsion Research

## CHEMICAL PROPULSION

R. F. Landel*

Environmental regulations require that nitrogen oxide emissions from aircraft be reduced by 1981. A concept for obtaining steady combustion at exceptionally lean fuel-to-air mixture ratio which has been conceived at JPL is currently being tested for applicability to gas turbine engines. Substantial progress has been demonstrated in that control of hydrocarbon, CO and $NO_x$ to within the desired target figure has been obtained over a substantial range of the gas turbine combustor operating range.

The apparatus to characterize combustion effects in liquid propellant rocket engine sprays, using a molecular beam sampler, has been completely redesigned and put into operation. True molecular beam signals have been obtained at combustion chamber pressures as high as 100-psig. Further refinements to improve the signal-to-noise ratio are being undertaken. The goal of this project is to characterize the effect of intense reactions in hypergolic propellant sprays on the mixing and efficient combustion in such engines.

A new concept in deriving power from the Venus atmosphere for missions to the surface of the planet is being researched. Carbon dioxide, which is the main constituent of the Venus atmosphere, is a relatively active reactant with light metals such as beryllium and lithium. The possibility of an electrochemical reaction to generate electric power as a primary battery is being tested under simulated Venusian surface conditions (470°C and pressures to 90 bars). Preliminary data leading to a prototype battery is being obtained. The project is significant in that if a high energy density primary battery is feasible, then a wide range of Venus surface probe missions can be contemplated as realistic options. Currently, surface probe activities are limited to thermal heatup period, hence are adequate only for short durations. With power for refrigeration of key electronic components, and for operating instruments and telemetry, longer duration missions are possible.



*Control and Energy Conversion Division, Energy and Materials Research Section

RTOP 506-21-51
Combustion Effects in Sprays
P. R. Ryason*

## MOLECULAR BEAM SAMPLING SYSTEM FOR ROCKET COMBUSTION CHAMBERS

To characterize the mixing processes in a liquid propellant rocket engine is the objective of this work. Rocket exhaust gas analyses are being performed by a molecular beam sampling device. A multiple orifice plate rocket exhaust end plate serves to isolate individual stream tubes in the rocket combustion chamber. Mass spectrometric analyses of individual stream tubes provide mixture ratios in each stream tube and the mass flux through each orifice. An extensive body of cold flow liquid jet impingement data exists. Various injector configurations have been characterized, and useful design guides have evolved from the nonreactive studies. When two reactive fluid jets impinge, however, new processes may occur such as gas generation at the interface, liquid mixture detonation, stream separation, etc. Reactive sprays are therefore likely to be different than nonreactive sprays. Mixture ratio data obtained by mass spectrometer sampling in this work will be correlated with cold flow data, and the mixing processes in reactive sprays characterized. This knowledge will advance the objective of injector design, eventually leading to a design methodology, to replace the current semi-empirical approaches requiring iterative alterations of real injectors.

During FY'76, a completely redesigned sampler was constructed and put into operation. This device generates a molecular beam of sampled gases for sample inlet pressures up to 100 psig. In operation, the existence of a beam signal is demonstrated by interposing a shutter in the molecular beam. The resulting decrease in signal is the signal due to the molecular beam. Compared to the previous apparatus, the current sampler differs in three important respects: improved first stage pumping speed (1600 cfm compared to 300 cfm); a decreased distance between sampling orifice and mass spectrometer (7.6 in. compared to 24 in.) and the molecular beam passes entirely through the third stage vacuum envelope, whereas in the previous device, all gas entering the third stage was pumped out through it. Some data have been obtained on rocket engine exhaust using this device. These indicate that mixing is better in the reactive case than the nonreactive case. However, a test of internal consistency reveals the data to be very imprecise (±24%, one relative standard deviation). This is inadequate for quantitative comparisons with the cold flow data. It is believed the poor precision is the result of obtaining beam signals as small differences between large signals; i.e., the beam signal is the difference in signal with the shutter open and the shutter closed.

Steps are being taken in FY'77 to convert the beam detection and measurement system from D.C. to A.C. Beam chopping and synchronous detection techniques will be used to discriminate against the nonbeam component of the signal. Since a relatively high D.C. beam signal (~9% of the total signal) is already available, the A.C. signal should be large, and will afford sufficiently precise results for comparison with cold flow data. A body of reactive flow data will be accumulated, and the quantitative comparison undertaken.

Molecular beam sampling of rocket engine exhaust is a goal of long standing in the liquid rocket engine research area. Both Air Force and NASA efforts date back many years. It is believed the current device solves the problems that have plagued this effort so long. The goals of quantitatively understanding liquid rocket engine combustion processes: physical (atomization and mixing), and chemical (reaction processes and incomplete combustion), can now be realized.

This technique can be extended to sampling other high pressure systems (e.g., flames, internal combustion engines, gas turbine engines, etc.). In principle, the design concept permits extension to very high pressure systems, requiring only that adequate pumping speed be provided.

*Control and Energy Conversion Division, Energy and Materials Research Section

RTOP 506-21-43
New Horizons in Propulsion
R. Kushida*
C. England*

# UTILIZATION OF PLANETARY ATMOSPHERE FOR POWER AND PROPULSION

A new concept for utilizing indigent planetary materials for power in Venus surface landers is being investigated. It is proposed that the Venus atmosphere, which is mostly carbon dioxide, be used in an electrochemical reaction with an on-board reactant such as beryllium, lithium, or aluminum to produce electrical power. The high ambient temperature at the planet's surface (470°C) means that fused salt electrolytes can be used which increases the power-density capability of this primary battery. The development of an efficient, lightweight power source for use on the Venus surface would make feasible a new range of lander probes.

The development of a new battery is desirable because currently available power sources either do not operate or operate with low efficiency at conditions found on the Venus surface. The radioactive thermoelectric generator, scheduled for use on the Mariner Jupiter/Saturn (MJS) spacecraft, requires heat rejection from a heat radiator at 300°C, hence, a design for Venus surface operation would call for considerably higher radiator temperature with a consequently lower electrical conversion efficiency. The radio-isotope thermoelectric generator (RTG) also has a relatively low power output per unit mass. Solar panels would be of doubtful value on the cloud-covered surface of Venus. Most storage batteries would not be operable at the ambient surface temperature, besides being relatively shortlived. The proposed battery would have capability for high energy density and high power output at high ambient pressures and temperature. Energy density is increased because only one reactant needs to be carried from Earth as payload. The power from the battery could be used to operate machinery such as scoops, augers, and rovers, as well as providing power for instruments and telemetry.

The concept is an outgrowth of previous studies on "New Horizons in Propulsion."

The battery uses a molten-salt electrolyte selected so that it has favorable conductive properties and is molten at the ambient Venus surface temperature. Mixtures of lithium and potassium chloride satisfy this condition. Beryllium reacts with carbon dioxide directly, so it is necessary to isolate the anode from contact either with the gas or with the $CO_2$ dissolved in the salt. Presumably the reactions occur with the carbonate ions in the following conjectured half-reactions at the metallic surface:

$$Be + CO_3^{=} \rightarrow Be\,CO_3 + 2e^-$$

and at the gas electrolyte interface

$$2e^- + 2CO_2 \rightarrow CO_3^{=} + CO\,.$$

The overall cell reaction is:

$$Be + 2CO_2 \rightarrow Be\,CO_3 + CO,$$

for which the theoretical cell voltage at a temperature of 470°C is 1.60 V. The effect of temperature on voltage is small (Fig. 1). The pressure does not affect the theoretical cell voltage since one mole of a gaseous product (CO) is discharged for each mole of $CO_2$ used. High pressure will favor the gas phase solution of $CO_2$ in the salt, and hence enable high current densities to be achieved at the gas electrode.

Preliminary experiments are being conducted to measure electromotive force and current in a molten salt electrolytic cell at elevated pressures (Fig. 2). Overall voltage of 0.92 V has been measured with an open circuit and 0.37 V with currents of 380 mA. The anode is a beryllium foil with an area of 2.5 $cm^2$. The gas electrode is a $CO_2$ bubbling tube wrapped in graphite felt and platinum lead wires. A bare platinum wire is used as a reference electrode. No change in voltage or current has been observed with changes in pressure from 1 to 5 bars. Experiments with a more refined design of the gas electrode and with better isolation of the beryllium from contact with dissolved $CO_2$ are in progress. Preliminary data are interpreted to indicate that high current densities are possible on the metal electrodes, but the limiting factor will be the design of the gas electrode, where effective reaction occurs only at a gas-liquid-solid interface.

Conceptual design of a prototype battery is in progress. Further research will be done to characterize the factors which limit current densities on the electrodes and useful life time of the battery.

*Control and Energy Conversion Division, Energy and Materials Research Section

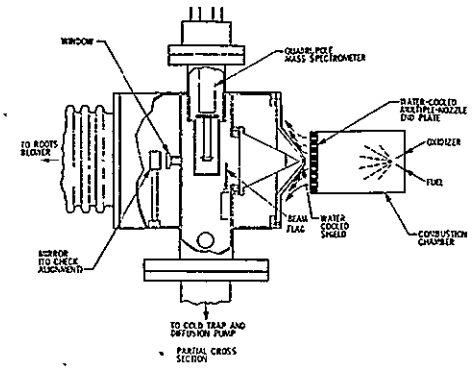


Figure 1. Molecular Beam Sampler and Rocket Engine

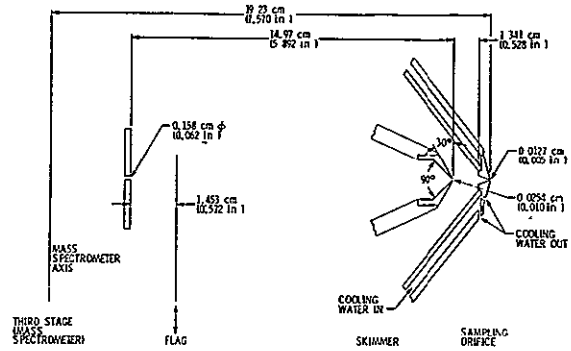


Figure 2. Geometry of Skimmer System

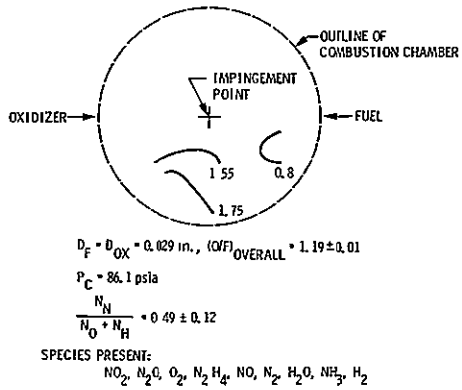


Figure 3. Preliminary Results O/F Ratio Contours

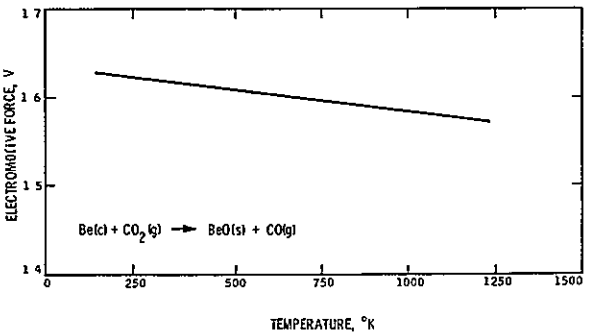


Figure 1. Theoretical EMF for a Beryllium Carbon Dioxide Cell

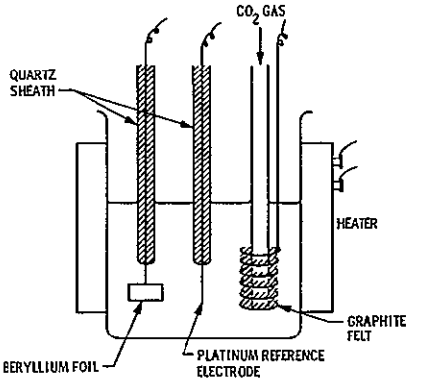


Figure 2. Schematic Diagram of the Beryllium Carbon Dioxide Cell

RTOP 506-21-32
Advanced Solid Propulsion and Pyrotechnic Concepts
K. Ramohalli*

## SOLID PROPELLANT COMBUSTION

The basic goals of this research program continue to be 1) to enhance our understanding of the fundamentals of the relationship between the interior ballistics and the physicochemical properties of the ingredients and 2) to apply our results to current problems of state-of-the-art technology. The applicability of fundamental research to immediate needs in complex situations is demonstrated.

The porous plate apparatus for scale modeling composite propellant combustion was extended to high pressure regimes. The response of the vapor phase combustion processes to pressure oscillations plays a key role in instability problems that frequently trouble motor development programs. The effect of vapor phase response is felt on the mass generation rate (through the heat transfer rate to the solid) via the flame standoff distance ($x^*$). The flame stand-off distance was measured at various flow rates of reactants (which correspond to various burning rates in an actual propellant) and pressures. Visual observations were made through quartz windows in the chamber and the flame stand-off distances were determined with photographic measurements. Over the range of pressures and flow rates in our experiments, the flame stand-off distance scaled linearly with the flow velocity and was independent of the chamber pressure. This "kinematic" scaling suggested that the vapor phase combustion processes were governed by geometrical factors and not by chemical kinetics. These observations suggested that the zone of importance to problems of solid propellant combustion (most of which are related to pressure effects in one form or another) is unlikely to be the vapor phase. The condensed phase processes are highlighted by these observations. Thus, the porous plate scale model that isolates the vapor phase processes answers an important question in solid propellant theory, design and performance. The quantitative results also yield numerical data for use in predicting propellant time-independent burning rate when the ingredients and pressure are specified. Thus would minimize, if not eliminate, costly trial and error methods of propellant formulation variations to achieve desired ballistic characteristics.

The microwave technique of measuring the dynamical combustion response of propellants was demonstrated by tests on the Space Shuttle booster candidate propellant. An oscillating pressure is imposed on a strand of propellant whose burning surface continuously reflects a microwave signal. By measuring the doppler phase shift between the incident and the reflected microwave, the instantaneous burning rate is determined. Since pressure is continuously measured, continuous determination is made of the response function (defined as the ratio of instantaneous burning rate fluctuation to the instantaneous pressure fluctuation, normalized by the mean values), the complex value of which dictates the instability tendencies of a propellant at that frequency and mean pressure. This technique works particularly well at the lower frequencies ($< 250$ Hz) which is also the region of great uncertainty in the conventional technique: The T-burner.

Some aspects of the unstable operation of rocket motors which depend purely on the fluid-mechanical details (without the influence of combustion) are studied in a cold flow apparatus with gas injection through a porous plate to simulate gas evolution from a burning propellant. The gains/losses of acoustic energy are quantitatively measured. The data from these simplified tests supply an important piece of information for use in calculations of rocket instability.

Actual technology problems were considered in the Space Shuttle separation motor program. To avoid problems associated with impingement on the main vehicle, it was required that the exhaust from the separation rockets be free of condensibles. This eliminated a major dampening of combustion oscillations inside these rockets. Stability was achieved by carefully balancing different oxidizer blends and a catalyst. However, instability was encountered in one of two static firings, both of which seemingly had the identical formulations. Careful examination of the ingredients showed one of the oxidizer distributions to be slightly different from the other. This work underscores the caution that needs to be exercised in quality control when working close to stability boundaries.

In future work the porous plate burner will be applied to oscillatory combustion and nitramine ingredients in propellants. Also, novel methods are being pursued to combat instability and heat transfer problems in solid rockets. Many of the results of this program have proved direct applicability to problems of fire safety.

*Control and Energy Conversion Division, Solid Propulsion and Environmental Systems Section

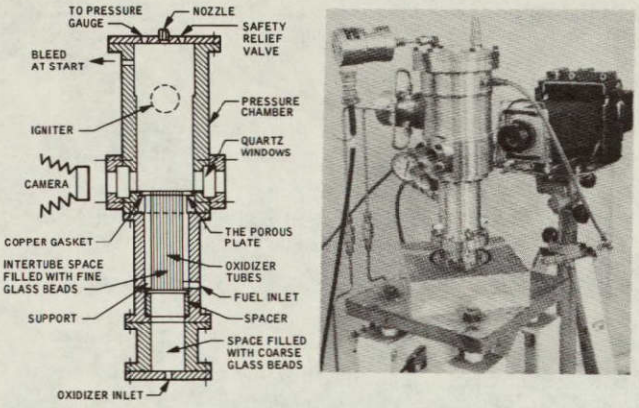


Figure 1. The Porous Plate Burner

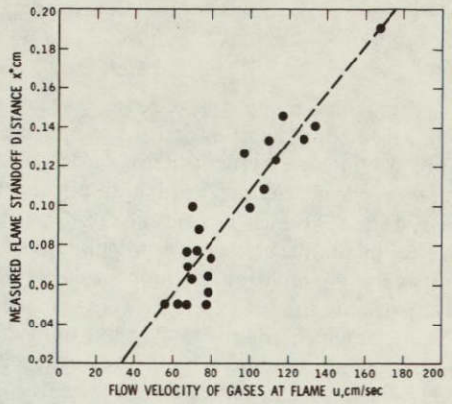


Figure 2. Flame Standoff Distance for all Pressures

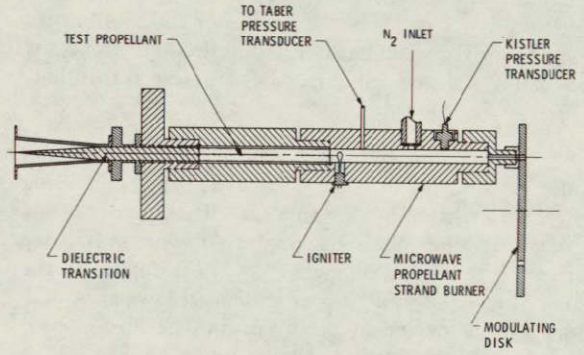


Figure 3. Variable-Frequency Oscillatory Regression Rate Burner

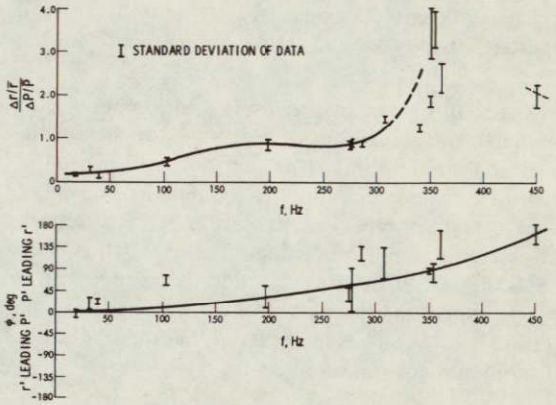


Figure 4. Combustion Response Function Test Results (Space Shuttle Booster Candidate Propellant)

RTOP 506-21-32
**Advanced Solid Propulsion and Pyrotechnic Concepts**
Ta-Jin Kuo*
Ki-Bong Kim**

## DETONATION PROPULSION

JPL's detonation propulsion program is aimed at carrying out a theoretical, experimental and computational effort toward developing a systems design capability that will produce dependable, durable and high performance propulsion systems. The high performance of detonation propulsion over conventional chemical propulsion in high pressure planetary atmospheres has been made manifest through theoretical studies and experiments, as summarized in Fig. 1. To better understand the gasdynamics of the blast wave propagation and its influence on the measured performance data, from which the criteria for the systems design are derived, we have started using an advanced hydrodynamic code to complement testing and the earlier simplified theoretical analysis. In the past year, this Eulerian code, DORF, was used for detailed computation of axisymmetric, finite-length conical nozzles with finite plug diameters. Results of this elaborate unsteady, inviscid computation further corroborate the previous findings.

The DORF program is well suited to compute multidimensional, two-component compressible flow fields with large flow distortions, which is our case, with a modest amount of computer time. Prior to computation, a mesh of Eulerian cylindrical cells fixed in space is defined, through which there is fluid convection. The calculation then proceeds in two steps: first the flow is computed in a Lagrangian sense, and then it is rezoned back to the original Eulerian grid. Artificial viscosity is introduced as a mechanism of shock front formation.

Figure 2 gives the time history of the computed specific impulse (using DORF) for a 10° half-angle cone with a thin disc of "detasheet" placed flat against the nozzle end wall. The ambient gas is $N_2$ at 69 bars. The experimental value of the specific impulse is about 280 sec, as vs the projected asymptotic value of the $I_{sp}$ transient at around 250 sec. This discrepancy, which is relatively small, can be partially attributed to a practical compromise between the grid resolution and computing time.

To account for the $I_{sp}$ undulation, Fig. 2(b) gives the pressure transient curves at 11.5 cm away from the end wall, about ¾ of the nozzle length. The agreement between the computed result and the pressure transducer measurement is excellent. At around 500 μsec the pressure there has dropped to around 30 bars, as a consequence of the overexpansion of the plume gas. This underpressure is the cause of the $I_{sp}$ dip in Fig. 2. Thereafter, compression waves arrive from the ambient gas and the local pressure begins to rise, resulting in the upward swing of the $I_{sp}$ curve. The $I_{sp}$ undulation is a direct consequence of the pressure field undulation over the nozzle wall.

Figure 3 shows the flow field evolution as computed in and around the same nozzle after the detonation. The shock heated ambient gas is represented by the shaded region, and the explosive product gas is represented by the crosshatched region. Transport mechanism is unaccounted for, as is evidenced by the existence of a clean contact surface throughout.

The shock still stays way inside the nozzle 35 μsec after the detonation, indicating that the thrust and $I_{sp}$ are still on the rise. At 453 μsec, when the shock front has passed the nozzle exit plane, and a weaker shock front is propagating backwards outside the nozzle, the plume has shot far out, implying an overexpansion within the nozzle is underway. At 974 μsec, the contact surface has receded deep into the nozzle, indicating that it has passed the first overexpansion stage, and is recovering or about to recover from the overexpansion effects. Reflections from the boundaries of the computer mesh are also seen at that time.

Progress has been made in setting up the shadowgraph optics for studying the flow field, as well as in optimizing the nozzle shape in an ambient atmosphere of low molecular weight. Such shadowgraph technique is being applied to verify the computed flow field outside of the nozzle. Figure 4 gives the sequential shadowgraphs of a firing plug detonated in the open air. The time interval between successive frames is approximately 7.5 μsec.

To continue acquiring elements for the formulation of design criteria, we intend to study the material response in FY'77, and to initiate computational and experimental studies on standoff firing, when the explosive is placed at a certain distance from the end wall, so as to evaluate the trade-off between system durability vs performance. We will also initiate testing in an $H_2$/He environment under elevated pressures to simulate the Jovian atmosphere, and carry out numerical and experimental studies in optimizing the nozzle configuration in an environment of low molecular weight. We also intend to compute cases when the ambient medium is not quiescent and to examine repetitive firing.

It has been possible to apply the computational portion of this research to other problems: recently the transient flow field generated by an air-launched rocket has been calculated successfully for the Air Force Rocket Propulsion Laboratory.

*Applied Mechanics Division, Thermophysics Section
**Control and Energy Conversion Division, Solid Propulsion and Environmental Systems Section

### References

Varsi, G., Back, L. H., and Dowler, W. L., "Development of Propulsion for High-Atmosphere-Pressure on Dense

Environments," JPL Quarterly Technical Review, Vol. 3, No. 2, July, 1973.

Back, L. H., and Varsi, G., "Detonation Propulsion for High Pressure Environments," AIAA Jour. Vol. 12, No. 8, pp. 1123 - 1130, Aug. 1974.

Varsi, G., Back, L. H., and Kim, K., "Blast Wave in a Nozzle for Propulsion Application," Acta Astronautica, Vol. 3, pp. 141 - 156, 1976.

Kim, K., and Johnson, W. E., "Exit of Blast Wave from a Conical Nozzle," AIAA Paper No. 76 - 401, 1976.

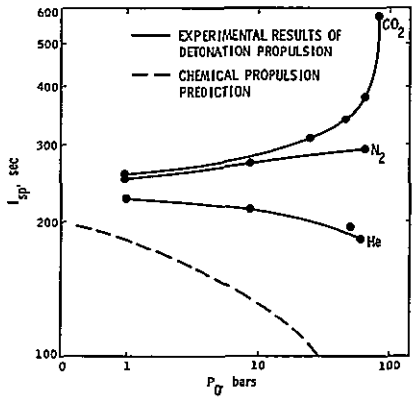


Figure 1. Background

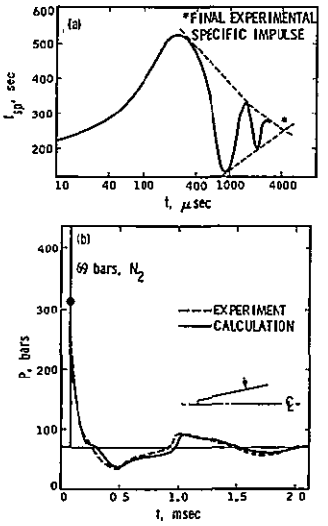


Figure 2. Transient Specific Impulse

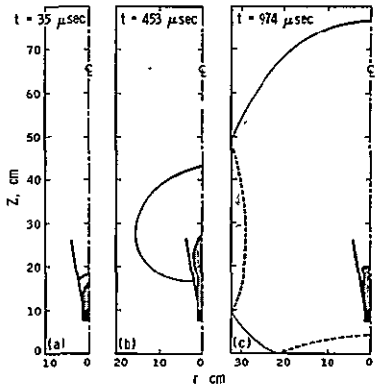


Figure 3. Flow Patterns at Three Different Times

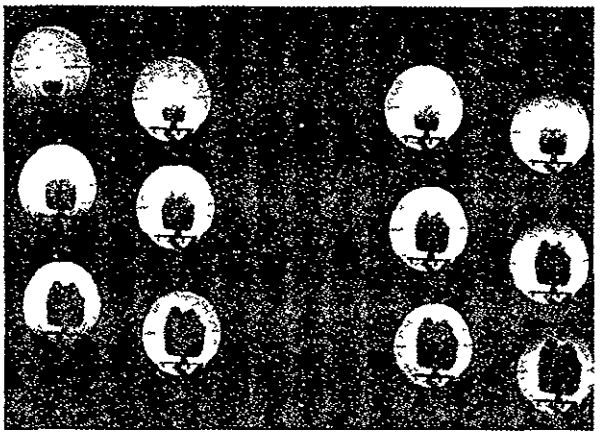

Figure 4. Shadowgraphs of a Firing Plug

RTOP 506-21-32
Advanced Solid Propulsion and Pyrotechnics Concepts
B. O. Stokes*

# MICROBIAL PRODUCTION OF PERCHLORATE

The projected increase in demand due to NASA's Space Shuttle Program will require a four- to five-fold increase in the present perchlorate production capacity. Today's methods for perchlorate synthesis involve electrolysis at energy costs as high as 7-9 kWh/lb of perchlorate produced. We are exploring a microbial method which offers cost and energy reduction potential for perchlorate synthesis. The goal is to develop an organism or system of organisms which would serve as the basis for an industrial process for perchlorate production.

The primary energy input in perchlorate production is the oxidation of $Cl^-$ to $Cl_2$ ($E^\circ$ = 1.36 V). The remainder of the oxidations are exergonic. Certain fungi are able to catalyze the oxidation of $Cl^-$ to $Cl_2$. The enzyme responsible (chloroperoxidase) has been isolated and characterized (Ref. 1). The enzyme appears to follow the mechanism shown in Fig. 1 and may be responsible for the occurrence of chlorine in antibiotics such as chlortetracycline, chloramphenicol, caldariomycin and griseofulvin. The key observation which suggests exploiting this system for commercial production of perchlorate is the fact that the enzyme can use chlorite instead of $H_2O_2$ and $Cl^-$ for the chlorination reaction (Ref. 2). This observation suggests that mutants which would produce chlorite should be readily obtainable under appropriate mutagenesis and selection conditions.

The microbial process for perchlorate production will occur in two steps which may or may not require separation. The first step is the oxidation of chloride to chlorite described above. The candidate organisms in this instance are those fungi possessing high chloride metabolism (Ref. 3). This group includes active cellulose degraders such as *trichoderma viride* and shows excellent potential for the utilization of organic wastes as a primary energy source for the oxidation of chloride ion. The second step is the oxidation of chlorite to chlorate or perchlorate. The observation that chlorate is an alternate substrate for the nitrate reductase enzyme (Ref. 4) suggests the approach of using nitrobacter organisms in the second step. These organisms grow by oxidizing nitrite to nitrate. Mutants able to oxidize chlorite to chlorate may be obtainable by relatively slight modification of the existing nitrite oxidizing system.

We are presently studying the effects of chlorite on fungi with high chlorine metabolism and on nitrobacter organisms. We will be mutagenizing these organisms with nitrosoguanidine and selecting for organisms which oxidize chlorite to chlorate or perchlorate. This will be followed by mutagenizing and selecting various fungi for the production of chlorite.

References

1. Morris, D. R., and Hager, L. P., Journal of Biological Chemistry 241, 1763, 1966.

2. Hollenberg, P. F., Rand-Meir, T., and Hager, L. P., J. Biol. Chem. 249, 5816, 1974.

3. Clutterbuck, P. W., Mukhopadhyay, S. L., Oxford, A. E., and Raistrick, H., Biochem. J., 34, 664, 1940.

4. MacGregor, C. H., and Schnaitman, C. A., J. Bacteriol. 108, 564, 1971.

5. Hagar, L. P., Thomas, J. A., and Morris, D. R., Biochemistry of the Phagocytic Process (ed. J. Schultz), North Holland Publishing Co., 1970.

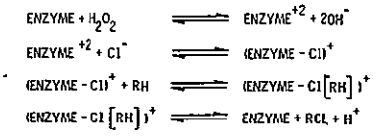


Figure 1. Mechanism of Chloroperoxidase

*Control and Energy Conversion Division, Solid Propulsion and Environmental Systems Section

RTOP 506-21-44
Generation and Storage of Activated Species
N. Jacobi*

## PHYSICAL PROPERTIES OF SUPERCONDUCTING TRANSITION-METAL HYDRIDES

To demonstrate the possibility of achieving high energy storage capability in metal hydrides for propulsion and other applications is the objective of research in this task. While the present task concentrates on superconducting transition-metal hydrides under moderate pressures, another task of Dr. J. S. Zmuidzinas, of JPL, is concerned with lighter hydrides and metallic hydrogen under very high pressures. The light hydrides are of particular interest, as rendering them metallic and perhaps superconducting under high pressure may prevent their reversion to their zero pressure form when the pressure is released ("superconductivity locking"). It is, therefore, natural to investigate in detail the mechanisms for superconductivity and other related physical properties in transition-metal hydrides ($PdH_x$, $PdD_x$, $TH_4H_{15}$) in which superconductivity has been observed under readily available pressures.

With this purpose in mind, extensive theoretical and experimental effort has been directed to explain the role of hydrogen location, ordering, mobility, and interactions with the host lattice, and correlating them with the observed physical properties in these systems, noticeably superconductivity. This activity will be briefly summarized under the following subgroups: (1) Electronic band structure calculations for PdH; (2) Phonon models and the superconductivity of PdH; (3) H-ordering related to specific heat and resistivity anomalies; (4) NMR measurements of thorium hydride.

1. Accurate band structure calculations have been performed for PdH by Prof. D. A. Papaconstantopoulos of George Mason University under subcontract from JPL. He has utilized his self-consistent scheme of augmented plane waves (SCF-APW), previously successfully applied to transition-metal carbides and nitrides, and has obtained a most reliable and widely quoted electronic band structure (Refs. 1 and 2). These results (Fig. 1) were combined with neutron scattering data and used in McMillan's theory of strong-coupling superconductivity. This scheme confirms that the superconductivity in PdH is mostly due to the optic phonon modes of the hydrogen atoms in the lattice. While these calculations were performed for the stoichiometric ratio, the concentration dependence of $T_c$ is of primary importance. $PdH_x$ becomes superconducting at $x \sim 0.8$, and $T_c$ increases monotonically with x. The calculations for the nonstoichiometric ratio are more elaborate, requiring the use of the coherent potential approximation (CPA), and will be undertaken in the coming FY.

2. While the work at George Mason University concentrates on the electronic aspects, an effort was undertaken at JPL to consider phonons in some detail. This was performed in close collaboration with Prof. L.-G. Caron, University of Sherbrooke, Quebec. We used a one-dimensional phonon model that reproduces the main features of the neutron scattering data. Combining these results with the electronic band structure obtained in George Mason University, we deviated from the conventional use of McMillan's theory, in which the contribution of optic phonon modes becomes somewhat ambiguous, and used an extended BCS-McMillan version, explicitly incorporating the relative role of acoustic and optic modes. We also reproduced the inverse isotope effect (Fig. 2) by varying the force constants from PdD to the stiffer PdH lattice. Best results are obtained when the Pd-D force constant is 11% smaller than that of Pd-H, while the D-D force constant is 18% smaller than that of H-H. Work is currently in progress on the concentration dependence of the electron-phonon coupling. Preliminary results indicate that when effective charges, consistent with the electronic band structure results, are included in a mean-field treatment, the variation of $T_c$ with hydrogen concentration is faithfully reproduced. This aspect of the problem is near completion, and will soon be prepared for publication. While the force constants, their isotopic dependence, and the Coulomb pseudopotential are empirically adjusted, a more basic approach will be undertaken in the coming FY to justify the values used so far.

3. Specific heat and resistivity anomalies occur in $\beta$-PdH at $T \sim 60$ K, which must be related to the hydrogen locations and possible phase changes or ordering processes. While a previous explanation (Ref. 3) in terms of hydrogen motion from octahedral to tetrahedral sites was disproved by recent neutron diffraction measurements, a more recent suggestion (Ref. 4) of formation of hydrogen clusters gave a poor fit to the experimental specific heat anomaly, both in shape and in magnitude. We have considered a two-level ("ordered" and "disordered") Schottky-type anomaly (Ref. 5), and find that this model agrees with experiment in magnitude far better than the previous explanations and without any adjustable parameters. However, the shape is not yet well reproduced (Fig. 3). The result suggests a possible ordering process taking place among the randomly occupied octahedral sites, and measurements of the resistivity anomaly just performed independently of our effort (Ref. 6) also suggest such an ordering process. The next step will be to apply a self-consistent version of the theory of order-disorder phase transitions in interstitial alloys to ordering processes in the hydrides.

4. Experimental NMR work was performed by Prof. R. W. Vaughan and his group, under subcontract to Caltech from JPL. They have completed an NMR study of low and high pressure samples of thorium hydride (Ref. 7), the other superconducting hydride, showing some very interesting features of the electronic spectrum and hydrogen mobility. Moment analysis of the line shapes confirms the proton locations suggested by earlier X-ray measurements of the thorium positions. A large change in activation energy for proton motion has been observed (Fig. 4)

*Earth and Space Sciences Division, Physics Section

between 350 and 390°K, implying more than a single mechanism for proton motion within thorium hydride. A noticeable temperature dependence of the line center position has been observed by multiple pulse techniques. This shift cannot be explained by either the chemical or the Knight shift, which are both smaller in magnitude and temperature independent, and reminiscent of a similar temperature-dependent line shift observed in A-15 structures.

## References


1. Papaconstantopoulos, D.A. and Klein, B. M., Phys. Rev. Lett. 35, 110, 1975.

2. Klein, B. M. and Papaconstantopoulos, D. A., J. Phys. F6, 1136, 1976.

3. Ferguson, G. A., Schindler, A. I., Tanaka, T., and Morita, T., Phys. Rev. 137, A483, 1965.

4. Brodowsky, H., Ber. Buns. Ges. Phys. Chem. 76, 740, 1972.

5. Jacobi, N. and Vaughan, R. W., Scripta Metallurg. 10, 437, 1976.

6. Ellis, T. E., private communication to N. Jacobi, Jet Propulsion Laboratory.

7. Lau, K. R., Vaughan, R. W., and Satterhwaite, C. B., Phys. Rev. B (in press).


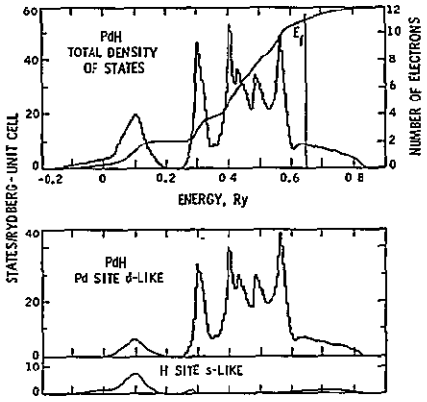


Figure 1. Total and Component Densities of States for PdH

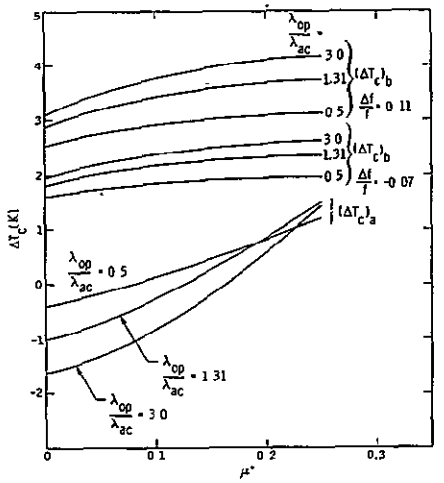


Figure 2. The Mass and Force Constant Components for the Inverse Isotope Effect in PdH/PdD

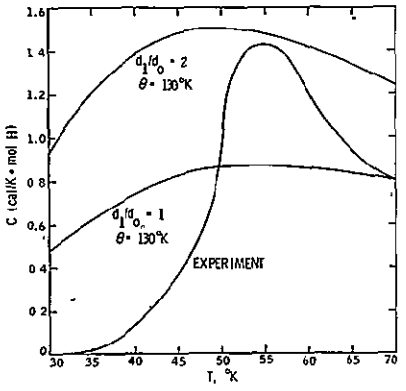


Figure 3. Comparison of Experimental and Calculated Specific Heat Anomaly in PdH

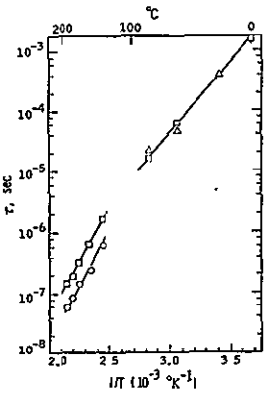


Figure 4. Estimated Correlation Times for Proton Motion as a Function of Inverse Temperature in $Th_4H_{15}$

RTOP 506-25-13
Basic Research in Advanced Energy Processes
P. F. Massier*

# BASIC RESEARCH IN ADVANCED ENERGY PROCESSES

It is anticipated that by 1990 with unmanned spacecraft, preliminary exploration of each of the planets will have been accomplished. For some planets, orbiters, entry probes and rudimentary landers probably will have been attempted; and some comets and asteroids also may have been encountered. There will be impetus to undertake more sophisticated missions within the solar system, to reduce trip time to the outer planets of the solar system, and to go beyond the planets into interstellar space.

The primary limitation to achieving these goals is propulsion technology. Propulsion historically has been one of the key pacing technologies in the advancements of space exploration, and it is evident that this condition also will be true in the foreseeable future. It is clear that investigation of advanced propulsion concepts is required now if these concepts are to be brought to a state of readiness for application when needed.

Current chemical propulsion systems being developed for the space programs are achieving close to the theoretical maximum attainable performance. The technology for solar electric propulsion is in the late stages of advanced development and the resultant systems are expected to find application well before 1990. These advanced technologies exhibit known limitations and will not be adequate for many of the more ambitious missions.

The concepts of concern to this study are those which have not yet been proven and are beyond the conventional approaches, but which hold the promise of significant performance improvements, and for which there exists some level of physical understanding to indicate that the concept is at least theoretically feasible.

Proposed concepts singled out for study:

(1) Studies pertaining to the production and storage of antimatter and the control of matter-antimatter annihilation will be continued. Production and storage will be investigated on contract by specialists in these areas.

(2) Methods of "tapping" energy available in space are being evaluated. An example is the interaction between a fluctuating magnetic field, which may be located in the vicinity of a planet, and an electrically conducting fluid in turbulent motion on board the spacecraft.

(3) Analyses will be made for propulsion and power using indigenous materials; for example, the materials contained in asteroids and small satellites of other planets.

(4) Efficient physical processes will be studied for converting energy from high-energy-density sources into electric energy and into directed kinetic energy of particles to produce thrust.

A matter-antimatter propulsion system has been conceived. It involves the storage of antihydrogen in an electric field, the transfer of antiprotons along magnetic field lines to an annihilation chamber, and the conversion of the annihilation energy into directed kinetic energy of hydrogen particles. A preliminary study of the concept was conducted by incorporating it in a vehicle which was assumed to weigh 20 tons. The mass of the antihydrogen was taken to be 1 gram with a hydrogen propellant mass of 10 tons. Results indicate that the average kinetic energy of the pions is 60% of the annihilation energy; thus 40% of the annihilation energy is lost by gamma radiation. Not all of the energy of the pions, however, is recoverable as directed kinetic energy of particles. The additional losses evaluated include: (1) collisions of the pions with the wall, which results in heating; (2) transmission of pions upstream, (3) momentum components perpendicular to the direction of thrust, and (4) energy of undirected neutrinos. As a consequence, 40% of the annihilation energy is finally available for utilization as directed kinetic energy of particles to produce thrust.

A comparison of the matter-antimatter propulsion system with chemical, solid core nuclear, fluid core nuclear, solar electric, and nuclear electric indicated that for given payload mass fractions, much larger velocity increments are achievable with the matter-antimatter system than with any of the others.

A method of converting high-density energy sources of electromagnetic radiation directly into electricity has been conceived. The concept is based on the principle of high-energy-photon absorption processes which convert most of the photon energy into kinetic energy of electrons or electron-like particles. The resultant high energy particles exchange a large fraction of their initial kinetic energy to atomic electrons producing an avalanche effect. The direction of the primary particles is predominantly in the same direction as that of the original photons. Thus with a thin absorber it may be possible to extract a substantial amount of the photon energy by the deceleration of high-energy electrons emerging from the back surface of the absorber. This electron flux is collected on a subsequent absorber which acquires a charge and therefore a potential which opposes the flow of electrons.

It has been demonstrated analytically that the energy associated with a fluctuating magnetic field in space can be transferred in the form of heat to a conducting turbulent fluid on board a spacecraft. The application of the concept in propulsion appears promising for flights in areas of relatively strong fluctuating magnetic fields such as, for

*Control and Energy Conversion Division, Energy and Materials Research Section

instance, those existing in the vicinity of Jupiter and other planets. The rate at which energy is gained by the conducting fluid in the form of heat during interaction with the fluctuating magnetic field is typically of the order of $10^2$ W when the rms value of the magnetic field is about 1 G. The concept becomes attractive in the case in which this energy is continuously collected and stored during prolonged flights in the areas of strong magnetic fields. For instance, the energy collected over a period of 24 hr at the rate of 120 W is equal to approximately $6 \times 10^5$ J.

The targets of this investigation are:

(1) Determine the possibility of increasing antiproton production rates, of producing antimatter in atomic and/or molecular forms, of storing antimatter and of controlling matter-antimatter annihilation rates as well as conceiving a matter-antimatter propulsion scheme by the end of FY'80.

(2) Determine the possibility of extracting energy from fields such as Alfven waves and fluctuating electric fields that may exist in space or in the vicinities of planets; and conceive a propulsion scheme utilizing such a concept for appropriate missions by the end of FY'80. Evaluate the potential application of the concept of the interaction between a fluctuating magnetic field and a turbulent electrically conducting fluid by the end of FY'80.

(3) Evaluate the possibilities of utilizing indigenous solid materials and planetary atmospheres for propulsion and power generation by the end of FY'79.

(4) Evaluate the possibility of converting photon energy directly to electrical energy by the end of FY'79.

The work done by University personnel and by specialists on contract consists of the following:

(1) Prof. Sandweiss, Yale University – Positron production, positron storage, utilization of $e^+ - e^-$ annihilation energy in propulsion systems and systems for the delivery of controlled amounts of positrons from storage to the annihilation chamber.

(2) Dr. David L. Morgan, Jr., Lawrence Livermore Radiation Laboratory – Utilization of positrons to provide auxiliary power generation, annihilation products, interaction of antimatter with matter surfaces.

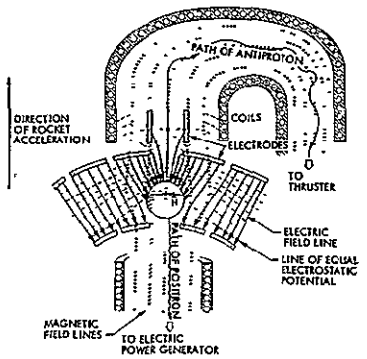


Figure 1. Transfer of Antimatter from Storage to Rocket Engine and Auxiliary Power Generator

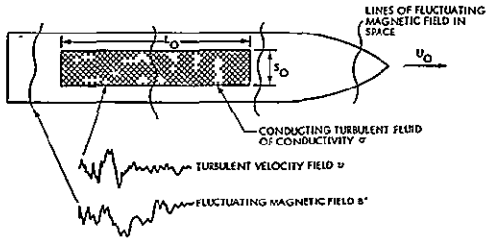


Figure 2. Concept of Turbulent Ionized Fluid on Board Spacecraft Moving Through Fluctuating Magnetic Field

- ESTABLISH COMPARATIVE MISSION ADVANTAGES DERIVED FROM THE REPLENISHMENT OF PROPELLANTS WITH EXTRATERRESTRIAL MATERIALS FROM SMALL BODIES IN THE SOLAR SYSTEM
- IDENTIFY METHODS OF USING THESE PROPELLANTS IN FLUID CORE REACTOR AND MPD THRUSTERS
- IF SIGNIFICANT MISSION ADVANTAGES OF INTEREST EXIST, DETERMINE REQUIREMENTS FOR PROCESSING THE MATERIAL

Figure 3. Indigenous Materials

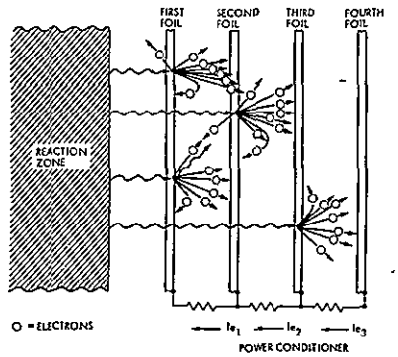


Figure 4. Photon to Electricity Conversion System

J. S. Zmuidzinas*

## METAL HYDRIDES AT HIGH PRESSURES

High-pressure phases of hydrogen, light elements, and light-element compounds, especially hydrides, are of great interest as fuels for space propulsion applications. When sufficiently highly compressed, every material, without exception, becomes metallic, if not already metallic at normal pressures. Considerable amounts of recoverable energy per unit mass could be stored in the metallic phases of light materials, should they prove to be metastable upon release of pressure, perhaps under favorable conditions (e.g., at low temperatures). The key issues of transition pressure to the metallic state, specific energy content, and metastability of a number of promising materials are being investigated in this research program.

In view of the contemporary limitations in achieving high pressures, it is desirable first to investigate materials with lowest possible metallization pressures. A study has been made (Ref. 1) of a number of low molecular weight materials to determine their metallization pressures and volumes, on the basis of the Herzfeld criterion (Ref. 2) and using available experimental data and extrapolations based on the Murnaghan Equation (Ref. 3). The results are summarized in Fig. 1 (Ref. 1). The main point to note is that lithium hydride, LiH, is predicted to metallize at about 1.1 Mbar with a molar volume estimated as 5.0 $cm^3$ $mole^{-1}$. The metallization pressure $P^*$ for LiH is seen to be much lower than for hydrogen ($H_2$). The value of $P^* \lesssim 10$ Mbar for $H_2$ is somewhat less reliable than that for LiH because the extrapolations involved occur over a larger range of pressures in the $H_2$ case. This is shown in Fig. 2 (Ref. 4).

In the light of these results, it appears that it should be much easier to produce metallic LiH than metallic hydrogen with the current high-pressure technology. Also, metallic LiH is of considerable interest from the viewpoint of metastability. It has been argued by Salpeter (Ref. 5) that metallic hydrogen would not be stable at one atmosphere, since protons would tunnel through the phase transition barrier. Because tunneling probabilities depend exponentially on mass, this transition path would effectively be eliminated for metallic H.

It is difficult to make reliable estimates of the specific energy storable in metallic LiH because the compressibility of this phase is presently unknown. In collaboration with Prof. J. R. Vaisnys, Yale University, and Prof. D. A. Papaconstantopoulos, George Mason University, calculations of various physical properties (e.g., electronic band structure, compressibility, superconductivity) of metallic LiH are in progress to further illuminate the basic questions of metastability and specific energy of this substance.

### References

1. Vaisnys, J. R., and Zmuidzinas, J. S., "Insulator-Metal Transitions of Low Molecular Weight Materials," to be submitted to Phys. Rev.

2. Herzfeld, K. F., Phys. Rev. 29, 701, 1927; J. Chem. Phys. 44, 429, 1966.

3. Murnaghan, F. D., Proc. N.A.S. 30, 244, 1944.

4. Vaisnys, J. R., and Zmuidzinas, J. S., "Formation of Metallic LiH," submitted to Phys. Rev. Lett.

5. Salpeter, E. E., Phys. Rev. Lett. 28, 560, 1972.

*Earth and Space Sciences Division, Physics Section

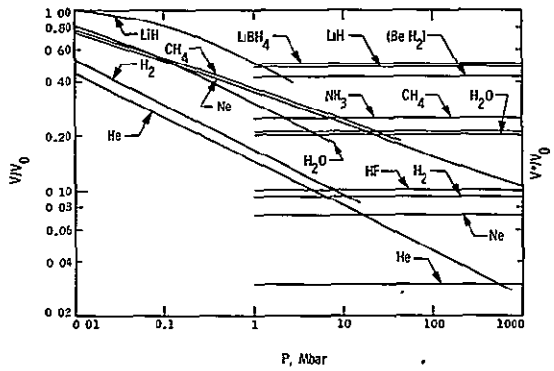


Figure 1. Metallization Pressures and Relative Volumes of a Number of Substances Given by the Intersections of (1) Curves ($V/V_0$) Based on Murnaghan Equation Extrapolations of Experimental Data and (2), Line Segments of a Number of Substances Showing the Predictions of the Herzfeld Criterion

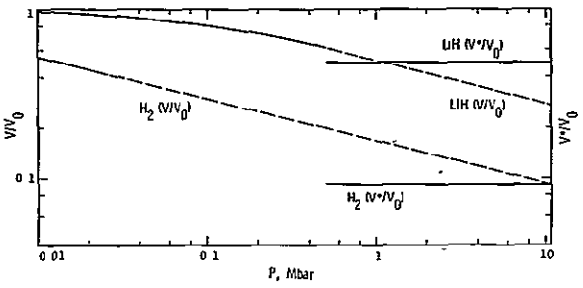


Figure 2. Solid Lines ($V/V_0$) are Experimental Data, Dashed Lines ($V/V_0$) are Extrapolation Based on Murnaghan Equation, and Solid Straight Lines ($V^*/V_0$) are Herzfeld Criterion Results

# Power

RTOP 506-23-46
Low Temperature Thermionic Converters
K. Shimada*

## LOW TEMPERATURE THERMIONIC CONVERTER RESEARCH

The long range objective of this research is to reduce barrier index from 2.0 eV to as low as 1.0 eV by reducing collector work functions and internal arc drops in a low temperature thermionic converter, so that the conversion efficiency would be as high as 35%.

However, recent system studies indicated that conversion efficiencies between 20 and 25% appear to be optimum for space nuclear electric propulsion applications since higher efficiency converters would require low heat rejection temperatures, thus an increased system weight. For terrestrial applications, however, higher efficiencies are still desirable because the reduction of fuel cost is of primary importance.

In FY'76 a polycrystalline silicon electrode achieved the work function of 1.05 eV after repeating several cesiation and oxygenation processes. It was found that the polycrystalline silicon electrodes are less susceptible to electrode processing for achieving low cesiated work functions. Above mentioned electrode research has been conducted with an extra clean test vehicle having a background pressure less than $10^{-9}$ torr. The primary method for work function determination is the photoelectron emission method. Thermionic emission method was used as an alternate. As it is shown in Fig. 1, very clean current saturation and an extremely small leakage current were achieved with this test vehicle. Interpretatons of such volt-ampere curves are shown in Fig. 2 as a square root of photo-electron yield versus photon energy. Intersection of the curve with abscissa determines the work function. As can be seen in Fig. 2, polycrystalline silicon electrode achieved work functions of 1.05 and 1.15 eV depending upon the activation process. In general, an increased number of cesiation-oxygenation cycles is required to achieve a lower work function. A class of metal-oxide electrode, Ta, $Ta_2O_5$, was also evaluated for its work function. The work function was 1.4 eV. Since this type electrode contains oxygen in the matrix, benefits of oxygen for reducing the work function would last longer than with electrodes having a relatively thin layer of oxide. The ability to dispense a desired amount of oxygen depends upon the chemical composition of, and the fraction of, metal oxide in the matrix.

Reduction of converter arc drop has been investigated with a converter that operates in a hybrid mode which is a combination of ignited and unignited mode. Cesium ions are mainly generated in the ignited region and those ions diffuse out to the unignited region to achieve space charge neutralization and arc drop suppression. The unignited region should not be collision dominated to minimize electron scattering. A test hybrid mode converter has a grooved molybdenum emitter and a molybdenum collector. The collector electrode is movable with respect to the emitter by means of a micrometer mechanism. An effective emission area of the emitter is 3.14 $cm^2$ (dia. = 2 cm) and parallel grooves, each of which is 0.05-cm wide and 0.05-cm deep, and are cut at 1-mm separation. These 1-mm-wide areas which are closest to the opposing collector, are thinly coated with rhenium metal. This coated area is to provide thermionic electron emission for power generation and the grooved region is to produce an efficient cesium ionization and to provide cesium ions to the unignited region. The hybrid mode converter has been operated with emitter temperatures up to 1500°K (Fig. 3). The minimum barrier index is 1.95 eV with an estimated arc drop smaller than 0.3 eV. The maximum power density is 1.2 $W/cm^2$. The calculated conversion efficiency is 9% at 1500°K emitter temperature. In FY'77, optimum geometrics for a hybrid converter will be determined and a test converter will be fabricated using a low work function collector. Candidate collectors include Nb, $NbO_2$ electrode and $Ba_3Sc_4O_9$ electrode, which will be evaluated separately in a demountable electrode test vehicle. The research goal for FY'77 is to achieve a barrier index of 1.7 eV so that the calculated conversion efficiency is 19% (Fig. 4). High temperature converter efficiencies and the projected converter efficiencies are also shown in Fig. 4.



*Control and Energy Conversion Division, Energy and Materials Research Section

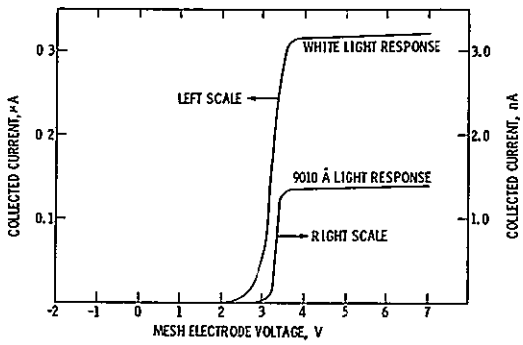


Figure 1. Photo Emission V-I Characteristics

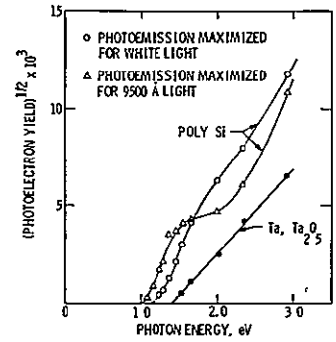


Figure 2. Photo-Electron Yield vs Photon Energy

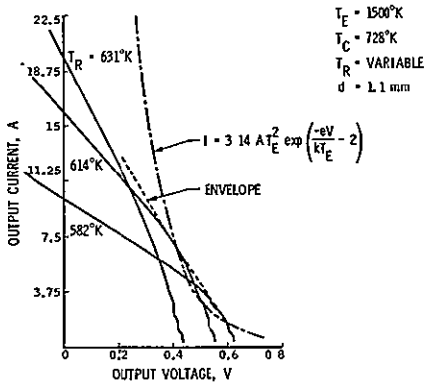


Figure 3. Hybrid Mode Converter V-I Characteristics

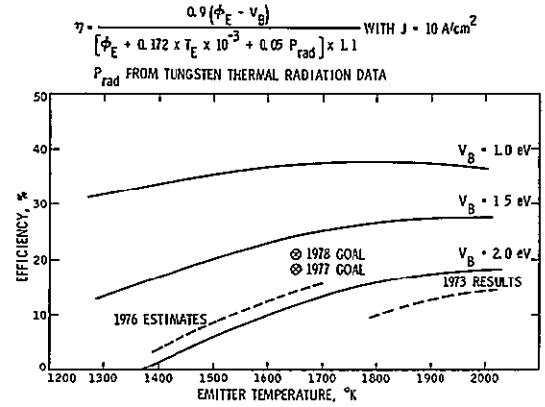


Figure 4. Conversion Efficiency vs Emitter Temperature

RTOP 506-15-25
Properties of Materials for Electronic Application
R. J. Stirn*

## HIGH EFFICIENCY METAL-OXIDE-SEMICONDUCTOR SOLAR CELLS

A research program to develop gallium arsenide (GaAs) Schottky barrier solar cells has been under way for several years. Such cells have promise for high efficiency, high radiation resistance, low cost fabrication, adaptability to thin film solar cells, and usefulness for both solar and laser energy conversion. An additional processing step – the growth of an interfacial oxide layer – was found to increase the open-circuit voltage ($V_{OC}$), and hence, efficiency by up to 60%. Consequently, maximum conversion efficiencies obtained to date have been about 30% for laser energy in the near IR and visible range, 15% for terrestrial sunlight, and 12-13% for space sunlight. The device has been called AMOS (Antireflection-Coated Metal-Oxide-Semiconductor) solar cell (Fig. 1).

Several oxidation techniques have been developed which will provide the necessary oxide thickness of 30 to 35 Å and chemical structure. In all cases there is an extreme sensitivity to the cleanliness of the chemicals used and the laboratory environment. GaAs will not oxidize in dry $O_2$ alone at temperatures below 400°C, but we have found that oxide growths are possible even at temperatures down to room temperature by the use of more reactive species of oxygen.

The highest value of $V_{OC}$ obtained so far with (100) GaAs has been with oxides formed at room temperature by passing water vapor-saturated $O_2$ over freshly etched GaAs. Figure 2 shows the ellipsometrically measured oxide thickness (t) and $V_{OC}$ as a function of exposure time. The relatively long exposure times are not desirable, however, for production rates. Much faster oxidation rates are obtained with ozone ($O_3$) passing over GaAs heated to about 120°C. With this method, 30 Å-thick oxides can be grown in 15-20 min. Even faster rates can be obtained with a RF-induced $O_2$ gas discharge. At room temperature with RF power under 10 W (the maximum available), suitable oxides would be grown in about 1 min. Anodic oxidations, both aqueous and non-aqueous, can also be very fast, but do not appear to be attractive for several reasons: (1) difficult thickness control since growth rates are sensitive to the degree of stirring, (2) difficult uniformity control, (3) high solubility of arsenic oxides in water leaving gallium oxide-rich layers, and (4) process complexity for large production rates.

Figure 3 shows some light current-voltage characteristics of oxidized AMOS solar cells. Unoxidized cells have values of $V_{OC}$ equal to 0.45 V. Curves 2 and 4 are of ozone and water vapor/$O_2$ growths on (100) surfaces, respectively. There is a strong crystallographic orientation effect as seen by curves 1 and 3, which are for ozone-generated oxide surfaces with (111) As-rich and Ga-rich orientations, respectively.

The curves shown are for cells with no antireflection (AR) coatings. The AR coating will increase the current output by 60%; however, the application of the coating by vacuum evaporation has been found to decrease the oxide-enhanced $V_{OC}$ by 100-150 mV. The effect appears due to migration of free metal atoms through oxide microcracks. The migration, induced by sample heating during the evaporation, apparently neutralizes charge within the interfacial states contributing to the enhanced voltage. Cooling the sample during evaporation reduces the effect pointing to a migration problem. A test system is being built by which AR coatings can be flash evaporated by means of a TEA-$CO_2$ laser. The apparatus should minimize sample heating, lead to highly stoichiometric dielectric layers, and allow for experiments with multiple-layer AR coatings for improved current outputs.

Studies using x-ray photoelectron spectroscopy (XPS) for chemical characterization indicate that a ratio of unity or less of arsenic oxide to gallium oxide gives the highest value of $V_{OC}$. Proportionately more arsenic in the +3 charge state, such as obtained with oxides grown by water vapor/$O_2$, also seems to lead to the highest values of $V_{OC}$. Figure 4 shows several XPS spectra in the region of the As 3d line. The higher energy peaks are due to oxides of As as indicated. The baseline cell spectra is that for a GaAs surface with the minimum native oxide of about 20 Å thickness.

The development of techniques to measure interface state densities and charge distribution in the ultra-thin oxides is a very desirable step for understanding the underlying physics, and to correlate with chemical information from XPS for optimizing the oxidation technique(s).

*Control and Energy Conversion Division, Energy and Materials Research Section

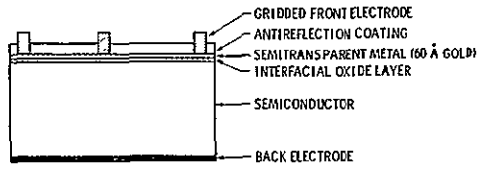


Figure 1. Physical Structure of AMOS Solar Cell

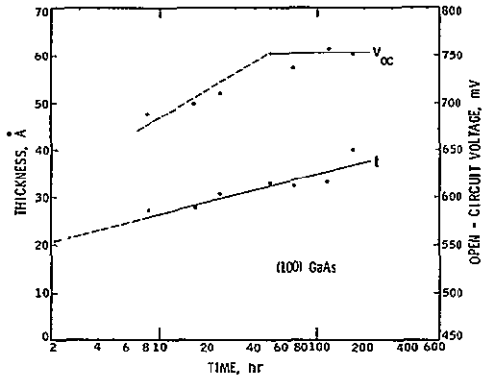


Figure 2. Dependence of $V_{OC}$ and Oxide Thickness on Exposure Time to Water Vapor/$O_2$

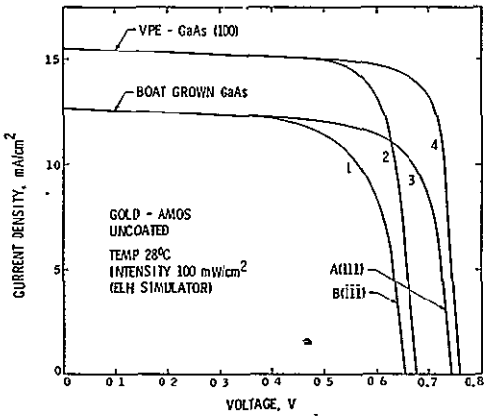


Figure 3. Light Current-Voltage Characteristics of AMOS Solar Cells

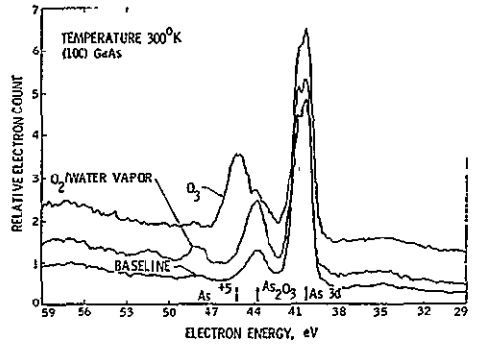


Figure 4. ESCA Scan of As Region for AMOS

RTOP 506-23-23
Electrochemical Energy Storage and Conversion
H. A. Frank*

# PULSE CHARGING OF ELECTROCHEMICAL CELLS

Prior reports in the literature indicate potential advantages of pulsed over direct current battery charging in terms of improved efficiency and charge acceptance as well as lower gassing and heat evolution. To this date there has however been no systematic study of the pulsed current charging process and no rigorous explanation offered as to why the process yields the above improvements.

The objective of this program is to obtain a fundamental understanding of pulsed battery charging with special emphasis on the nickel-cadmium battery. With such an understanding it will then be possible to identify the key pulsed current parameters (frequency, amplitude, and duty cycle) that influence cell performance. Further, with follow-on applied studies, it should then be possible to define the optimum types of pulsed currents for maximum cell performance.

Efforts performed consisted of charge acceptance, electrochemical and structural measurements during the course of pulse charging individual positive $Ni(OH)_2$/NiOOH electrodes and negative $Cd(OH)_2$/Cd electrodes.

In the case of the nickel electrode, it was found that the solid state mechanism describes the electrode reactions satisfactorily, with the rate controlling step being the proton transfer through a solid phase. This is in agreement with the findings of McArthur (J. Electrochem. Soc. 117, 442, 1970). The overall electrode reaction is represented by the following equation,

$$6(\mathrm{NiOOH} \cdot \tfrac{7}{6}\mathrm{H_2O} \cdot \tfrac{3}{8}\mathrm{KOH}) + 3\mathrm{H_2O} + 6e^- \underset{\text{Charge}}{\overset{\text{Discharge}}{\rightleftharpoons}} 3(\mathrm{Ni(OH)_2} \cdot \tfrac{2}{3}\mathrm{H_2O}) + \mathrm{Ni_3O_4} + \tfrac{9}{8}\mathrm{KOH} + 6\,\mathrm{H_2O} + 4\,\mathrm{OH^-},$$

and its mechanism is shown in Fig. 1. The effect of pulsed charging on the charge acceptance of the electrode is relatively small, which is because the rate controlling step is mass transfer of a proton through a solid phase and this is relatively insensitive to the mode of charging. In general, charge acceptance is found to increase slightly with increasing duty cycle and charging rate. At low duty cycles, self-discharge during the off period of the pulse is an important factor causing a decrease of charge acceptance. Pulse charging can affect the reaction kinetics which in turn can modify the structure and composition of the electrode as shown in Fig. 2. From the scanning electron microscope (SEM) pictures and performance data there was observed a tendency for formation of blisters at low duty cycles. The phenomena of low charge acceptance with blister formation has been reported in the literature by Chua (Ph.D. Thesis, Rensselaer Polytechnic Institute, Troy, New York, 1973).

In the case of the cadmium electrode, it was found that the solid state dissolution precipitation mechanism describes the electrode reactions satisfactorily, with the rate controlling step being $Cd^{++}$ transfer through both solid (CdO) and a liquid (electrode-solution interface) phases. Schematic representation of the reaction mechanism is shown in Fig. 3. The effect of pulsed charging on the charge acceptance is also relatively small. It is nevertheless more pronounced than that in the case of the Ni-electrode. This is because the reactions at the Cd-electrode have greater dependence on mass transfer through a liquid phase. This dependence also causes variations in the crystal size of the active material with duty cycle and charging rate as shown in Fig. 4. The formation of smaller crystals at faster charging rates improves the charge acceptance. This could be explained by the fact that at a solid-solid interface nucleation, rather than crystal growth, is the predominant factor for new phase formation under fast charging conditions (Ohara, M. and Reid, R. C., "Modeling Crystal Growth Rates from Solution," Prentice Hall, New Jersey, 1973). The kinetics of the reactions are also affected by pulsed charging. From SEM pictures and x-ray diffraction patterns, there is evidence for the formation of two different materials, in addition to Cd, on the electrode surface. One is identified as $Cd(OH)_2$, the amount of which seems to increase with decreasing duty cycle. The other compound which is amorphous in nature could not be identified by the x-ray diffraction technique. In addition, self-discharge becomes important for shorter duty cycles, causing a decrease of charge acceptance.

The performance of both Ni and Cd electrodes shows no dependence on frequency in the range of 50 to 200 Hz but some dependence on self-discharge, type of active material formed and, in the case of the Cd electrode, on crystal size of the active material. All of these factors are functions of pulse characteristics. Pulsed charging also causes a postponement in gas evolution. These findings have practical implications in charging Ni-Cd cells. For instance, by using a pulse of optimum characteristics, improvement in charge acceptance, shorter charging time, and power savings due to postponement of gas evolution can be achieved.

The experimental work on this investigation was completed in October 1976 and a final report will be issued in January 1977.

*Control and Energy Conversion Division, Electrical Power and Propulsion Section, Electrochemical Power Group, Columbia University Contract 953970, Principal Investigator: Prof. H. Y. Cheh

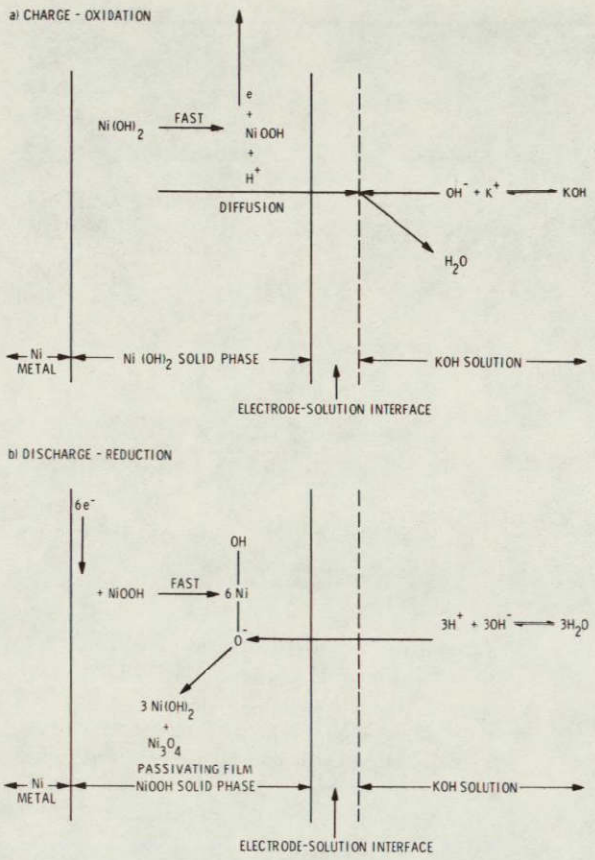


Figure 1. Mechanism of the Reactions Occurring at the Ni-Electrode

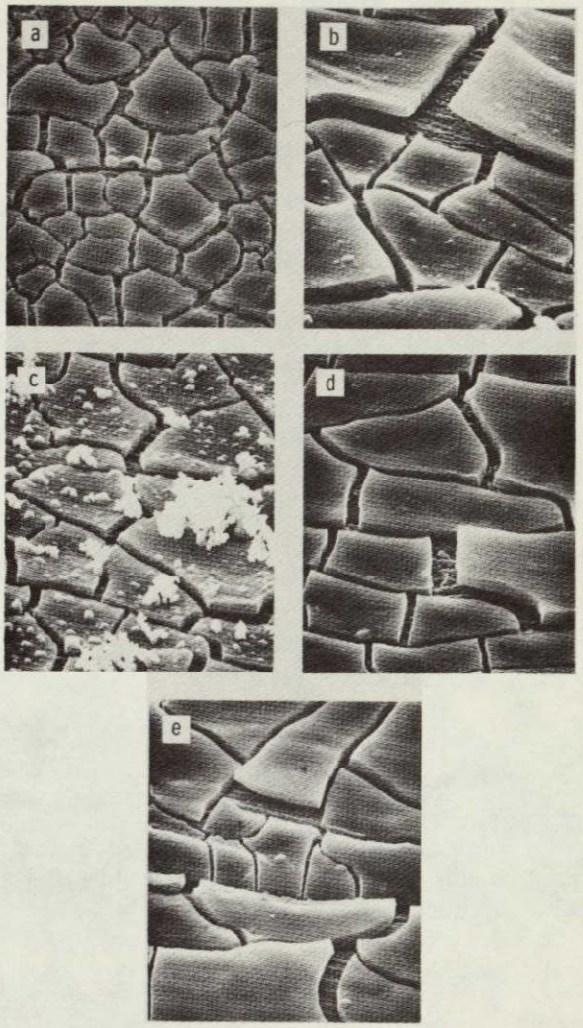


Figure 2. Scanning Electron Micrographs of Ni-Electrodes Charged Under D-C and Variety of P-C Conditions, Magnification of 3000 X. Charging Currents of: a) 5 mA D-C; b) and c) Instantaneous P-C of 5 mA, $\theta_1/\theta$ of 0.25 and Frequency of 50 Hz; d) Instantaneous P-C of 5 mA, $\theta_1/\theta$ of 0.50 and Frequency of 50 Hz, Dried in Air; e) Instantaneous P-C of 5 mA, $\theta_1/\theta$ of 0.5 and Frequency of 50 Hz, Dried in Vacuum

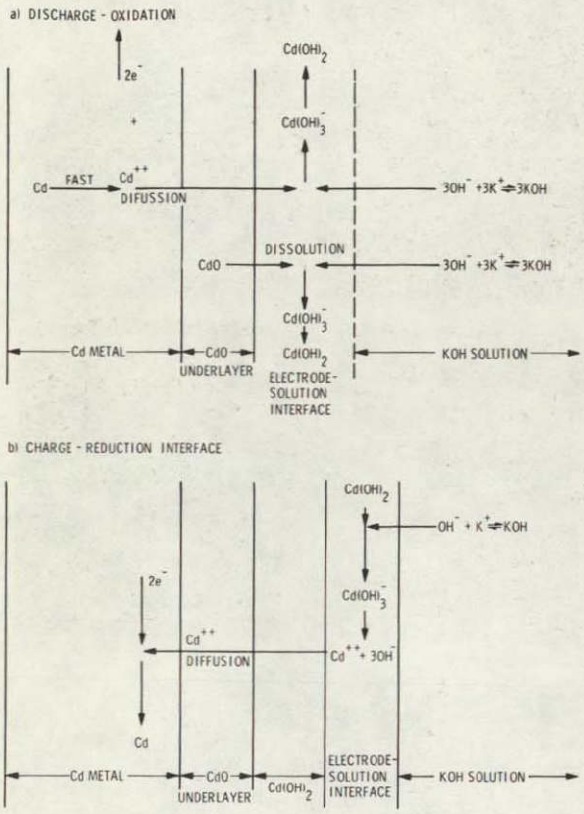


Figure 3. Mechanism of the Reactions Occurring at the Cd-Electrode

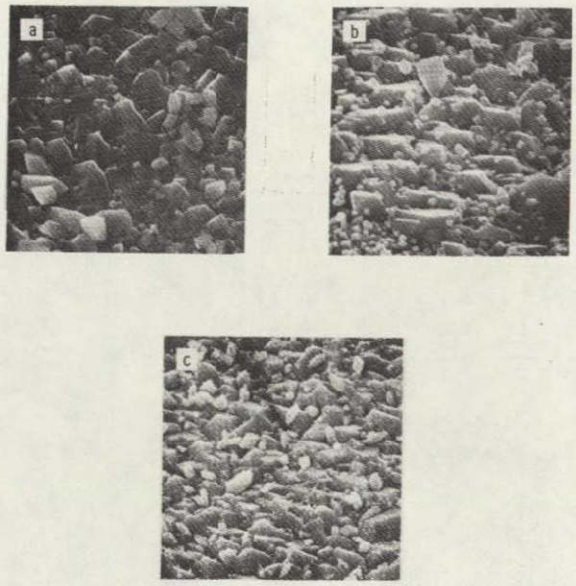


Figure 4. Scanning Electron Micrographs of Cd-Electrodes Charged Under D-C and Variety of P-C Conditions, Magnification of 10,000 X. Charging Currents of: a) 5 mA D-C; b) 5 mA Instantaneous P-C, 0.1 Duty Cycle and 50 Hz Frequency; c) 5 mA Instantaneous P-C, 0.25 Duty Cycle and 50 Hz Frequency.

# Guidance and Navigation

G. J. Bierman*

# TRIANGULAR FACTORIZATION ALGORITHMS FOR KALMAN FILTERING

Statistical estimation of linear discrete nonstationary systems is of major importance for navigation as well as other engineering and scientific disciplines. Kalman filtering methods which involve sequential processing of data are extremely well suited for real time digital computer implementation. There is a variety of theoretically (algebraically) equivalent algorithms which can be used for recursive estimation. These algorithms involve different amounts of computer storage, have different speeds of execution, and most importantly they are affected by numerical roundoff in different ways. Orbit determination problems using Earth-based radio data are especially sensitive to the effects of numerical roundoff errors. This motivated JPL navigation researchers to develop efficient and numerically accurate matrix factorization algorithms.

To illustrate the problems inherent in the existing state-of-the-art Kalman filter algorithm implementations and to demonstrate the value of our research we applied a variety of estimation algorithms to a typical orbit determination problem. The algorithms compared included the conventional and (Joseph) stabilized Kalman filter mechanizations, the Potter-Schmidt square root covariance filter and the Bierman-Thornton triangular factorization filter (which was developed, in the main, under RTOP 506-19-21). The algorithms involved here involve the U-D factors of the estimate error covariance; i.e., $P = UDU^T$ where U is an upper triangular matrix with unit diagonal elements and D is diagonal with nonnegative entries.

A portion of the forthcoming MJS'77 planetary tour, approaching Saturn, was chosen for the demonstration, and simulated radio data were generated. The various algorithms used these data and *a priori* nominal trajectory information to estimate the state of the spacecraft and other related parameters (19 in all). Spacecraft position and velocity mean square errors (actual minus estimated) for a sample simulated problem are shown in Figs. 1 and 2. Perusal of these results shows that the single precision factorization results are numerically reliable and give very accurate results. The simulations were carried out on a UNIVAC 1108 having 8-9 decimal digits of accuracy in single precision (SP) and 18 decimal digits in double precision (DP). The Kalman conventional and Joseph covariance formulated algorithms give markedly different single precision results; these differ by having errors which are orders of magnitude larger than their factorization counterparts. To show that the sample simulation results are not serendipitous, a statistical covariance analysis of the algorithms was performed. The results, shown in Figs. 3 and 4, confirm the sample simulation results.

The results of our numerical simulation studies, documented in JPL TM 33-771 and TM 33-798, show that the newly developed factorization algorithms are numerically reliable and accurate, require no additional storage, and are as fast as the conventional Kalman algorithm (which is generally considered to be the fastest, albeit numerically unstable, recursive estimater).

Although the Potter formulation SP algorithms give comparable results they require more than twice the storage and computation requirements of the U-D factorization formulations. Of all the filter algorithms available in the literature, the new U-D factorization algorithms seem to best satisfy the requirements of minimum storage and computation while retaining numerical integrity in the results.

The fast triangular estimation algorithms developed at JPL are of general utility. Applications of these algorithms, of which we are aware, include:

1. Onboard autonomous guidance and navigation.
2. Navigation for aircraft and marine users of the NAVSTAR Global Positioning System (GPS)
3. Precise navigation to support the SEASAT satellite experiments.

Because of the excellent computational performance of the U-D algorithms it has been suggested that they be used for all of the next generation NASA on-board satellite navigation work.

Current research relating to this area and needing further development includes:

1. More efficient U-D time propagation algorithms for real time problems.
2. Algorithms which better exploit model structure to reduce storage and increase speed of operation.
3. U-D algorithms for efficient and accurate post flight data processing.

References

1. Bierman, G. J., "Measurement Updating Using The U-D Factorization," Proc. 1975 Conf. Decision and Control, pp. 337-771, June 1975.
2. Thornton, C. L. and Bierman, G. J., Proc. 1975 Conf. Decision and Control, pp. 489-498, Dec. 1975.
3. Thornton, C. L. and Bierman, G. J., "Numerical Comparison of Discrete Kalman Filtering Algorithms: An Orbit Determination Case Study," JPL TM 33-771, June 1975.

*Systems Division, Navigation Systems Section

4. Thornton, C. L., "Triangular Covariance Factorization for Kalman Filtering," JPL TM 33-798, Oct. 1976.

5. Bierman, G. J., "A Comparison of Discrete Linear Filtering Algorithms," Trans. Aero. Elect. Sys. Vol. AES-9, No. 1, Jan. 1973.

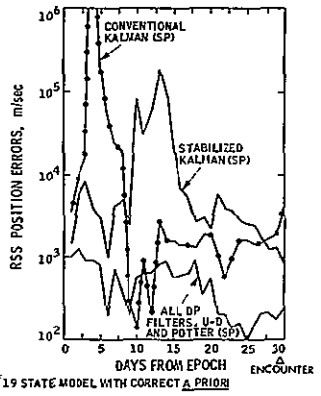


Figure 1. Comparison of Position Errors,* Single Simulation Result

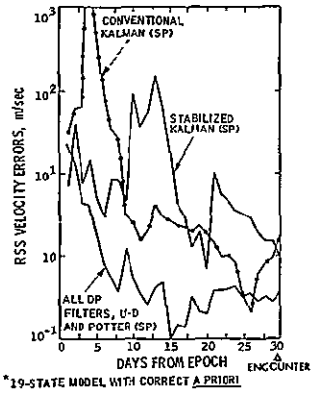


Figure 2. Comparison of Velocity Errors,* Single Simulation Result

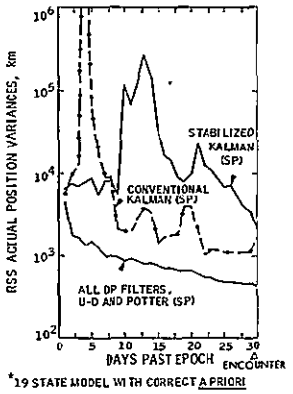


Figure 3. Comparison of Actual Position Uncertainties*

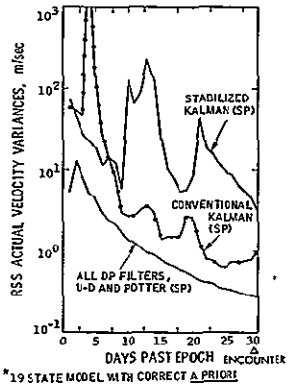


Figure 4. Comparison of Actual Velocity Uncertainties*

# Communication and Information Sciences

# ARTIFICIAL INTELLIGENCE FOR INTEGRATED ROBOT SYSTEMS

The long-range goal of the JPL Robotics Research Program is to develop methods whereby remote systems can carry out certain procedures autonomously that would otherwise require step-by-step human control. A prime candidate for the application of such methods is remote planetary surface exploration. Sending commands to a roving vehicle on Mars or a Jovian satellite, and verifying their execution over a communication link with a long time delay and a limited channel capacity, could yield unacceptably slow performance of many scientific and engineering tasks. If some of the control loops, especially those requiring the processing of images and the control of mechanical movement, could be closed by the remote machine itself, many missions could be conducted more efficiently and more of the communication channel could be devoted to the transmission of scientific information. Thus, one tangible and measurable benefit of the capabilities developed in this program would be an increase in the quantity and value of data returned from a remote spacecraft for a given mission duration or a given mission cost. The automation of many of the functions that are needed in a semi-autonomous roving vehicle presents many problems that are still unsolved.

A rover in a natural environment, outside a laboratory, must be able to perceive features of the environment that the designers could not specifically foresee; shapes, obstacles, barriers, objects, must be discovered in the sensed image and related to the commanded task, whether it be moving the vehicle safely to a designated location, manipulating objects for sample collection, or deploying a scientific instrument. The robot executive control program must be flexible enough to plan a response to a command that is sensitive to both the context of the command and the states of the environment and the robot. A simple example demanding flexibility is a request to the robot to pick something up when it is already grasping something. In addition, the robot executive must be able to monitor execution of plans, to be sensitive to the failure of individual steps and capable of correcting errors of execution. These are inevitable for either a machine or a human being in dealing with the real world. Methods for dealing with such errors in an automatic fashion have received scant attention. A related research problem is to endow the robot with the ability to learn the significance of previously unknown objects or situations from experience and to acquire motor skills. Only by adapting itself to novel environments can a robot be expected to succeed outside a laboratory.

The JPL research program, which was begun in FY'72, has developed a roving vehicle test bed as a tool for understanding and solving the problems just described. In FY'76 the roving vehicle (Fig. 1) was completely assembled and brought into operation. The significance of this achievement is that we now have in hand a complete working test bed vehicle/computer system which is being used actively to pursue the solutions to theoretical problems as well as many other practical engineering innovations that are of importance in achieving satisfactory robot performance. Among the latter is a special memory called RAPID which has speeded up the processing of TV images by an order of magnitude. New proximity sensors are now mounted on the manipulator to enable it to correct errors of placement. The path-planning software module described last year has been fully implemented and is in the process of being integrated into a complete vehicle-eye locomotion system. During FY'76 a new computer language called CSA was installed and brought into working order for research into error-correction and learning.

The emphasis in FY'77 will be to create a dynamic planning, error correction and learning capability and integrate it into the robot system. A parallel effort will be made to augment the perception programs that interpret the sensory input so that object identification (semantic image processing) can be made reliable and integrated into the learning system. Studies on employing micro-processors in the robot system will be undertaken and the display of status to permit control of the robot remotely will be studied. In conjunction with the research on automatic learning, program personnel are serving as technical monitors for a University of Maryland research project in natural language understanding. The principal investigator (C. J. Rieger) developed the CSA computer language we are employing for this project. The objective of the work is to permit a robot to communicate with a human operator at a higher level of "understanding," using English forms in both input and output.

Project personnel are also supporting and serving as advisors to a number of Caltech graduate students working on theses connected with robotics. A Ph.D. has already been granted to S. M. Udupa for a thesis entitled "Collision Detection and Avoidance in Computer-Controlled Manipulators."

The two papers following this overview amplify on two important aspects of the research program: the cognitive system, and automated perception.



*Information Systems Division, Information Systems Research Section

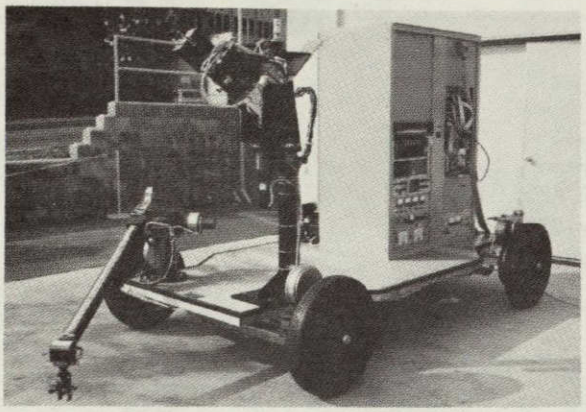

Figure 1. The JPL Robot

RTOP 506-19-32
Artificial Intelligence for Integrated Robot Systems
L. Friedman*

## RECOGNIZER: A COGNITIVE SYSTEM

### Planning

A host of engineering issues must be met in getting a robot to function successfully. Also, the robot requires cognitive capabilities to cope with an environment that is only partially known to the designer in advance. Such capabilities are now under development and will be integrated with the other robot systems during the coming year.

Increasingly, research on cognitive systems in artificial intelligence has come to focus on the proper representation of data as the crucial issue. One of the leaders in this research has been C. J. Rieger of the University of Maryland, who has been working on natural-language understanding of stories. As part of this effort he has invented a new high-level computer language that contains special representations of actions, states and state-changes, and the causal relations linking actions and states. One of the features of his language is a planning mechanism that automatically synthesizes plans to accomplish a commanded goal. The operation of the planner depends on the special representation forms linking actions to state-changes, provided proper preconditions are met. In addition, some pre-existing knowledge of the world has to be organized in appropriate "chunks" stored in memory. These representations are retrievable with action labels as cues, and the planner assembles them into a sequence of actions and intermediate goal states leading to the final desired state. An example of an input to the Robot Planner is a human command such as "Put the rock which is on the floor in the box." The planner translates this into a string of executable actions such as: *Move* the TV cameras to look at the rock; *analyze* the scene and locate the rock; *move* the manipulator fingers around the rock; *grasp* the rock; *move* the manipulator fingers to above the box; *ungrasp* the rock.

### Expectation Models

During the coming year a cognitive system called RECOGNIZER will be constructed using the concept of expectation models which will contain all known outcomes of a given action or sequence of actions. The outcome referred to is an interpretation of sensory inputs, or robot perception, resulting from an action. For example, after the robot has grasped an object successfully, the two touch sensors on its fingers would be "on". For each action about to be executed, RECOGNIZER will "sensitize" an appropriate set of outcomes while flagging the likely outcome as "expected". A monitor will compare the actual outcome with the expected outcome. If they are not the same, two subsystems of RECOGNIZER are activated. These are the Error-Correction and Learning Subsystems. Expectation models will not be limited to those directly concerned with primitive actions. An example is an environmental state such as "unsupported" which would be linked to a model of gravity. Another example is a completed mechanical assembly. This would not be predictable as a result of primitive actions such as *MOVE TO*, *GRASP*, and *UNGRASP*, but some notion of what the final assembly should be must be available for comparison to detect deviation and error.

### Error Correction

An outcome may be unexpected but not affect achieving the desired sub-goal state. If the sub-goal of the action was not achieved, a corrective procedure is necessary. For failure outcomes of specific robot actions that can be uniquely characterized by the robot's perception capacities, a corrective action can often be specified in advance. An example of such an error would be misplacing the hand in the act of grasping so that the tip of the left finger is touching the object to be grasped. An obvious correction is to move the hand left. It will be necessary to invoke goal-connected rather than action-connected concepts to provide more sophisticated corrective actions. For example, if the initial human command, which becomes the robot's goal, involved changing the location of an object, RECOGNIZER would "sensitize" the concept "unsupported" before planning actions. This is because one of the more likely failure modes during a change-of-location of an object is to drop it. This pattern would be triggered if, after the arm grasped and lifted an object above the floor, both touch sensors of the fingers went "off". Once triggered, RECOGNIZER would invoke a model of gravity to predict the location of a falling object. RECOGNIZER would sense the failed goal when it dropped the object. It would then find, as one of its preconditions for planning a recovery, that it needed to know the present location of the object. From the activated trigger pattern it would know that the gravity model would be appropriate to predict the present location of the dropped object.

There are times when correcting errors by characterizing the failure outcome is not possible. It may be necessary instead to find the reason for failure by analyzing the steps preceding the state in which failure was detected. This would involve retracing the steps of the plan in reverse order and checking for earlier failure. One technique of failure reason analysis would be to have models of failure outcomes available to provide sensing criteria normally too time-consuming to use. These could be applied during such an analysis to isolate an error and suggest a correction. An extremely simple example of the need for failure-reason analysis would be moving the fingers around an object to grasp it. If the arm missed completely there is no way to detect this at present, until actually trying to grasp and finding the touch sensors do not come on until the fingers

*Information Systems Division, Information Systems Research Section

are completely closed. The reason for failure would have to be found in the actions leading to the sensed grasp failure before specifying a corrective action.

### Learning

Detecting an unexpected outcome may call not only for correction, but also learning. The learning paradigm planned for implementation during FY'77 involves the operation of two decision nets interacting with each other. Both nets are activated by a planned action about to be executed. The first net makes semantic decisions about the nature of the object which is the target of the action (Fig. 1). The second net is the expectation-model net. Using information obtained from the semantic net, it chooses the expected outcome for performing the action and provides the list of other possible sensory outcomes. In addition it provides a decision about whether to execute or inhibit the planned action (Fig. 2).

The semantic net is organized according to abstract, higher-level knowledge about how the robot's world is categorized. For example, if the action is *grasp* object, the tests in the decision net would first ask about the size of the object, with a preference for hand size. We will base our sample decisions on the attributes "fragility" and "danger". We shall assume hypothetically that the robot can sense high temperature and that there are extremely hot (and therefore dangerous) objects in its environment. Initially, there is no knowledge stored in the net to point to "fragile" or "dangerous" terminations. Default answers always point to "manipulable object". The possibility for obtaining this knowledge lies in the organization of the expectation net. The expectation net is set up to sense the presence of the unusual states. (In this example, dangerous – hot, and fragile.) These states must be characterized by virtually unambiguous sensory signals to be of value. If they can be so characterized, as in our example, then the experience of encountering a very hot object can be detected by the monitor as discrepant from the expected. When this is done, the system can perform a reverse search of the expectation net starting from the actually experienced trigger. It can find the first node that is common to both the wrong decision path and the correct path. This node will point to the corresponding node (say, $N_2$ or $N_3$ in Fig. 1) in the semantic net where an incorrect decision was made. RECOGNIZER then asks the scene-analysis system to find attributes of the object grasped that differ from the attributes previously used to select the path to the node Ni. If such attributes (A, B, C) can be found, they can be inserted in the node-test in the form ["Does the object possess (A, B, C)?" If yes, then choose the path labeled "dangerous".] In this manner, meaningful knowledge, based on actual experience, can be incorporated.

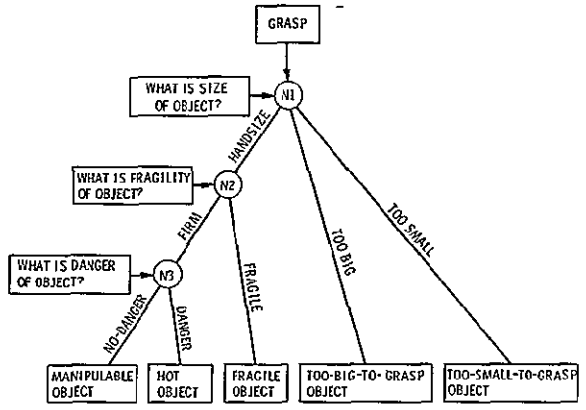


Figure 1. Semantic Net for Grasp

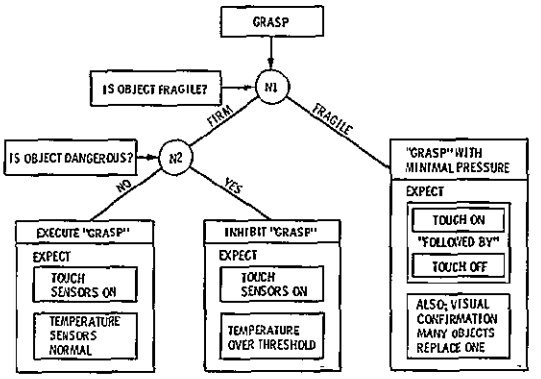


Figure 2. Expectation Net for Grasp

RTOP 506-18-23
Fiber Optics for Data Transmission and Processing
A. R. Johnston*

# FIBER OPTICS FOR DATA PROCESSING AND TRANSMISSION

Fiber optic data transmission will have applications in many areas, both in space and on the ground, because of resistance to electromagnetic interference (EMI) and crosstalk, size and weight advantages, and large bandwidth capability. Fibers can be used virtually anywhere that information must be transported. These technical advantages are important, but ultimately, it is the promise of lower cost that will determine where fiber links are used.

Two applications are presently being investigated and breadboarded in order to evaluate the capability of fiber optics. First, a paper study of a Shuttle payload bay closed-circuit television (CCTV) system has been made, and elements of the system will be breadboarded. Second, a breadboard-type demonstration of a TV link between buildings at JPL is planned. Other digital applications are being sought.

The research reported here is in support of the applications mentioned above.

The use of bit error rate (BER) data for evaluation of fiber optic electronic terminal modules was investigated and reported in Ref. 1. The interest in this topic stems from the probability of sealed terminal packages for digital links being available in the near future. Testing and evaluation of such components must be done from their digital terminals. It is possible to gain some information on internal parameters of the modules, as well as measuring overall link performance, by means of BER measurements. BER versus signal power plots, shown in Fig. 1, yield information on comparator threshold and receiver noise level, although it is difficult to separate basic noise from pickup or other parasitic effects. BER vs bit rate data, an example of which is given in Fig. 2, can measure amplifier bandpass, and detect ringing effects.

Our study of the Shuttle payload bay CCTV application (Ref. 2) indicates that large temperature excursions are likely. As a result, the effect of temperature on fiber transmission has been measured for a number of fiber types. For the pure fused silica plastic clad fibers which use a silicone compound for the cladding, transmission cuts off sharply below approximately −80°C, as shown in Fig. 3. We believe the cause is a temperature coefficient of the refractive index of the silicone compound much larger than the silica, resulting in a decrease in NA with decreasing temperature. Core and cladding index become equal at −80°C, cutting off waveguiding by the core. Further work will verify this assumption. On the other hand, chemical vapor deposited (CVD) doped fused silica shows no measurable temperature dependence of transmission, also shown in Fig. 3. We conclude that the plastic clad type, if the silicone compound is used, is not suitable for spacecraft application, but CVD types are quite satisfactory with regard to temperature. A different type of plastic clad fiber (Ref. 3), not using silicone has been tested also. This type has higher loss, but shows a linear temperature dependence of transmission, which is small enough to permit its use at even −150°C with an acceptable loss penalty.

A third type of data has been obtained, using the CVD (doped fused silica) type of fiber, related to transmission around bends in the fiber. Optical wave guiding, as is well known, is perturbed by curvature of the guide, resulting in light leakage. The leakage as a function of radius is an extremely sharp function, increasing rapidly at the critical radius. Figure 4 shows the results of our initial measurements, which are the first reported data of this type known to us. They indicate that no significant loss occurs until the radius of bending is very small, of the order of 1 mm, so bending radius in installation will not be a problem.

## References

1. Bergmann, L. A., and Johnston, A. R., "Bit Error Rate Measurement for Evaluation of a Fiber Optic Link," SPIE Symposium Proceeding on Fibers and Integrated Optics, Vol. 77, p. 78, Palos Verdes, CA., 1976.

2. Johnston, A. R., Katz, J., Donovan, M., and Yeh, C., "Fiber Optic Links for the Shuttle Orbiter CCTV System," Jan. 9, 1976, unpublished.

3. Dupont Corp., Wilmington, Del.

*Control and Energy Conversion Division, Guidance and Control Section

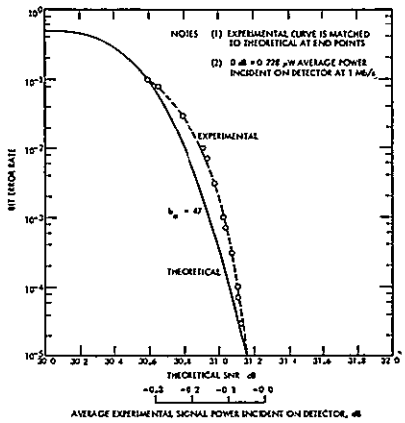


Figure 1. Bit Error Rate vs Signal Level of a Test Link

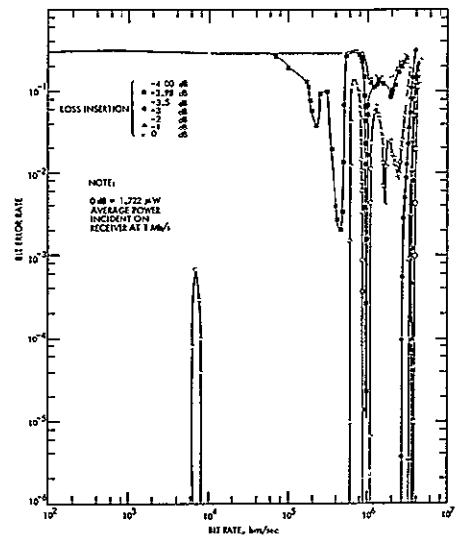


Figure 2. Bit Error Rate vs Bit Rate of a Test Link at a Fixed Optical Signal Level at the Receiver

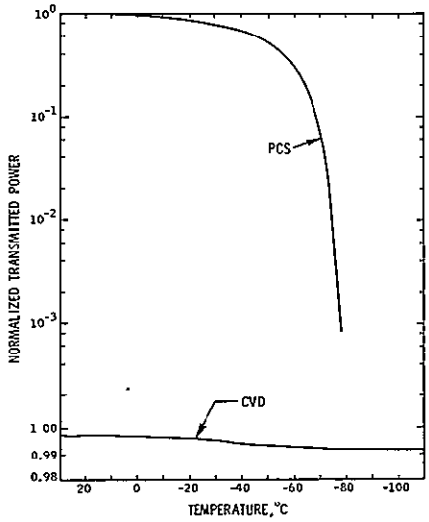


Figure 3. Transmission of Plastic Clad Fused Silica (PCS) Fiber and Doped Fused Silica (CVD) Fiber as a Function of Temperature

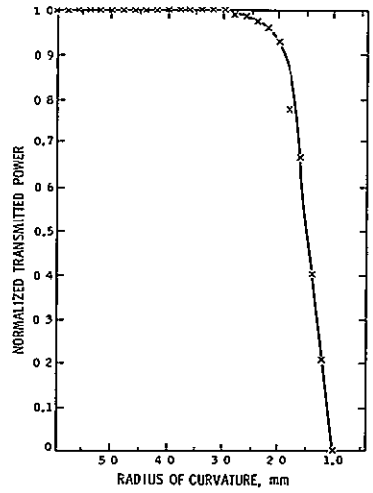


Figure 4. Transmission of CVD Step Index Fiber as a Function of Bending Radius

RTOP 506-19-32
Artificial Intelligence for Integrated Robot Systems
R. T. Cunningham*

## AUTOMATED PERCEPTION

The two major areas of vision research in FY'77 will be semantic interpretation of scenes and real-time object tracking as they apply to an integrated robot system. Semantic interpretation will be investigated specifically as it applies to the problems of object location and obstacle avoidance for manipulation and vehicle navigation. Our efforts in real-time object tracking will also be concerned with these tasks, but the results will generalize to many applications.

There are several implemented algorithms for segmenting a digitized TV image into regions based on grey-level data. The robot must be able to assign meaning to the regions in order to use visual information in decision making. Meaning is defined in the vision context as the assignment to a region of a label that is a useful parameter. An important task involving this capability is creating a terrain map for vehicle navigation. Meaningful labels in this case are "traversable" and "nontraversable" applied to definite regions of the map. Producing a terrain map is a problem in 3-D measurement; however, there is much information in a 2-D image which can be used to detect probable traversable and nontraversable regions. Obtaining precise 3-D measurements over a large area is very time-consuming. Establishing which regions are likely to be traversable first in the 2-D image, and then making 3-D measurements in these regions is a much more efficient map-making process, and this technique will be implemented.

The semantic interpretation of scenes employs an abstract model of the environment which specifies measurable or inferrable attributes of objects and the relationships between objects in a scene. Some examples are: large untextured regions at the top of an outdoor image may be sky, dark regions adjacent to bright regions may be shadows; regions of a certain size, shape, and texture may be rocks or mountain peaks. If the measured or inferred attributes agree with the model patterned relations, a label can be assigned.

In the case of navigation, the regions will fall into two classes – traversable and nontraversable – as mentioned before. Within these categories there may be several types of regions. In the case of nontraversable regions, there are obstacles such as large rocks, holes, overhangs, and areas where the slope is too steep for safe traversal. Another factor which will have to be analyzed is surface composition. The model should classify surfaces as sandy, icy, hard rock, etc., since these may also affect traversability.

Similar techniques will be applied to problems of manipulation. For this task, useful labeling categories are movable objects and obstacles to manipulation. In addition, during the assembly of complex objects, such as scientific experiment packages, labeling of component parts is indispensable.

In FY'77 we will address ourselves to two applications of real-time object tracking. The first is tracking the manipulator while it is performing a task. By tracking several points on the manipulator while it is in motion, the vision system will be able to provide trajectory correction feedback in real-time. This will reduce errors in manipulation as well as enhance error-recovery capabilities.

The second application is tracking landmark points in the terrain while the vehicle is moving. Landmark navigation is essential since dead-reckoning is subject to errors, primarily due to wheel slippage and gyro drift. The vehicle must have a reliable estimate of its position at all times to avoid obstacles and reach the desired goal location. By tracking several landmark points, the vehicle position can be updated while it is in motion, insuring a successful traversal to the goal.

In both cases, the major problem will be integrating the tracking software into the manipulator and vehicle control loops. This has to be done in a manner which allows a normal mode of operation while providing enough computer time for the tracking program to operate effectively. This will ultimately require several microprocessors operating in parallel, but preliminary results are achievable using the present minicomputer as the sole processor.

The tracking capability that we are developing is general in the sense that the system will respond to arbitrary grey level patterns in a digitized TV image. The system will be able to track a great variety of objects and will have the capability of deducing the signature of the object to be tracked at run-time. In the case of landmark navigation, the semantics program will be used to select the set of feature points to be tracked. Thus, the robot will have the capability of deciding what is "interesting" or relevant in the context of a given task, and establish tracking of those objects as needed. This may be contrasted with present systems which are preprogrammed to a specified signature in a limited domain; for example, optical tracking of bright objects such as rocket or jet exhausts.

*Earth and Space Sciences Division, Science Data Analysis Section

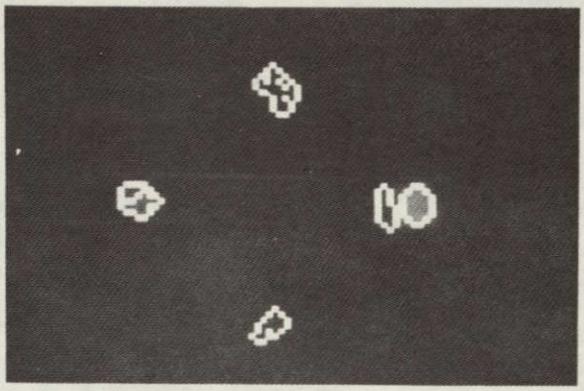

Figure 1. Rocks Are Outlined by Region Grower as Part of Object Location for Manipulator

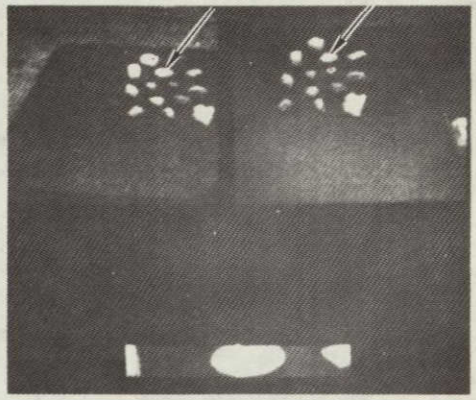

Figure 2. Arrows in Stereo Display Show Match Points in Left and Right Images Used for 3-D Measurement. Display at Bottom Shows Sampling Use by Stereo Correlation Program to Obtain the Match Points

# Physics and Chemistry

RTOP 506-25-31
Fundamental Photonics
G. R. Russell*

# HIGH ENERGY LASER RESEARCH

Research carried out during the last several years at JPL to determine the feasibility of developing efficient, high energy visible lasers has resulted currently in the development of continuously pulsed copper halide lasers with pulsing rates of 10-20 kHz, 1% efficiency, average laser power output in the range of 10-20 W, and with lifetimes of several hundred hours. Because visible lasers with this level of performance have several important applications (Earth and planetary remote sensing, sea water laser propagation, and isotope separation), research during the last year has been focussed on the determination of the laser characteristics and ultimate performance of copper halide lasers operating in this power range (10-20 W).

The first paper deals with the temporal measurement of the electron temperature in a double-pulsed copper chloride laser using microwave diagnostic techniques. The study was initiated to attempt to determine the reason for the decrease in laser performance of copper chloride lasers at lasant temperatures larger than the optimum (about 400°C). It was anticipated that beyond the optimum lasant temperature, inelastic and elastic losses as well as decreases in joule dissipation in the laser electrical discharge would cause a decrease in the electron temperature below that required for selective excitation of the upper laser level in the copper vapor. Surprisingly, the measurements showed that the electron temperature increased rapidly beyond the optimum lasant temperature. It was shown subsequently that Penning ionization of the copper by metastable buffer gases was the cause for the electron temperature increase and the resulting rapid ionization of the copper ground state which ultimately led to a decrease in laser performance.

Because the laser tube temperature and, therefore, the laser performance is a nonlinear function of the various operating parameters in continuously pulsed lasers, it was decided to conduct a parametric study of a continuously pulsed copper chloride laser to determine the effect of specific operating parameters on the laser performance. Emphasis is placed on the determination of the effect of copper chloride feed rate and laser electrode configuration. This study is currently being carried out. The results obtained to date are summarized in the second paper.

To date, the best performance has been attained with continuously pulsed copper bromide lasers, particularly with respect to reliability; 100 hr of operation have been completed with a laser operating routinely at the end of the test. In the third paper a summary is given of the design and performance of a copper bromide laser operated with an LC power supply utilizing a 3 to 1 step-up transformer. Currently, tests with copper bromide lasers have been extended to include the use of a Blumlein power supply (which does not require the use of a transformer and can attain higher laser discharge current rise times). In addition, a parametric study has been initiated to compare the operation of continuously pulsed copper chloride and bromide lasers. Upon the completion of these studies it will be possible to design optimum copper halide laser amplifier modules which can be used in series with a laser oscillator to extend the laser performance to 100-200 W of laser average power.

An oscillator-amplifier study of a double-pulsed laser was initiated to identify the crucial problems that would have to be solved in the development of a continuously pulsed laser amplifier chain. This work is described in the fourth paper. In this study, a comparison was made of the known characteristics of continuously pulsed lasers, such as pulse amplitude stability and pulse jitter, and the requirements for successful operation of a double pulsed oscillator-amplifier. It was shown that although continuously pulsed operation of a chain of amplifiers will be more difficult than a single double-pulsed oscillator-amplifier, no problems have arisen thus far that would preclude the development of an amplifier chain capable of producing an average laser power output of 100-200 W at pulsing rates of 10-20 kHz with an efficiency of 1%.



*Control and Energy Conversion Division, Energy and Materials Research Section

RTOP 506-25-31
Fundamental Photonics
C. J. Chen*

# MICROWAVE DIAGNOSTIC STUDY OF A COPPER CHLORIDE LASER

Previous experiments (Ref. 1) with CuCl lasers have indicated that there is an optimum tube temperature of about 400°C at which the laser power is at maximum. The reason for the power decrease at low temperatures is understood to be a lack of a sufficient number of copper atoms but the reason for the decrease at temperatures above 400°C is not understood. One speculated reason (Ref. 1) was that the electron temperatures ($T_e$) decrease, due to elastic and inelastic electron energy losses, as the CuCl density is increased. This experiment is designed to measure the electron temperature as a function of the laser tube temperature.

The technique used to determine $T_e$ is based on the measurement of the microwave range incoherent radiation emitted from a plasma (Refs. 2 and 3). The origin of this radiation is primarily free-free collision of electrons in the fields of ions and atoms and the radiation energy is related to the mean electron energy which, for a Maxwellian distribution of electron velocities, is defined by $T_e$.

The experimental apparatus consisted of a laser tube enclosed in a microwave cavity and the associated equipment to operate the laser and to measure a sample of the radiation emitted from the laser tube as a function of time after the laser pumping pulse. The equipment, microwave calibration techniques, and the measurement of the signal delay time of the electronic circuits are described in Ref. 4.

Figure 1 shows the typical time-dependent relation among the pumping current pulse, laser output, and $T_e$. The peak electron temperatures for pure helium and pure copper chloride vapor are shown in Figs. 2 and 3. The trend shown in Fig. 2 agrees with von Engels theory (Ref. 5). Deviations from this trend at very low gas pressures have been observed previously (Ref. 2) and also with pure copper chloride as shown in Fig. 3.

The maximum electron temperature as a function of the tube temperature for a mixture of CuCl and helium is shown in Fig. 4. It can be seen that at lower laser tube temperature, the descending portion of the electron temperature curve agrees in trend with von Engels' theory, while the ascending portion is contrary to theory. The curve exhibits a minimum electron temperature at a tube temperature of about 400°C. This is also the optimum tube temperature for maximum laser output for the present experimental arrangement. Similar data were obtained with pure neon and with mixtures of neon and CuCl vapor. Although the variations in $T_e$ were not as pronounced with neon as that shown in Figs. 2 and 4, the trends were the same. The minimum electron temperature for the neon-CuCl mixture also occurred at a tube temperature of about 400°C.

Comparison of Figs. 2-4 indicates that the increase in $T_e$ at higher tube temperature is due to the interactions of the buffer gas and the lasant and may be Penning ionization by metastable buffer gas atoms. This reaction may be represented by

$$He(2^1S,2^3S) + X \rightarrow He(^1S_0) + (X^+)^* + e \rightarrow He(^1S_0) + X^+ + e + \Delta E \qquad (1)$$

where X represents either a copper or a chlorine atom.

The excess energy, $\Delta E$, is transferred to the electron gas and causes an increase in $T_e$. Because the copper chloride density increases as the tube temperature is raised, the total excess energy released increases and accounts for the increase in $T_e$ shown by Fig. 4. At 500°C, Fig. 4 shows $T_e$ to be nearly 25 eV; at this electron energy level the copper atoms should be fully ionized. Thus, the depletion of the ground state copper atom density by ionization would account for the decrease in laser power at the higher tube temperatures.

References

1. Chen, C. J., Nerheim, N. M., and Russell, G. R., Appl. Phys. Lett. 23, 514, 1973.

2. Bekefi, G., and Brown, S. C., J. Appl. Phys. 32, 25, 1961.

3. Sugawara, M., and Gregory, B. C., Phys. Rev., 2, A439, 1970.

4. Sovero, E., Chen, C. J., and Culick, F. E. C., J. Appl. Phys. 47, 4538, 1976.

5. von Engel, A., and Steenbeck, M., Elestrische Gasentladungen, ihre physik and technik, Springer-Verlag, Berlin, Germany, Vol. 2, p. 86, 1932.

*Control and Energy Conversion Division, Energy Conversion Systems Section

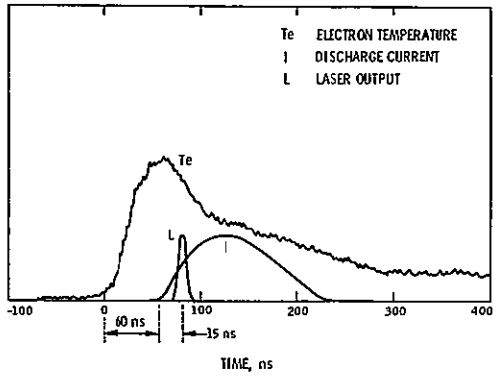


Figure 1. Typical Time-Dependent Relations

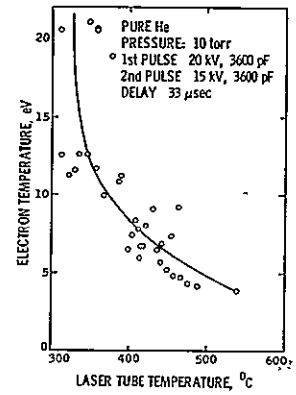


Figure 2. Electron Temperature (Pure He)

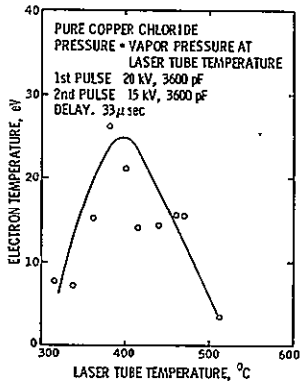


Figure 3. Electron Temperature (Pure CuCℓ)

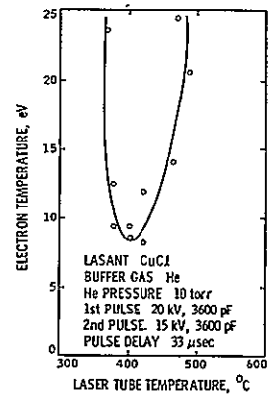


Figure 4. Electron Temperature (Mixture of CuCℓ and He)

RTOP 506-25-41
High Power Laser Systems
T. J. Pivirotto*

# PARAMETRIC STUDY OF A CONTINUOUSLY PULSED COPPER CHLORIDE LASER

There are two main objectives of this experimental effort: (a) to develop a cathode that will operate reliably with a lifetime of the order of 100 hr at pulse repetition rates between 10 and 30 kHz and peak pulse currents of the order of 100 A, and (b) to control and maintain the copper chloride vapor density in the laser tube in the range $10^{14}$ to $10^{16}$ $cm^{-3}$.

The experimental setup is shown schematically in Fig. 1. The laser tube is 150 cm long between electrodes and has a 2.5-cm inside diameter. The unique feature of this design is that the copper chloride is vaporized in a reservoir that is thermally isolated from the laser tube discharge. The vapor is carried to the laser tube with a controlled flow of neon and there diluted with a second flow of neon entering the laser tube at the anode. By varying the copper chloride melt temperature and the two neon flow rates, the vapor density in the laser tube can easily be varied between levels below which lasing will not occur and above which the discharge becomes unsteady. The pressure in the tube is controlled by a valve at the exhaust port of the laser tube.

The pulse power supply consists of an energy storage capacitor (variable between 0.002 and 0.050 $\mu$f in steps) LC charged from a high voltage D.C. power supply. The capacitor is discharged through the primary of a pulse transformer with an EG&G Hydrogen Thyratron which is controlled by a Velonex pulse generator. Lasing has been obtained at pulse repetition rates in the range 8 to 35 kHz.

To date two types of cathodes have been studied. The first is a commercial, dispenser-type, independently heated cathode in the form of a helix and made of porous tungsten filled with barium oxide. The second is a form of the self-heated, hollow cathode made from a length of 3-mm-diameter tantalum tubing. Neon is injected through this tubing into the laser tube. Plain tubes, tubes with a coating of $BaCO_3$ on the inside, and tubes with a cylinder of rolled tantalum foil coated with $BaCO_3$ and inserted into the tube end have been tried. Of these cathodes the last one mentioned operates more reliably than the others. It can be used continuously for several hours before the tip overheats and the tantalum begins to slowly vaporize. It is believed that the overheating is caused by a depletion of the barium oxide; hence a larger version of this cathode with a greater store of barium oxide will be tried in the future.

In the laser tube under study, the copper chloride is vaporized in a heated glass container separate from the laser tube and the copper chloride vapor is injected into the laser tube with a flow of neon. Of the three parameters that determine the vapor density in the laser tube the most important is the temperature of the copper chloride melt. A typical plot of the average power vs temperature is shown in Fig. 2.

It was found experimentally that lasing starts at a temperature of about 400°C. The average laser power rises smoothly and then peaks out at a temperature of approximately 480°C. Above about 480°C the average power begins to fall and above around 500°C the discharge becomes spatially unsteady and the average power becomes very unsteady.

The second parameter controlling the tube vapor density is the mass flow rate of neon which carries the vapor from the vaporizer to the laser tube. Figure 3 shows how the average laser power varies as this flow rate is varied. The degree of control of laser power and the ease of optimizing it by controlling the copper chloride vapor density is clearly indicated. When the copper chloride melt temperature is above about 480°C it is possible to increase the vapor density in the tube above its optimal value. This causes a reduced average power and discharge instability at high neon flow rates.

The third parameter is the diluent mass flow rate. Its effect on the average laser power is shown in Fig. 4. It is clear from Figs 2-4 that the vapor density and its replenishment rate can be independently controlled and optimized.

The maximum recorded performance to date for this laser tube is:

| | |
|---|---|
| Average pulse power | 28 kW |
| Average power | 12 W |
| Pulse energy | 700 $\mu$J |
| Capacitor efficiency | 0.47% |
| Pulse rate | 17 kHz |
| Gas pressure | 12 torr |

Future efforts will be devoted to improving the average power, efficiency and lifetime, and to studies of the effects of discharge circuit capacitance and inductance on performance.

*Control and Energy Conversion Division, Energy Conversion Systems Section

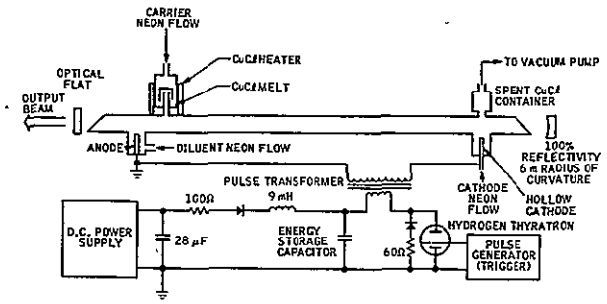


Figure 1. Schematic Diagram of Experimental Setup

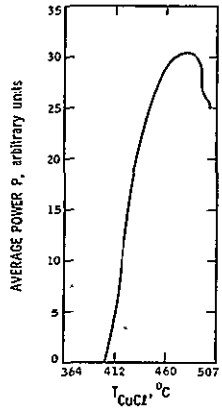


Figure 2. Effect of Copper Chloride Temperature on Average Power

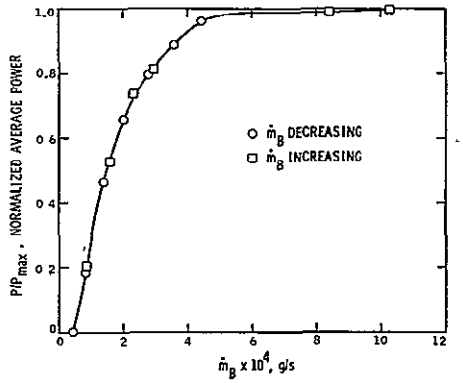


Figure 3. Effect of Neon Flow Through Copper Chloride Vaporizer

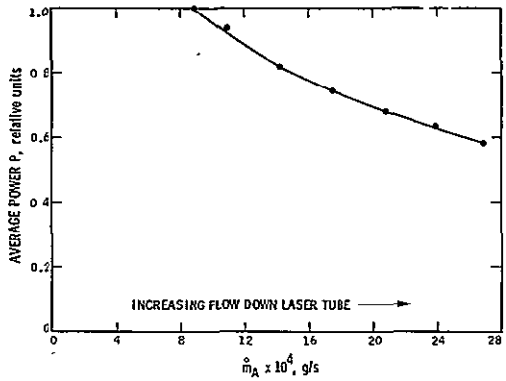


Figure 4. Effect of Diluent Flow Rate on Average Power

RTOP 506-25-31
Fundamental Photonics
G. R. Russell*

## COPPER BROMIDE LASER RESEARCH

During the last year, experimental work dealing with copper halide lasants has been extended to include copper bromide. Preliminary work carried out utilizing double-pulsed lasers indicates that the laser energy/pulse is the same as previously obtained in double-pulsed copper chloride lasers. However, the performance (efficiency, power output, reliability) of continuously pulsed copper bromide lasers is superior to copper chloride lasers.

A schematic diagram of the experimental setup of a copper bromide laser currently under investigation is shown in Fig. 1. The laser discharge tube is quartz, 2.5 cm in diameter having an electrode separation of 200 cm. The optical cavity consists of an optical flat and a 6-m radius of curvature, 5-cm mirror, dielectrically coated for maximum reflection at 510.6 nm. A heated receptacle containing copper bromide supplies copper bromide vapor to the discharge tube. A small bleed flow of neon at a pressure of from 80 to 100 torr, initiated upstream of the copper bromide receptacle, aids in maintaining a uniform distribution of copper bromide in the discharge tube, in addition to preventing the condensation of copper bromide on the discharge tube brewster windows. The discharge tube copper bromide vapor pressure is controlled by means of separate heaters for the tube and copper bromide receptacle. The electrodes consist of two 0.64-cm (¼-in.) tungsten rods housed in water-cooled jackets placed perpendicular to the discharge tube axis. The energy storage capacitance consists of RG 214/U coaxial cables connected in parallel. The capacitor is charged with the LC charging circuit shown in Fig. 1.

Currently, an average power level of 16 W has been attained at a pulsing rate of 17 kHz and an efficiency of 1%. The laser operating conditions are shown in Fig. 1. The reliability of copper bromide lasers, tested to date, is excellent. Laser operation of 100 hours was accumulated by operating 8 hours a day making only minor adjustments in laser operation. The laser was operating routinely at the end of 100 hours and was arbitrarily shut down at that time. Examination of the discharge tube showed a small amount (< 0.2 gm) of metallic copper deposits and very little electrode deterioration. The general condition of the laser tube, brewster windows, electrodes, and electrode housings indicated that laser operation probably could have been continued for several hundred hours. It is currently believed that the lifetime of the laser is dependent on electrical components such as the thyratron rather than on the discharge tube operating characteristics.

Table 1. Laser Operating Conditions

| | |
|---|---|
| Pulse repetition rate | 16.7 kHz |
| Pulse width (FWHA) | 40 nsec |
| Pulse amplitude stability | <±5 nsec |
| Gain | 45 dB/m (510.6 nm),<br>38 dB/m (578.2 nm) |
| Beam divergence | $4 \times 10^{-3}$ rad (~150 λ/D) |
| Polarization | 80% linear |
| Neon buffer gas pressure | 80-100 torr |
| Copper bromide container temperature | 400-500°C |

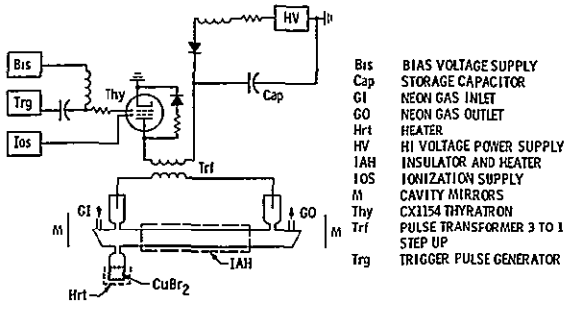


Figure 1. Schematic Diagram of Experimental Setup

*Control and Energy Conversion Division, Energy and Materials Research Section

RTOP 506-25-41
High Power Laser Systems
A. A. Vetter*



# OSCILLATOR-AMPLIFIER OPERATION OF A DOUBLE-PULSED COPPER CHLORIDE LASER

An oscillator-amplifier can be used to scale short-pulse-duration lasers to higher power. This configuration, illustrated schematically in Fig. 1, consists of a single laser, termed the oscillator, that has its output beam directed into the amplifier, where the power is increased. The amplifier is essentially a laser without mirrors. Optical equipment is placed between the oscillator and amplifier to select portions of the oscillator output to be amplified.

For this study, the oscillator and amplifier consist of double-pulsed copper chloride lasers. The oscillator has a maximum output of 1.5 mJ per pulse. The optical equipment is used to collimate the beam and to select polarization, wavelength, and energy of the oscillator beam. For pulsed lasers, the amplifier must have gain when the light from the oscillator is passing through, otherwise amplification will not occur. It was determined that for maximum energy extraction, the oscillator and amplifier discharges which excite the copper atoms are required to be timed with an accuracy of 2 ns. The time that is required for the light to travel from the oscillator, through the optics, to the amplifier must be taken into account.

The energy extracted from the amplifier as a function of input energy is illustrated in Fig. 2. The data indicate that maximum energy (8.4 mJ) is extracted from the amplifier with an oscillator energy of around 0.8 mJ. The amplifier, when operated as an individual laser, has an output of 8.4 mJ. When the oscillator output is linearly polarized, the output from the amplifier is almost totally in that same polarization. The oscillator has a pulse width (FWHM) of 32 ns and the amplifier section, when operated as an individual laser, has a pulse width of 34 ns. When operated for maximum energy extraction, the pulse width of the oscillator-amplifier was 30 ns.

This double-pulsed copper chloride laser configuration has shown characteristics of oscillator-amplifier operation. The oscillator energy is large enough to saturate the amplifier. Pulse narrowing has been observed, and polarization of the input beam has been preserved without loss of amplification.

Experiments are in progress to further define the characteristics of double-pulsed copper halide oscillator-amplifiers. Small signal gain will be determined, and the lasers will be optimized for peak instantaneous power. Determination of an upper bound on the rate of kinetic mixing of the two upper laser levels is also planned.

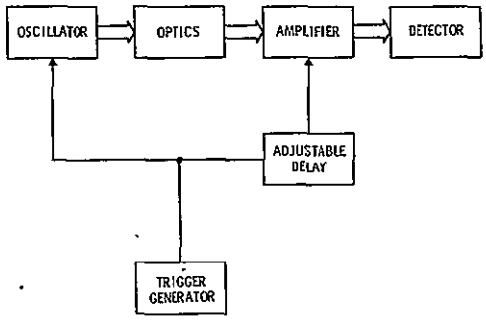


Figure 1. Block Diagram of Oscillator-Amplifier Laser Apparatus

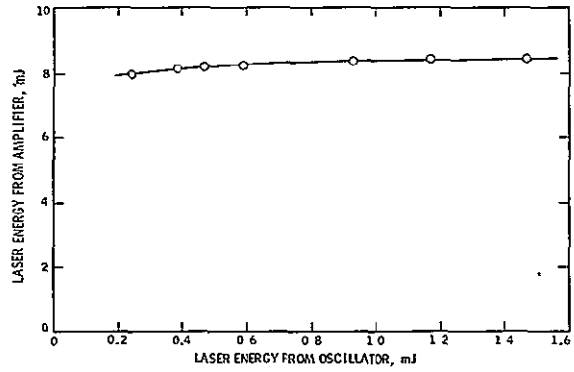


Figure 2. Energy Extracted from Amplifier



*Control and Energy Conversion Division, Energy Conversion Systems Section

RTOP 506-25-31
Fundamental Photonics
J. B. Laudenslager*

## PHYSICS OF MOLECULAR INTERACTIONS

The physics of molecular interactions program is primarily a basic research task which emphasizes experimental studies of the fundamental interactions of ions, metastables, electrons, and photons with molecules. Unique research instrumentation and capabilities have resulted from this task which has in the past produced a high level of significant basic research. Close interactions with universities and outside research institutions have been maintained throughout this work. The basic research performed in this task has been successfully applied in several areas of practical applications for NASA, including the development of new UV and visible lasers.

In previous years we have predicted that collisional excitation processes, such as excitation transfer from excited rare gas species to neutral molecules, would be an efficient means for achieving laser emission at short wavelengths. In FY'76 we have successfully demonstrated this concept by achieving laser action at 427.8, 351, and 249 nm from three different collisional excitation transfer reactions. We have also developed a unique tabletop double discharge laser capable of operating at many atmospheres of total pressure (Fig. 1). This capability is necessary for operating these new laser systems at high powers. In FY'77 we will optimize this discharge system to obtain even higher output powers from those lasing systems we have operating, and we will search for other, new laser systems which operate on the same principle of rare gas excitation transfer chemistry.

The underlying principles for the excitation transfer laser concept can be illustrated by the $He_2^+/N_2$ charge transfer laser system. Figures 1 - 4 depict the operating characteristics of this laser. Preionization is necessary to eliminate discharge instabilities which occur for electric discharges in large volume high pressure gas mixtures. The discharge device depicted in Fig. 1 has been used successfully to achieve stable discharges in a variety of high pressure gas mixtures. Figure 2 depicts the optimum concentration of $N_2$ in helium for the $N_2^+$ laser which is pumped by charge transfer reactions and the measured optimum partial pressure of $N_2$ is in the range of partial pressures which the kinetics for the charge transfer reaction would predict. Figure 3 demonstrates that the output power for this laser system scales with the input power of the main discharge. This is an essential characteristic for potential high power lasers. Figure 4 demonstrates that the $N_2^+$ laser is indeed pumped by an excitation transfer reaction. The delay between the discharge current pulse and the $N_2^+$ laser output pulse is due to the time needed for the charge transfer reaction sequence to occur. The $N_2$ laser at 3371Å, which is produced directly by electron impact, has no delay between the current onset and the lasing pulse.

The significance of this work is that these new lasers scale with volume, number density, and input power. They also operate in the visible and ultraviolet regions of the electromagnetic spectrum which has several potential NASA applications:

(1) Short wavelengths can be readily used for energy conversion schemes. There is no need to convert IR photons to visible or UV photons with subsequent loss of efficiency.

(2) Photochemistry requires UV or visible lasers and these lasers open up new applications in remote atmospheric sensing.

(3) Communication and detection capabilities are more favorable for short wavelength photons.

(4) These lasers have both high peak and average power capabilities, and we can achieve this in a small compact flyable package.

(5) Because we can obtain a variety of new high power UV laser lines from the same discharge device, we will have unique capabilities to study the interactions of high intensity UV laser light with molecules. This will help extend the fundamental knowledge of these processes which may lead to other significant NASA applications.

Along with our refinement of double discharge excitation transfer laser technology, we will continue in FY'77 our fundamental research in the area of ion chemistry and excitation transfer reactions. We will also apply these new high power lasers to various problems in photochemistry for possible NASA applications in remote atmospheric sensing.

Reference:

Laudenslager, J. B., Pacala, T. J., and Wittig, C., "Electric-Discharge-Pumped Nitrogen Ion Laser," J. Appl. Phys. 29, 1976.



*Earth and Space Sciences Division, Physics Section

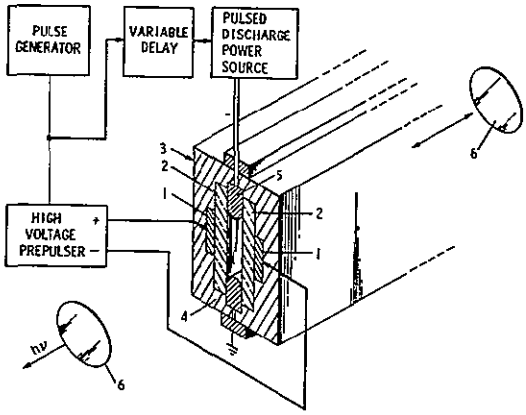


Figure 1. Schematic of the preionized transverse electric discharge device used to generate the $N_2^+$, $XeF^*$, and $KrF^*$ lasers. The preionization electrodes (1) which are glued behind glass plates (2) are fired by a high voltage prepulser before the primary discharge is fired between the main electrodes (4) and (5). The laser cell is fabricated of lucite (3) and has Brewster angle end windows. An appropriate optical cavity (6) is used to provide the necessary feedback for stimulated emission.

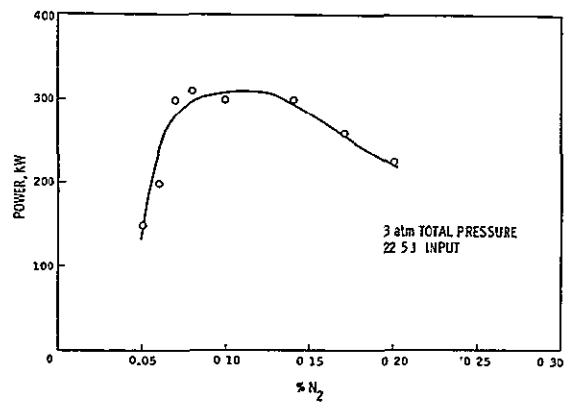


Figure 2. Pulse power output characteristics of the $N_2^+$ laser for the 4278Å laser line as a function of $N_2$ partial pressure in high pressure helium gas. This laser is pumped by a charge transfer reaction of $He_2^+$ with $N_2$.

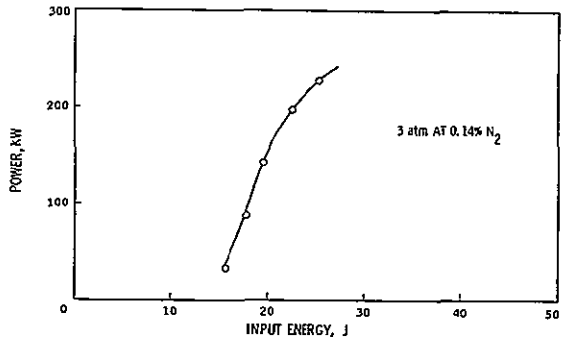


Figure 3. Output power characteristics of the $N_2^+$ laser for the 4278Å line as a function of the electric discharge energy input.

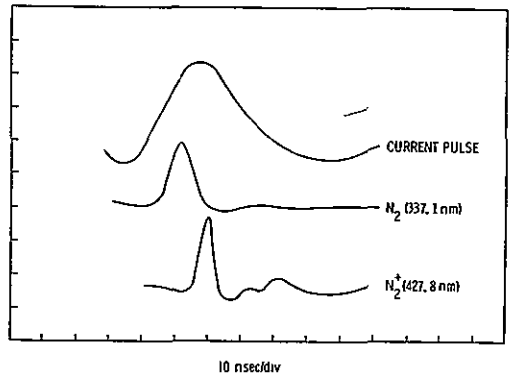


Figure 4. Laser pulse shapes for the $N_2$ laser at 3371Å and the $N_2^+$ laser at 4278Å produced in the discharge device depicted in Fig. 1. The current pulse shape for the electric discharge is represented by the top trace.

RTOP 506-25-31
Fundamental Photonics
W-K. Rhim*

# NUCLEAR ZEEMAN AND GAMMA-RAY LASERS

The primary objective of this task is to study nuclear spin dynamics and apply it to produce stimulated gamma-ray effects for a potential gamma-ray laser. The resonance cross sections of those isomers that can be pumped with laboratory scale pumping equipment are very small due to the broad linewidth caused by interactions such as the static dipole-dipole, quadrupolar or the hyperfine interactions. Our effort at JPL is to adopt the artificial line-narrowing technique to increase the gamma-ray resonance cross section.

There are numerous applications of coherent gamma-ray sources. For example, the short wavelength graser would allow the $\gamma$-ray holography of molecular systems. Direct holography of the three-dimensional structure of molecular systems would revolutionize chemistry, biology, metallurgy and crystallography. The energy conversion from a laser to a high temperature plasma is, in general, proportional to the square of the laser frequency; thus, the graser may be utilized to induce a controlled fusion reaction. There is also the possibility of the controlled release of energy from a graser; using the graser as an energy storage device, $10^5$ J/gm of energy may be stored and released through the $\gamma$-ray output.

It is also worthwhile to emphasize the importance of the side products generated from this task. The line-narrowing sequence developed at JPL is being widely recognized in the field of high resolution solid-state NMR spectroscopy (Refs. 1-3). In contrast to liquid state NMR, which has become an essential tool for analytic chemistry, solid state NMR has not yet become an analytic tool because of the wide structureless lines obtained. This broadening is caused by the static dipolar interaction. However, using a properly programmed line narrowing sequence, one can eliminate this interaction and observe a spectrum with various structures which reveal information such as anisotropic chemical shifts or indirect exchange coupling constants. These anisotropic interactions are valuable for the study of electronic structures of molecules and crystaline solids, and are normally obscured in liquids because of molecular motion. Application of the same technique to Mossbauer spectroscopy will create a high resolution Mossbauer spectrometer by which fine interactions within long-lived isomers can be explored. Even more important, the success of such an experiment would mean great progress toward the actual construction of a gamma-ray laser.

In FY'76 we have observed a new spin-locking effect under conditions of pulsed RF excitation. The transverse nuclear polarization was locked along the RF phase for nearly 10 sec in a $CaF_2$ crystal under this condition. Figure 1 shows the effect of RF pulse angles on the lifetime of nuclear polarization. When we used conventional pulse sequence which utilized 90° pulses, the nuclear polarization disappeared after 30 msec. However, when 45° pulses were applied the nuclear polarization could be preserved longer than a second. And this total time of polarization was limited by the spin-lattice relaxation time of the crystal rather than the imperfection of the new pulse sequence. An interesting phenomenon is that the spin system can be described using spin temperature even under the multiple pulse excitation condition (Refs. 4, 5). For example, the spin system could be adiabatically cooled down through adiabatic demagnetization process which was achieved by gradually decreasing pulse amplitudes as shown in the beginning part of Fig. 2(a) and (b). In this demagnetized state, the polarization disappeared, the entropy preserved and the spin temperature was only a few degrees Kelvin. The proof that this was indeed the case was demonstrated by showing reverse processes, i.e., when the RF pulse sequence was gradually turned on, the nuclear polarization started growing from a completely demagnetized state to its full original value, as shown in the latter part of Fig. 2. Such quasi-equilibrium spin states are very susceptible to any abrupt change of the system which might be caused by the atomic jumps or the molecular reorientation in the crystal. Therefore, it will provide a sensitive technique to probe molecular dynamics in the solid phase. Also, present multiple pulse approach enables us to observe the whole dynamics of spin polarization almost instantly, therefore saving the experiment time tremendously. For instance, several cycles of adiabatic demagnetization–remagnetization process as shown in Fig. 3 could be observed in less than a second while it could have taken more than 4 hours if conventional techniques were used.

Primary activities in FY'77 will be the study of spin systems in which quadrupolar and hyperfine interactions are the dominant line-broadening mechanism. We will be seeking ways to control these interactions. The problem of Mossbauer line scanning scheme by means of chemical shift will also be analyzed.

Prof. G. C. Baldwin at the Rensselaer Polytechnic Institute has a contract with NASA, being monitored by JPL, on the theory of gamma-ray laser related problems.

References

1. Rhim, W–K., Elleman, D. D., and Vaughan, R. W., "Analysis of Multiple Pulse NMR in Solids," J. Chem. Phys. 59, 3740, 1973, ibid, 60, 4595, 1974.

2. Rhim, W–K., Burum, D. P., and Vaughan, R. W., "Extraction of Quadrupole Phase Information From Multiple Pulse NMR Signals," Rev. Sci. Instrument 47, 720, 1976.

3. Stoll, M., Rhim, W–K., and Vaughan, R. W., "Heteronuclear Spin Dynamics Using Multiple Pulse NMR Technique," J. Chem. Phys. 64, 4808, 1976.

*Earth and Space Sciences Division, Physics Section

4. Rhim, W–K., Burum, D. P., and Elleman, D. D., "Spin-Temperature and Multiple Pulse NMR in Dipolar Solids," XIXth Congress Ampere, Heidelberg, Germany, 1976.

5. Rhim, W–K., Burum, D. P., and Elleman, D. D., "Multiple Pulse Spin-Locking in Dipolar Solids," Phys. Rev. Letters, submitted 1976.

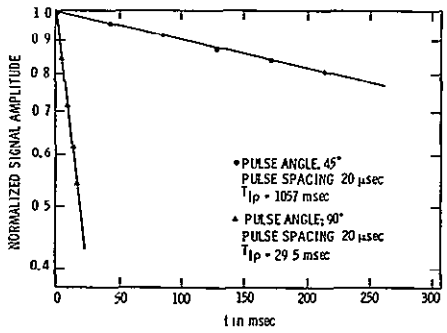


Figure 1. Effect of Pulse Angle on the Lifetime of Polarization

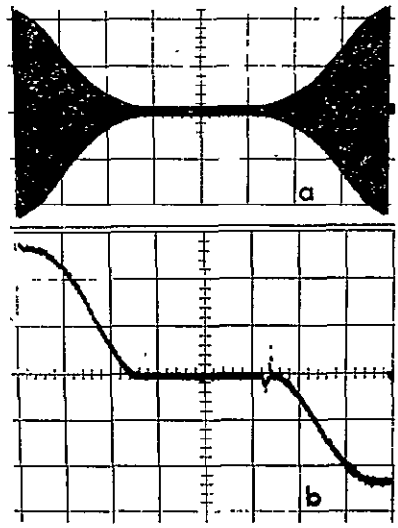


Figure 2. Adiabatic Demagnetization and Remagnetization Process

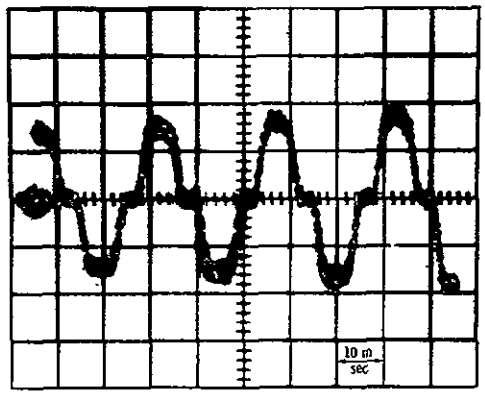


Figure 3. Cycles of Adiabatic Demagnetization and Remagnetization Processes

RTOP 750-01-52
Definition of Physics and Chemistry Experiments in Space
M. M. Saffren*

# PHYSICS AND CHEMISTRY EXPERIMENTS IN SPACE

The specific objective of the NASA OAST Physics and Chemistry Experiments in the Space Experiments Program is to identify, develop, and perform experiments for fundamental physical science investigations in space. These investigations utilize the unique environment provided by shuttle flight, such as microgravity and macrovacuum, to perform experiments not possible or practical on Earth.

The JPL program is presently directed toward four areas of experiment: liquid drop dynamics, wall-less chemistry, behavior of quantum fluids, and relativity and gravitation experiments. The experiments in drop dynamics and quantum fluids exploit the microgravity available in orbital flight, while those in wall-less chemistry utilize the extensive vacuum provided by space; the delicate relativity and gravitation experiments take advantage of the absence of appreciable low frequency seismic noise.

Work in the program proceeds through both in-house work and study contracts to university scientists.

Current study contracts are listed in Table 1.

Work at JPL on the dynamics of liquid drops has led to an experiment module, the Drop Dynamics Module to be flown on Spacelab 1, furnished by JPL through the Drop Dynamics Module Project. JPL has also proposed an experiment for that module. Dr. Wang describes that experiment later in this review. In developing the module and experiment, both KC-135 aircraft and sounding rockets are employed to provide periods of weightlessness less than those available on the Shuttle, but useful enough to test hardware, experiment techniques, and perform precursor experiments. For drop dynamics, neutral buoyancy tanks in the laboratory are also used for the same purposes.

In relativity, aside from sponsoring study contracts, JPL is planning together with MSFC a miniconference on relativity modelled after the Quantum Fluids in Space miniconference held at the University of Oregon in July 1975.

That conference uncovered several possible experiments on quantum fluids. One of these, experiments on superfluid helium agglomerates, is currently being funded for study. In these experiments mixed phases such as $^3$He droplets in HeII, and foams of HeII and its vapor, may be new superfluid phases not observable on Earth. The idea is that in these systems, liquid phases can have thicknesses less than or comparable with the coherence distance; so, for example, superfluidity is induced in thin normal metal films in intimate contact with superconductors. In any case, in the quantum systems studied, the superfluid is simply connected but with an extremely large surface area so that surface phenomena will be enhanced and thus more easily studied.

Another experiment study, approved but not yet funded, is observation of HeII at temperatures closer to the lambda point than is possible on Earth. The lambda transition is the archetype for second-order phase transitions because of the "cleanness," literally and figuratively, of the HeII transition. Study of HeII at the lambda transition to temperatures within $10^{-7}$ °K of the lambda point will be a stringent test of the current theory of critical exponents now being applied to the study of thermodynamic phase transitions.

The JPL studies on quantum fluids are directed to three experiments: the dynamics of a HeII drop; visualization of HeII vortex lines; and the behavior of capillary waves on thick HeII films. In studying the feasibility of these experiments; use will be made of calculation, laboratory studies, and experiments in the near weightlessness provided by flight of the NASA KC-135 aircraft.

## Visualization of Vortex Lines

Visualization of vortex lines hinges on decorating the lines with visible particles. The necessary sizes of the particles have been calculated. Laboratory tests will be conducted to determine the lighting that renders the particles most visible without causing objectionable heating of the helium. Strobe lighting currently appears to be most suitable. The type of decorating particles will be chosen on the basis of optimum size, density, and uniformity.

Clumping of the decorating particles would prevent visualization of one entire line. To prevent the tendency to clump, the particles must be electrically charged. Calculations show that the experiment duration is one hour, consequently the particles must retain their charge for that length of time. Capacitative techniques will be used to determine the charge lifetime.

Slight temperature variations in the superfluid can cause irregular motions of the vortices, consequently strict temperature regulation of the dewar is necessary. Sloshing of the superfluid bath surrounding the experiment dewar can introduce undesirable temperature variations. Methods of reducing slosh will be tested in the laboratory and on the KC-135. Candidate methods include use of a superleak plug to keep vapor and liquid from mixing, and various capillary control devices such as styrofoam, at one extreme, or arrays of rods at the other.

## Superfluid Helium Drop

Because of the extremely low viscosity of liquid helium, a rotating drop must be spun up very slowly to maintain rigid body rotation. Even if the drop is spun up so that initially there is differential rotation, the low viscosity requires a long time for the drop to relax to rigid body rotation. Since the drop must not collide with the dewar

*Earth and Space Sciences Division

walls during spin up, the spin-up time determines the spacecraft accelerations allowable during the experiment. Spin-up rates of superfluid helium will be determined by spinning superfluid helium in a laboratory vessel.

Formation of a superfluid helium drop is made difficult because superfluid easily leaks past the sides of even the tightest piston. We will study a pistonless injector based on the fountain effect.

Quantum Capillary Waves on Thick Films

Because the severe attenuation of capillary waves on thick films in normal gravity makes them unobservable in the laboratory, no calculations have ever been performed to predict their behavior. The attenuation on films in zero-gravity is, on general grounds, predicted to be less severe and so should be observable; calculations will be undertaken to determine their behavior. The analysis will utilize the simple two-fluid model of HeII and will serve both as an aid in designing the experiment and providing a comparison for data taken in the actual experiment.

Capacitive detectors have been developed for gravity waves on films. Determining the optimum detector for capillary waves will require flight on the KC-135. Because of the relatively poor quality of near-weightlessness, both in terms of value and duration, the KC-135 experiments will be necessarily crude but will nevertheless be the first capillary wave experiments on a thick film and so will be useful in checking, if indeed, capillary waves can begin to propagate in a low-gravity environment.

Table 1. Study Contracts

1. Completed
   - Free Jet Experiments in a Spacecraft Environment
     J. B. Fenn - Yale University
     Monitor - W. T. Huntress, JPL
   - Gravitational Radiation Experiments
     J. Weber - University of Maryland
     Monitor - P. V. Mason, JPL
2. New
   - Study of Superfluid Agglomerates
     L. Campbell - Los Alamos Scientific Laboratory
     Monitor - M. M. Saffren, JPL
   - Feasibility Analysis of Experiments on Gravitation in Space
     F. Everitt - Stanford University
     Monitor - M. M. Saffren, JPL

Table 2. Accomplishments in FY'76

1. The Proceedings of the International Colloquium on Drops and Bubbles was published.
2. The Proceedings of the miniconference on Quantum Fluids in Space was published.
3. The final draft of the Proceedings of the miniconference on Fluid Dynamics in Zero-Gravity was completed.
4. A preliminary report on Gravitational Radiation Experiments has been prepared and the final report is being drafted.
5. The final report on Free Jet Experiments in a Spacecraft Environment is being drafted.
6. A preliminary report on Feasibility Analysis of Experiments on Gravitation in Space is being drafted.
7. Four presentations on the Physics and Chemistry in Space Program have been given to European and American scientists.
8. Six preliminary study proposals and two feasibility studies have been submitted to PACE.
9. A dewar for the visualization studies of superfluid helium has been constructed for KC-135 flight.
10. A capacitive sensing technique for "visualizing" superfluid helium has been undergoing laboratory test.
11. Calculations to study the feasibility of decorating quantized vortex lines to render them visible have been completed.
12. Both user and review groups for superfluid helium experiments in space have been established.

RTOP 506-25-35
Electron Impact Spectroscopy
S. Trajmar*

## ELECTRON-ATOM (MOLECULE) COLLISION PROCESSES

This task is concerned with the physics of electron-atom (molecule) collision processes and is closely coordinated with needs in the areas of plasma and laser physics and isotope separations. Cross sections for the various electron collision processes (including elastic scattering; momentum transfer; rotational, vibrational, and electronic excitations; ionization; dissociation; electron capture; superelastic scattering; and their combinations) are determined and the methods of electron impact spectroscopy are also exploited to gain spectroscopic information and insight into the basic nature of electron-atom interactions.

The main emphasis during FY'76 has been on metal vapors which have been predicted (and in some cases shown) to be excellent candidates for high power visible lasers. The predictions have been based mainly on the energy level schemes. No electron impact cross sections have been available, however, for evaluating, modeling and improving the systems from the cross section (population inversion) point of view. Laboratory measurements were carried out to fill these needs on a number of metals (Li, K, Mg, Ba, Cu, Zn, Pb, Bi). Extensive measurements were carried out on Cu which is presently the best laser medium. The normalization of the cross sections is the most difficult problem which has not yet been satisfactorily solved. We have devised an experimental and a theoretical scheme for achieving this normalization and work is in progress along these lines. The measurements are also being extended to inner shell and multiple excitation processes which overlap the ionization continua and are responsible for the major fraction of actual ionization. Although this is a completely unexplored area, several papers have been published dealing with it.

Work on $UF_6$ has been continued to support the $UF_6$ gas core reactor, nuclear-pumped laser, and uranium isotope separation modelings. Some of the results have been published in three papers, while others are being evaluated and prepared for publication.

Work on rare gases (He, Ar, Kr) and diatomic molecules ($N_2$, CO, $O_2$) is continuing, and about a dozen papers have been submitted or are being prepared for publication.

The design, fabrication, and part of the testing of a new generation electron impact spectrometer have been completed. This is a very flexible instrument of modular construction which makes it possible to carry out a large number of complicated measurements. One of the first measurements planned on this instrument will concern electron collision processes with excited species (laser and discharge excitations). In laser and plasma devices a large number of excited species are present and their collisions with electrons can significantly influence the behavior of the system. However, practically no information exists at the present time on these processes.

The program planned for FY'77 includes: continuation of measurements on metal vapors; absolute cross section calibrations against He; improvement of He standard; electron/photon coincidence work on Kr, $UF_6$; electron scattering from laser excited species; vibrational excitation of polyatomic molecules; and completing survey work on CO, $O_2$ and $H_2$.

Figures 1-4 show, respectively, typical examples of an energy-loss spectrum, the energy dependence of cross sections in resonance regions, a set of differential cross sections, and integral cross sections.

*Earth and Space Sciences Division, Physics Section

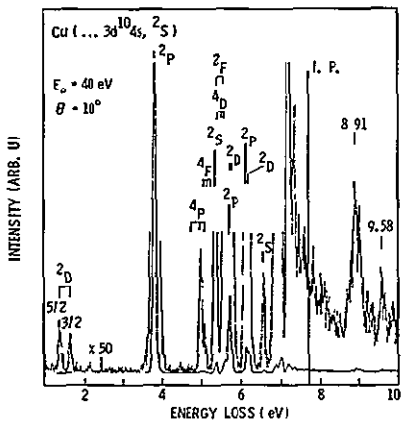


Figure 1. Energy-loss Spectrum of Cu at 40 eV Impact Energy and 10° Scattering Angle. Note the Presence of Strong Autoionizing Features Above the First Ionization Limit

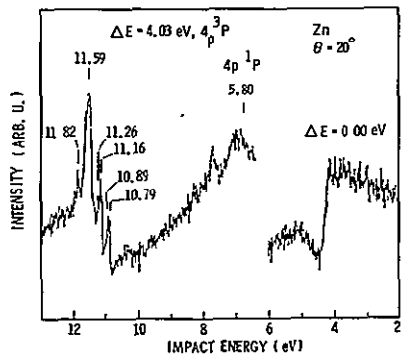


Figure 2.. Resonances in the Elastic and 4p $^3$P Excitation Channel for Zn at 20° Scattering Angle

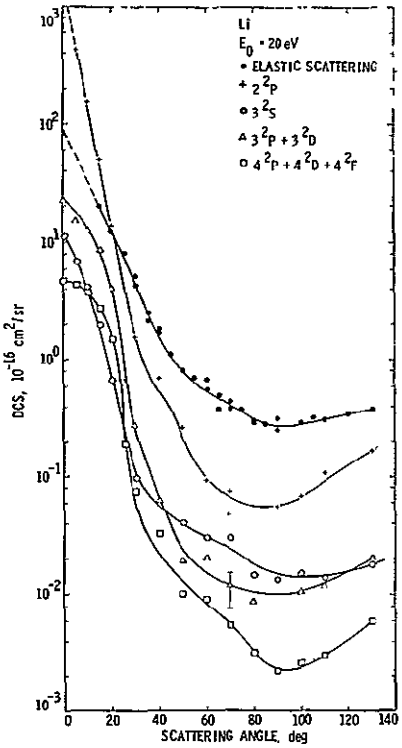


Figure 3. Differential Cross Sections for Li at 20 eV Impact Energy

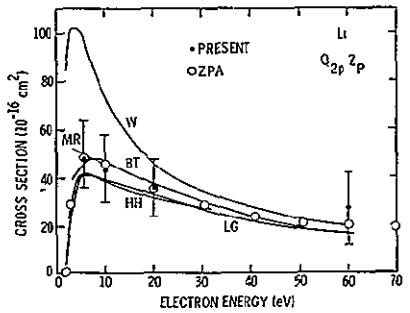


Figure 4. Integral Cross Sections for the Excitation of the 2p $^2$P state (6708 Å) of Li. Dots with Error Bars are Present Results. Curves and Circles are Other Experimental and Theoretical Results Given for Comparison



C.7

RTOP 750-03-01
Development of a Shuttle Flight: Drop Dynamic Module
T. G. Wang*

## DYNAMICS OF LIQUID DROPS IN ZERO GRAVITY

The theory of the dynamics of a free drop has been well-studied in the approximation that dynamic quantities deviate linearly from those of a resting drop. With a few exceptions, there is no nonlinear theory of the dynamics of a fluid drop. Not only are definitive experiments for the large amplitude behavior of fluid drops lacking but there are few definitive experiments even for linear behavior. This is a consequence of the limitations involved in conducting experiments in an Earth laboratory. Among these limitations are insufficient droplet sizes for accurate observation, limited available time for experiments, and perturbing effects due to the method of suspending the droplets.

The proposed Drop Dynamics Experiment will utilize the zero-g environment provided by the orbiting Space Shuttle to investigate the dynamics of a free drop. The results of the proposed experiment will be used to verify existing theory, and to provide the necessary insight for further theoretical development of this subject. The deficiencies of the existing theory, which disregards viscosity, internal flows, virtual mass, and other parameters, are exemplified by the different results of Plateau's system of two immiscible fluids (Ref. 1) and the Skylab science demonstrations (Ref. 2).

Aside from fundamental interest, a better physical understanding of the behavior of the dynamics of free liquid sperioids is required in many areas of science and technology, as demonstrated by the scope of the program presented at the Drops and Bubbles Colloquium (Ref. 3).

The objectives of the proposed Drop Dynamics Experiment are shown in Fig. 1. The experiment will examine the equilibrium shape, the bifurcation points, the instability and hysteresis of bifurcation points, and the oscillation and fission process of a rotating drop. The experiment will also examine the shape, frequency and damping of an oscillating drop, and the mode coupling and aperiodic motion of a drop oscillating with large amplitude.

To ensure the scientific significance of the JPL Drop Dynamics Experiment scheduled for flight on Spacelab in 1980, four parallel development efforts as shown in Fig. 2 are under way to define, modify and improve the 1980 experiment parameters, procedures, and sequences within the constraints of cost, manpower, and scheduling.

These efforts are not only of scientific interest but also will develop the expertise of JPL's investigation team on all phases of the experiment. In the next two figures, we describe some of the Laboratory results obtained from this development effort. In Fig. 3, new stable equilibrium shapes (Ref. 4) of rotating drops have been observed in our immiscible system. Those shapes appear to be higher modes of triaxial shape as theoretically described by Chandrasekhar (Ref. 5). However, those shapes have been believed to be highly instable, and unlikely to be observed. This result will significantly modify and improve our spaceborne drop dynamics experiment. In Fig. 4 the first order acoustic torque measurements have been carried out in our acoustic system. This is the first time that a non-zero time average torque not associated with second order effects has been observed (Ref. 6). This measurement will refine the parameters and procedures of our spaceborne drop dynamics experiment.

### References

1. Plateau, J., Smithsonian Report, 270, 1963.

2. Gibson, E. G., "Skylab Fluid Mechanics Demonstration," Proceedings of the International Colloquium on Drops and Bubbles, 1976.

3. International Colloquium on Drops and Bubbles, Pasadena, CA., 1974.

4. Wang, T. G., Elleman, D. D., and Saffren, M. M., Bull. Am. Phy. Soc., 1975.

5. Chandrasekhar, S., Proc. Roy. Soc. (London) 286, 1, 1965.

6. Wang, T. G., Kanber, H., and Rudnick, I. (Submitted to Phy. Rev. Lett.).

*Earth and Space Sciences Division, Physics Section

- DETERMINE EQUILIBRIUM SHAPES OF A ROTATING SPHEROID
- STUDY LARGE AMPLITUDE OSCILLATIONS

Figure 1. Drop Dynamics Experiment Objective

- LABORATORY STUDY
- THEORETICAL CALCULATION
- KC-135 AIRPLANE FLIGHT
- ROCKET FLIGHTS

Figure 2. Development Program

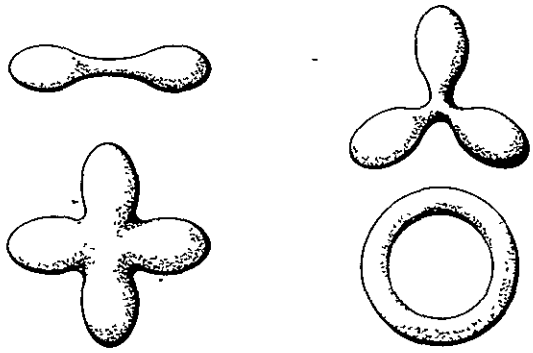

Figure 3. Equilibrium Figures of a Rotating Drop

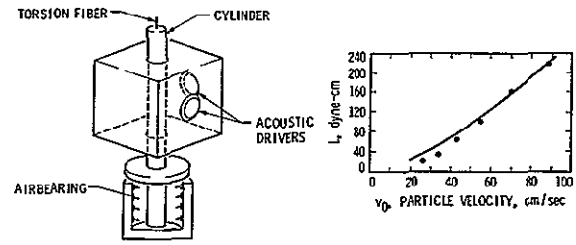


Figure 4. The Acoustic Torque

RTOP 506-15-25
Properties of Materials for Electronic Applications
P. V. Mason*

# SUPERCONDUCTING INFRARED DETECTORS

The development of higher performance detectors in the far infrared is of particular interest to NASA because the opaqueness of the atmosphere from 50 to 1000 $\mu$ forces the astronomer interested in obtaining high performance to use space-based telescopes. Three missions now under way or planned will accomplish the investigation of this last major unexplored region of the spectrum. These are: The Infrared Astronomy Satellite (IRAS), which is to accomplish an all-sky survey in the region from 8 to 300 $\mu$; the Shuttle Infrared Telescope Facility, which will perform short-duration high-resolution investigations; and the Space Telescope, which will have an infrared facility to perform long-duration high-accuracy investigations.

Two peculiarities of detectors for these wavelengths make it likely that superconducting devices will play a major role in far infrared astronomy. The first, which is fundamental, is that all high performance detectors must be cooled below 2°K. Thus, superconductors, which typically require temperatures below 6° or 8°K, impose no new demands for a cryogenic system.

The second is that the performance of present detectors is far short of that available in other regions of the spectrum in terms of sensitivity, selectivity, and speed of response. These limitations are not fundamental, and it is predicted that superconducting detectors, particularly those based on the Josephson effect, will offer improvements of one to several orders of magnitude in these parameters.

A program to develop improved detectors has been under way at JPL for several years. The Low Temperature Physics group at Caltech has played an important part in this effort.

During the period from October 1975 to October 1976, the following tasks were accomplished:

(1) Work on efforts to fabricate films of $Nb_3Ge$, the superconductor with the highest known transition temperature, has been re-started. The proposed technique involves the deposition of Nb films on $GeO_2$, and subsequent high-temperature reaction of the two to form $Nb_3Ge$. Earlier work at JPL failed because the $GeO_2$ melted before a reaction could take place. A hexagonal crystalline form of $GeO_2$ with a higher melting point has been obtained and the effort is now under way to fabricate high temperature films.

(2) Investigation by the Caltech group of the impedance of single element Josephson junctions have been successful in producing a phenomenological model which is in good agreement with the measured behavior (Ref. 1). Investigations have also been made of the more difficult problem of the impedance of arrays of junctions. These will be continued in the next year.

(3) Investigations by T. Ganz of Caltech of the coupling of Josephson junctions to strip transmission lines were reported to the last OAST Research Council Review. The work has been completed, and will make significant contributions to the solution of the problem of coupling the detected output of the junctions to external room-temperature circuitry (Ref. 2).

(4) An important question is the existence of fundamental physical limits on the high frequency response of Josephson junctions. Recent work by the Caltech group and others has led to an understanding that non-equilibrium effects play a major role (Ref. 3). In particular, the relaxation time of the hot electrons generated in the superconductor by the Josephson processes appears to be the fundamental limitation.

(5) Work has been under way for several years to form more sensitive and selective Josephson detectors by incorporation of infrared active materials into or onto the junction. It was thought that the IR active material would selectively absorb the incident radiation with very high efficiency, thus overcoming one of the major obstacles to development of high performance Josephson effect detectors. It was expected that the activated IR material would modify the Josephson junction electrical characteristics in a manner that would be measurable.

A key step in the development of such a detector is the demonstration that coupling exists between the IR active material and the junction. At the time of the last review, we reported that we were in the process of incorporating dipheynl picryl hydrazyl (DPPH) onto the junction. The DPPH can be made IR active at a frequency determined by an applied magnetic field. It was hoped to demonstrate the effect in the 50-MHz range rather than the technically more difficult 100-300 GHz range. This hope has not been borne out. No coupling was demonstrated in several attempts made in different ways. It has been concluded that further effort at this time would not be fruitful.

For FY'77, the Caltech group will continue to investigate the impedance of arrays and the fundamental limitations imposed by the non-equilibrium processes. JPL will continue its efforts to develop films of very high transition temperatures in forms which can be fabricated into Josephson effect structures.

Another task to be undertaken at JPL will be the development of a composite bolometer consisting of a low thermal capacity substrate coated with an infrared absorptive material and a Josephson effect thermometer. Similar devices incorporating semiconductor and superconducting transition edge thermometers have yielded improved detectors, and it is expected that use of Josephson effect thermometers would lead to further improvements.

*Earth and Space Sciences Division, Physics Section

References

1. Franson, J. D. and Mercereau, J. E., "Microwave Impedance of Superconducting Weak Links," J. of Appl. Physics, 40, 3261, 1976.

2. Ganz, T., "I. The Phase-Current Relation at Zero Voltage in Bridges with Superconducting Microstrip Resonators," Doctoral Thesis, Calif. Inst. of Tech., March 1976.

3. Mercereau, J. E., "Properties of Real Junctions," IC-SQUID-Superconducting Quantum Interference Devices Conferences, H. Hahlbohm and H. Lubbig, Eds., Proceedings to be published by Walter de Gruyter, Berlin, New York, 1977.

RTOP 506-25-24
Superconducting Digital Microcircuits
R. K. Kirschman*

## SUPERCONDUCTING DIGITAL MICROCIRCUITS

This is a new program, with funding for FY'TR and FY'77. The long-range objective is to determine to what extent the projected superior performance of digital circuitry, based on superconducting technology and the Josephson effect, can be realized in practice, and to develop a technology base for subsequent applications. A significant part of the technological groundwork for this task is provided by previous work on superconducting devices and microcircuits for linear applications, carried out at JPL and Caltech.

IBM and a few other establishments have been working on superconducting digital microcircuitry and have demonstrated its feasibility and superior performance in the laboratory. However, this work has been based on the barrier-junction type of Josephson device, which requires an extremely thin oxide layer, resulting in difficulties in fabrication and reliability.

The approach to be used in this program will avoid the thin oxide, and its associated difficulties, by employing another type of Josephson structure, known as the proximity device, as the active electronic circuit element. Thus, this approach should provide a more practical technology for superconducting digital microcircuits.

During FY'TR a paper was presented at the 1976 Applied Superconductivity Conference, covering work begun in 1975 in collaboration with Caltech and Langley Research Center (Ref. 1). This work concerned the use of ion implantation to fabricate proximity devices and compared the properties of such devices with those fabricated by other processes. Dependence of the behavior of the devices upon geometrical and material parameters was elucidated. On the basis of this study and work by others, it appears that ion implantation could be a valuable technique for fabricating superconducting microcircuitry.

In addition, two international meetings devoted to superconducting Josephson-effect devices were attended. These three meetings provided a good overview of the present situation in this field and a number of valuable ideas.

The goal for FY'77 will be to demonstrate basic digital logic gates based on the proximity device. Although many approaches have been envisioned, by others as well as ourselves, no work has been done to implement them with actual hardware. Thus the first task will be to evaluate, theoretically and experimentally, the possible approaches. The most promising will serve as the basis for more thorough study of the basic gates. Subsequently, in FY'78, work will begin on fabrication of digital microcircuits composed of a number of these basic logic gates.

### Reference

1. Kirschman, R. K., Hutchby, J. A., Burgess, J. W., McNamera, R. P., and Notarys, H. A., "Comparative Studies of Ion-implant Josephson-effect Structures," presented at the 1976 Applied Superconductivity Conference, Stanford, CA, August 17-20, 1976. To appear in IEEE Transactions on Magnetics (Jan. 1977).

*Earth and Space Sciences Division, Physics Section

RTOP 506-25-31
Fundamental Photonics
A. Chutjian*

## ELECTRON-ION COLLISION PROCESSES

The area of elastic and inelastic scattering of electrons from positive ions is an unstudied field of physics which has important applications in the development of future energy sources, such as controlled thermonuclear fusion devices (Tokamak, Z-pinch) and lasers (gas-ion, nuclear-pumped). An experimental apparatus is currently being assembled to study the scattering of low-energy electrons (1-200 eV) from singly-charged positive ions. A crossed-beam geometry is being used, with the ion beam both velocity and momentum-selected. Quantities measured will be normalized, cascade-free elastic and inelastic integral cross sections. Autoionization features (electron-ion resonances) will also be studied by detecting the autoionized electrons. Systems to be studied have relevance to the understanding of plasma environment ($Ar^+$, $Kr^+$, $Mg^+$, $Cu^+$, $U^+$ and others); and planetary atmospheres ($He^+$, $H_2^+$, $H^+$, $N_2^+$, $N^+$, $O_2^+$, $O^+$, $S^+$, $Na^+$, $Ca^+$ and others). The present measurements will also be useful in testing various electron-ion scattering theories. Those theories proving to be successful may then be used to calculate cross sections for electron-highly stripped ion scattering: cross sections which are extremely difficult and time-consuming to measure experimentally.

A second thrust of our work in ion physics is in the area of threshold photoionization of atoms, molecules and radicals. Using a new technique recently developed in our laboratory (Ref. 1), we are able to measure routinely and simply in positive ions, energy levels, ionization potentials, threshold photoionization cross sections, and Franck-Condon factors. The technique is referred to as "Threshold Photoelectron Spectroscopy by Electron Attachment" (TPSA). It involves (a) photoionization of the gaseous species, (b) attachment of the threshold (~ 0 eV energy) electron to $SF_6$ or $CFCl_3$, and (c) mass detection of the attachment product ($SF_6^-$ or $Cl^-$, respectively). The yield of negative ion vs photon wavelength is the TPSA spectrum of the species. In Fig. 1(a) we show the TPSA spectrum of $Ar^+$, along with the photoionization spectrum [Fig. 1(b)]. The onset of the $^2P_{1/2}$ ionization limit is clearly seen in (a), while that limit is obscured by autoionization in (b). Also evident in Fig. 1 are features lying below the $^2P_{3/2}$ limit arising from collisional ionization of high-Rydberg levels of Ar. The importance of this process in the ionization of atoms and molecules has never been estimated.

### Reference

1. Ajello, J. M., and Chutjian, A., J. Chem. Phys., in press.

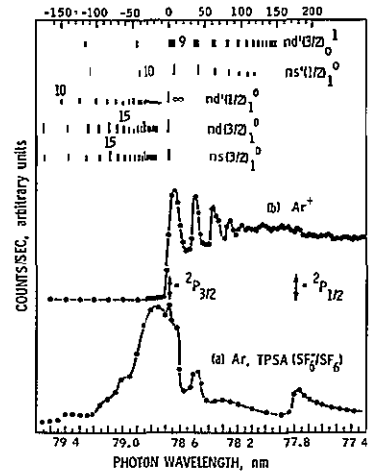


Figure 1. TPSA Spectrum of $Ar^+$ Compared to the Photoionization Spectrum in Fig. 1(b). Features Lying Below the $^2P_{3/2}$ Ionization Limit Arise from Collisional Ionization by $SF_6$ of the High-Rydberg Level Excitations in Ar. The Relevant Rydberg Series are Indicated Above the Spectra.

*Earth and Space Sciences Division, Physics Section

J. S. Zmuidzinas*

# A NEW CONCEPT FOR A VACUUM UV LASER

As a result of the research activities aimed at finding ways of storing energy in electronically excited condensed (solid and superfluid) phases of helium, a novel method for stabilizing excited $He_2(a\ ^3\Sigma_u^+)$ molecules in superfluid helium has recently been proposed (Ref. 1). An important application of this stabilization method is to obtain lasing in the vacuum ultraviolet wavelength regime around 800 Å.

Previous attempts to obtain lasing in this regime by utilizing excited states in superfluid helium were based on brute-force electron-beam pumping to obtain the requisite population inversion of the $A\ ^1\Sigma_u^+$ level of the helium molecule. Because of the very short lifetime of this level, extremely high electron-beam currents had to be delivered over correspondingly short intervals of time, leading to such difficulties as boiling of the liquid and making it impossible to maintain periodicities in liquid helium established for distributed feedback purposes.

The new approach is to utilize a "gentle" double-pumping scheme to achieve the necessary inverted populations. The first step in this scheme is to obtain a high concentration of the metastable $He_2$ ($a\ ^3\Sigma_u^+$) molecules in superfluid helium. With reference to Fig. 1, a comparatively low-current electron beam (100-200 keV, 1-10 $\mu$A) is used to produce these molecules from ground-state helium atoms. Normally the metastable molecules are quickly destroyed by mutual collisions. As a result, the achievable metastable populations are about $10^{12}$ - $10^{13}$ $cm^{-3}$ (Ref. 2). However, if the metastables are spin-aligned by means of optical pumping, then their mutual destruction is strongly inhibited by the mechanism of spin conservation, and much higher metastable concentrations are expected. By modeling the various metastable production and destruction processes in the presence of optical pumping ($c\ ^3\Sigma_g^+ \leftarrow a\ ^3\Sigma_u^+$, Fig. 1), it has been predicted (Ref. 1) that metastable concentrations of order $10^{18}$ $cm^{-3}$ can be achieved with quite modestly powered CW laser pumps operating at 9096 Å. The results are shown in Fig. 2. An alternate optical pumping scheme ($e\ ^3\Pi_g \leftarrow a\ ^3\Sigma_u^+$) might be more attractive in practice because it would utilize the more accessible laser wavelengths of about 4650 Å.

Once a high concentration of spin-aligned $He_2$ ($a\ ^3\Sigma_u^+$) molecules is achieved (lifetimes being long, ~ 1 ms), the second step is to quickly populate the upper lasing level, $A\ ^1\Sigma_u^+$, by applying a strong microwave signal tuned to the Zeeman resonance frequency of the $a\ ^3\Sigma_u^+$ molecule (situated in a magnetic field ~ 1 kG). This destroys the spin alignment and induces a quick collisional destruction of $a\ ^3\Sigma_u^+$ molecules in favor of those in the $A\ ^1\Sigma_u^+$ state. The $A\ ^1\Sigma_u^+$ populations and the feeding rates into the $A\ ^1\Sigma_u^+$ level are expected to be some $10^6$ and $10^{12}$ times higher, respectively, than those achievable by the previous simple electron-beam excitation technique. Rough estimates show that, under these conditions (super-radiant) ultraviolet lasing ($A\ ^1\Sigma_u^+ \rightarrow X\ ^1\Sigma_g^+$) might be possible, with suitable geometries, even without any feedback provisions.

The shorter wavelengths, increased resolution, and higher power densities of coherent radiation in the UV and vacuum UV regimes, as contrasted with optical wavelengths, are of great importance in applications, e.g., in physics and chemistry experiments (especially for molecular reaction studies), power transmission in space, and biomedical experiments and practice.

References

1. Zmuidzinas, J. S., "Stabilization of $He_2(a\ ^3\Sigma_u^+)$ in Liquid Helium by Optical Pumping," submitted to Phys. Rev., 1976.

2. Keto, J. W., Soley, F. J., Stockton, M., and Fitzsimmons, W. A., Phys. Rev. A 10, 872, 1974.

*Earth and Space Sciences Division, Physics Section

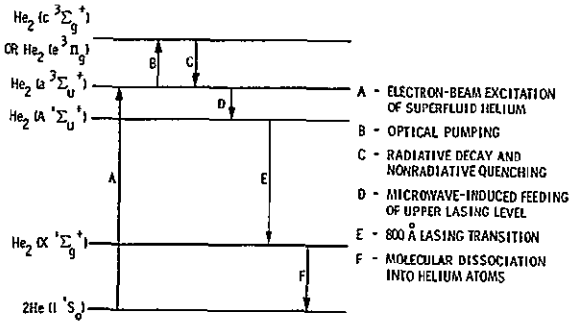


Figure 1. Spin-Aligned Excited Species VUV Laser Scheme

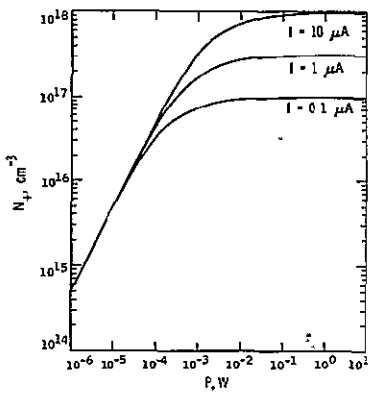


Figure 2. Metastable Populations